

Radium-226 and Radium-228 in the Atlantic Sector of the Southern Ocean

Radium-226 und Radium-228 im Atlantischen Sektor des Südozeans

Claudia Hanfland

**Ber. Polarforsch. Meeresforsch. 431 (2002)
ISSN 1618 - 3193**

Nothing in life is to be feared;
it is only to be understood.

Marie Curie

Claudia Hanfland
Alfred-Wegener-Institut für Polar- und Meeresforschung
Am Handelshafen 12
D - 27570 Bremerhaven

Die vorliegende Arbeit ist die inhaltlich unveränderte Fassung einer Dissertation, die im Januar 2002 dem Fachbereich Geowissenschaften (FB 5) der Universität Bremen vorgelegt wurde.

Eine Farbversion dieser Arbeit ist unter der nachfolgenden Internet-Adresse zugänglich:
A coloured version of this thesis is available at the following internet link:

<http://www.awi-bremerhaven.de/GEO/Publ/PhDs/CHanfland.html>

Table of contents

TABLE OF CONTENTS

Abstract	3
Kurzfassung	5
1 Introduction	7
1.1 The iron hypothesis	8
1.2 Transport mechanisms for iron into the Atlantic sector of the Southern Ocean.....	10
1.3 Objectives.....	11
2 Hydrography of the sampling area	13
2.1 General features of the Southern Ocean	13
2.2 Circulation within the South Atlantic.....	14
2.2.1 Frontal systems in the South Atlantic.....	15
2.2.2 Water masses of the Atlantic sector of the Southern Ocean.....	20
3 Radium in the marine environment	23
3.1 Physical and chemical properties.....	23
3.2 Geochemical behaviour of radium.....	24
3.3 Origin of ^{228}Ra in sea water.....	28
3.4 Distribution of $^{226}\text{Radium}$ in the Southern Ocean.....	30
3.5 Distribution of ^{228}Ra and ^{228}Th in the Southern Ocean	30
4 Material and methods	33
4.1 Sampling strategy and techniques	33
4.1.1 Surface water sampling for $^{228}\text{Radium}$	34
4.1.2 Profile sampling for $^{228}\text{Radium}$	35
4.1.3 Sampling for $^{226}\text{Radium}$	36
4.2 Measurement techniques for ^{228}Ra and ^{226}Ra	36
4.3 Sample preparation and measurement.....	37
4.3.1 Direct determination of $^{228}\text{Radium}$ on cartridge ash by γ -spectrometry	41
4.3.2 Indirect determination of $^{228}\text{Radium}$ via the $^{228}\text{Thorium}$ -ingrowth method	41
4.3.3 Determination of initial $^{228}\text{Thorium}$ on vertical water profiles.....	45
4.3.4 Determination of $^{226}\text{Radium}$	46
4.3.5 Blank determination	47
4.3.6 Error determination	48
4.3.7 Comparison of different measuring techniques	50
4.4 Spectroscopic instruments for the detection of radiation	51
4.4.1 α -Spectrometer	51
4.4.2 γ -Spectrometer	51
4.4.3 Preparation of standards for γ -spectrometry and spectrum analysis	53
5 Distribution of ^{226}Ra and ^{228}Ra in the South Atlantic	56
5.1 Surface water activities of ^{226}Ra	56
5.2 Surface water activities of ^{228}Ra	58

Table of contents

5.2.1	Shelf regions	59
5.2.2	Open ocean waters	61
5.3	Surface water activities of ^{228}Th	64
5.4	Vertical distribution of ^{226}Ra and ^{228}Th within the ACC and the Weddell Gyre	66
6	Biogeochemistry of radium and thorium in the South Atlantic	71
6.1	Bio-intermediate behaviour of radium in the upper ocean.....	71
6.1.1	The role of acantharians for the biogeochemistry of radium	74
6.1.2	Implications for radium analytics	75
6.2	Removal of ^{228}Th from surface waters	76
7	$^{228}\text{Radium as a tracer for iron input into the open South Atlantic$	80
7.1	The continental shelves as source regions for ^{228}Ra and iron	80
7.1.1	Iron distribution in coastal waters of the Southern Ocean.....	80
7.1.2	Shelf regions as sources for ^{228}Ra	82
7.2	Transport mechanisms for shelfwater signals into the open South Atlantic	85
7.2.1	Subtropical eddies.....	85
7.2.2	Oceanographic fronts.....	89
7.3	Comparison of ^{228}Ra with other geochemical tracer data	90
7.3.1	Distribution of Al and ϵNd as tracers for continental input.....	91
7.3.2	Distribution of $^{227}\text{Ac}_{\text{ex}}$ as a tracer for deep upwelling.....	94
7.4	Iron pathways into the Atlantic Sector of the Southern Ocean: a synthesis.....	95
8	Naturally occurring radium from man-made sources.....	97
8.1	Hydrocarbon exploitation on the Argentinean shelf.....	98
8.2	Naturally occurring radioactive material.....	98
8.3	Radium in produced water.....	99
8.3.1	Chemical composition of formation water	99
8.3.2	Process of radium enrichment in formation water	99
8.3.3	Radium concentrations in produced water.....	100
8.4	Discharge volumes and fate of radium after release to the marine environment.....	101
8.5	Implications of man-made sources for the use of ^{228}Ra as a tracer for shelfwater	106
9	Conclusions	107
10	References.....	109
	Acknowledgements	123
	Appendix	124

Abstract

ABSTRACT

This study investigates the distribution and the biogeochemical behaviour of ^{226}Ra and ^{228}Ra (half-lives 1600 and 5.75 years, respectively) in the Atlantic sector of the Southern Ocean. Both are important tracers in oceanographic issues on time-scales from months to years. ^{226}Ra with a deep-sea source has been suggested as a tracer for ocean mixing processes. ^{228}Ra gets enriched in shallow water regions and represents a suitable tracer for advection of shelfwater into the open ocean. In the context of iron as a growth-limiting factor for primary productivity in the Southern Ocean, ^{228}Ra is used in this study to investigate the role of iron input from coastal regions into the Atlantic sector. For a better understanding of the biogeochemical behaviour of radium in circumpolar waters, the distribution of ^{226}Ra was compared with Si concentrations.

During six cruises, ^{226}Ra and ^{228}Ra have been measured in high resolution in surface waters of the Antarctic Circumpolar Current (ACC), the Weddell Gyre, on the continental shelves and on a vertical transect across the ACC at 20° E. ^{226}Ra and ^{228}Ra samples with high activities were analyzed by γ -spectrometry. Determination of the open ocean ^{228}Ra activities was done by the ^{228}Th -ingrowth method via α -spectrometry.

^{226}Ra activities approximately double from north to south across the ACC. Highest activities (up to 18 dpm/100kg) are found in the southeastern corner of the Weddell Gyre where upwelling of Circumpolar Deep Water occurs. A correlation between ^{226}Ra and Si yields best results for surface water samples south of the Polar Front (PF) and for intermediate water masses. The correlation does not hold north of the PF, where ^{226}Ra depletion continues when Si is already exhausted. Acantharians, SrSO₄-building microzooplankton, are proposed as an important carrier phase in the marine biogeochemistry of radium.

^{228}Ra activities have been determined for the first time on both sides of the Antarctic Peninsula and on the Argentinean shelf. On the continental shelves in the Weddell Sea and along the Antarctic Peninsula, ^{228}Ra activities range from 0.2 to 2 dpm/100kg. Highest values have been determined on the Argentinean Shelf (3.7 dpm/100kg). Associated residence times for water masses on the Antarctic and Argentinean shelves vary between 2 and 10 months. In the open ACC, ^{228}Ra activities have a mean of 0.1 dpm/100kg but are below the detection limit within the Weddell Gyre. On two N-S-transects, extremely high ^{228}Ra signals of 4.3 dpm/100kg occur and coincide with the approximate position of the PF. They are suggested to originate from a temporary merging or a close proximity of the Subantarctic and the Polar Front at 40° W. Increased activities in the Argentine Basin and south of Africa could be related to the Brazil and the Agulhas Current, respectively. Satellite altimetry enabled the correlation of ^{228}Ra signals with cyclonic and anticyclonic eddies spawned from the Agulhas Retroflection Area. The subtropical intrusions containing ^{228}Ra enriched water could be traced as far as 45° S.

Vertical $^{228}\text{Th}/^{230}\text{Th}$ AR have been determined in the upper 1000 m along 20° E. It could be shown that the $^{228}\text{Th}/^{230}\text{Th}$ AR can be used as a qualitative indicator of ^{228}Ra

Abstract

activities. The depth profiles showed that ^{228}Ra enrichment is limited to a shallow surface layer north of the PF.

The distribution of ^{228}Ra was set in context to the distribution of tracers for iron input via terrigenous input (Al and the isotopic composition of neodymium) and deep upwelling (^{227}Ac) that had been determined in associated studies. Input of shelfwater seems to occur rather sporadically in restricted areas associated with the PF and the Southern ACC Boundary as elevated ^{228}Ra are not a regular feature of the frontal jets in the ACC.

A compilation of world-wide data from produced waters released during oil and gas exploitation reveals extremely high activities of ^{226}Ra and ^{228}Ra in these effluents. Several large hydrocarbon fields in operation are located in the influence of the Falkland or the Brazil Current on the continental shelf or slope of South America. It must be assumed that these discharges are subject to the same transport processes as ^{228}Ra released from shelf sediments and may complicate the distinction of the two sources.

KURZFASSUNG

Die vorliegende Arbeit untersucht die Verteilung sowie das geochemische Verhalten von ^{226}Ra und ^{228}Ra (Halbwertszeiten 1600 bzw. 5.75 Jahre) im Atlantischen Sektor des Südozeans. Beides sind wichtige Isotope für die Untersuchung von ozeanographischen Prozessen, die auf Zeitskalen von Monaten und Jahren ablaufen. Aufgrund seiner Freisetzung aus Tiefseesedimenten wurde ^{226}Ra als Tracer für großskalige ozeanische Zirkulation vorgeschlagen. ^{228}Ra hingegen reichert sich in Flachwassergebieten an und kann als Tracer für Advektion von Schelfwasser in den offenen Ozean benutzt werden. Im Zusammenhang mit Eisen als wachstumslimitierendem Faktor für die Primärproduktion des Südozeans soll im Rahmen dieser Arbeit die Rolle von Eiseneinträgen aus küstennahen Gebieten in den Atlantischen Sektor näher untersucht werden. Ein Vergleich von ^{226}Ra mit Si-Konzentrationen soll zu einem besseren Verständnis der Biogeochemie von Radium in zirkumpolaren Gewässern führen.

Die Verteilung von ^{226}Ra und ^{228}Ra wurde in hoher Auflösung auf sechs Expeditionen im Oberflächenwasser des Antarktischen Zirkumpolarstroms (ACC), des Weddellwirbels, auf den kontinentalen Schelfen sowie auf einem Vertikalschnitt durch den ACC gemessen. Die Bestimmung von ^{226}Ra sowie ^{228}Ra in Proben mit ausreichend hoher Aktivität erfolgte mittels γ -Spektrometrie. Alle übrigen ^{228}Ra -Proben wurden über die ^{228}Th -Nachwachsmethode analysiert.

Die ^{226}Ra -Aktivitäten verdoppeln sich von Nord nach Süd über den ACC. Die höchsten Aktivitäten (bis 18 dpm/100kg) wurden im südöstlichen Weddellwirbel gemessen, wo Zirkumpolares Tiefenwasser bis an die Oberfläche aufsteigt. Die Korrelation von ^{226}Ra zu Si ist am ausgeprägtesten für Oberflächenproben südlich der Polarfront (PF) sowie für intermediäre Wasserproben. Nördlich der PF, wo die Si-Konzentrationen nahe null sind, ist keine Korrelation mehr gegeben. Den SrSO_4 -bildenden Acantharien könnte eine wichtige Rolle für die Biogeochemie des Radiums zukommen.

^{228}Ra wurde zum ersten Mal auf den Kontinentschelfen der Antarktischen Halbinsel sowie auf dem argentinischen Schelf gemessen. Die Aktivitäten auf den Schelfen des Weddellmeeres reichen von 0.2 bis 2 dpm/100kg. Auf dem argentinischen Schelf wurden Aktivitäten bis 3.7 dpm/100kg gemessen. Die Residenzzeiten der zugehörigen Wassermassen variieren zwischen 2 und 10 Monaten. Die mittleren Aktivitäten im offenen ACC liegen bei 0.1 dpm/100kg. Proben im zentralen Weddellwirbel lagen unterhalb der Nachweisgrenze. Jedoch konnten im Bereich der PF auf zwei Transekten stark erhöhte ^{228}Ra -Aktivitäten gemessen werden (4.3 dpm/100kg). Ein temporäres Verschmelzen der Subantarktischen mit der Polarfront bei etwa 40° W wird als Ursache für diese erhöhten Signale an der PF angenommen. Erhöhte Aktivitäten im Argentinischen Becken sowie südlich von Afrika konnten auf den Einfluß des Brasilien- bzw. des Agulhas-Stroms zurückgeführt werden. Mit Hilfe von Satellitenaltimetrie ließ sich ein Zusammenhang zwischen ^{228}Ra -Aktivität und zyklonischen bzw. antizyklonalen Wirbeln herstellen, welche ihren Ursprung im Gebiet der Agulhas-

Kurzfassung

Retroflektion haben. Der Einfluß subtropischen Wassers mit erhöhten ^{228}Ra -Werten konnte bis 45° S nachgewiesen werden.

$^{228}\text{Th}/^{230}\text{Th}$ -Aktivitätsverhältnisse (AR) wurden in den oberen 1000 m entlang eines Tiefenprofils bei 20° E bestimmt. Es konnte gezeigt werden, daß das $^{228}\text{Th}/^{230}\text{Th}$ -AR als qualitativer Anzeiger für ^{228}Ra -Aktivitäten verwendet werden kann. Anhand der Tiefenprofile wurde deutlich, daß erhöhte ^{228}Ra -Werte nur in einer flachen Schicht im Oberflächenwasser nördlich der PF auftreten.

Die Verteilung von ^{228}Ra wurde im Zusammenhang mit Informationen über weitere natürliche Eiseneintragswege untersucht, welche mittels der Tracer Al und Neodym-Isotopie (für terrigenen Eintrag) sowie ^{227}Ac (für Aufstieg von Tiefenwasser) im Rahmen anderer Arbeiten gewonnen wurden. Da nur sporadisch erhöhte ^{228}Ra -Werte an den ozeanographischen Fronten nachzuweisen waren, muß davon ausgegangen werden, daß der Eintrag von Schelfwasser keine kontinuierliche Eisenquelle für den Südatlantik darstellt und nur in beschränkten Gebieten entlang der PF oder der Südlichen ACC-Grenze von Bedeutung ist.

Eine Zusammenstellung von weltweit erhobenen Daten über Produktionswässer, die bei der Öl- und Gasförderung anfallen, zeigt, daß diese Abwässer zum Teil extrem hohe ^{226}Ra und ^{228}Ra Aktivitäten aufweisen. Entlang des südamerikanischen Schelfs sowie des Kontinentalhangs werden an mehreren Stellen große Mengen Kohlenwasserstoffe gefördert. Diese Gebiete befinden sich im Einflußbereich des Falkland- und des Brasiliengstroms. Eine Verdriftung der künstlich freigesetzten ^{228}Ra -Aktivitäten ist daher wahrscheinlich und könnte die Unterscheidung von natürlich freigesetztem ^{228}Ra erschweren.

1 INTRODUCTION

Many issues in marine research rely on tracer studies that allow a more detailed study of the many aspects of such general topics like ocean circulation, mixing or biogeochemical cycles. While mixing of two water masses might prove difficult to be seen from θ -S-properties alone, the admixture of a trace element or compound can be readily discernible, provided that it is characteristic for a certain water mass.

Not least because of its uniqueness compared to other oceans, e.g. the formation of bottom water, the linkage between the Atlantic, Indian and Pacific Ocean by the Antarctic Circumpolar Current (ACC) or the upwelling of nutrient rich Circumpolar Deep Water, the Southern Ocean has been deemed increasingly important by the scientific community. Antarctica and the Southern Ocean are considered to play a key-role in the modern climate. Any precise reconstruction of the palaeoclimatic conditions as well as reliable predictions of future trends both involve a close investigation of the processes and interactions that govern the climate system, and with it the Southern Ocean, today. In this respect, tracer studies contribute valuable information.

The naturally occurring decay chains ^{238}U , ^{235}U and ^{232}Th provide a number of radionuclides with half-lives in the order of days to thousands of years that are of particular use in marine issues (Appendix A 6). Their distribution, apart from radioactive decay, is mainly governed by the reactivity of the respective elements: e.g. uranium, radium or actinium tend to stay in solution while thorium or protactinium are quickly scavenged by particles and transported to the seafloor. Disequilibria between parent and daughter nuclides are the consequence of this partitioning. For water mass studies, preferentially soluble radionuclides come into application. Their supply to the water column is mostly by diffusion from sediments through decay from a particle-reactive parent while their distribution in the water column is governed by their respective half-lives. The naturally occurring radium isotopes ^{223}Ra , ^{224}Ra , ^{226}Ra and ^{228}Ra have been used extensively for mixing and advection studies on different timescales in various regions (Broecker and Peng 1982).

For ocean-wide and mesoscale processes, ^{226}Ra and ^{228}Ra (half-lives 1600 and 5.75 years, respectively) are particularly suitable tracers. Both are released to the water column from the sediment through decay of thorium isotopes, but in consequence of a difference in parent nuclide distribution and half-life, ^{226}Ra is liberated rather from deep-sea sediments while ^{228}Ra accumulates to higher activities in shallow water regions. ^{226}Ra is used as a deep sea tracer for mixing processes (e.g. Ku and Luo 1994) or as a tracer in studies of particle cycling, notably barite (Legeleux and Reyss 1996). ^{228}Ra has been proven to be an excellent tracer for advection of shelfwater into the open ocean (e.g. Moore 1969b, Kaufman et al. 1973, Moore et al. 1980).

Within the Southern Ocean, the data base for both radionuclides is rather scanty and has for the most part been ascertained during the world-wide Geochemical Ocean Sections Study (GEOSECS) program between 1976 and 1979. At that time, extremely

Introduction

low ^{228}Ra activities in the open ocean could partly not be determined with the available analytical techniques and many of the samples taken south of the Polar Front were below the detection limit. Despite the progress made in the development of measurement techniques and the successful application of radium isotopes in other oceans, only few studies in southern polar waters have made use of either ^{226}Ra or ^{228}Ra as a tracer. One of the reasons might be the comparatively little information about the geochemistry and, especially in the case of ^{228}Ra , distribution of these radionuclides.

1.1 The iron hypothesis

In recent years, the recognition that primary production in the open South Atlantic might be co-limited by the availability of iron has attracted the interest of biologists and climatologists alike. The growth of phytoplankton in the world's oceans is directly linked to the availability of light and the macronutrients N, P and Si in the euphotic zone. But despite its replete nutrients, the Antarctic waters sustain only moderate primary production (Fig. 1), a phenomenon that has for a long time been known as the "Antarctic Paradox".

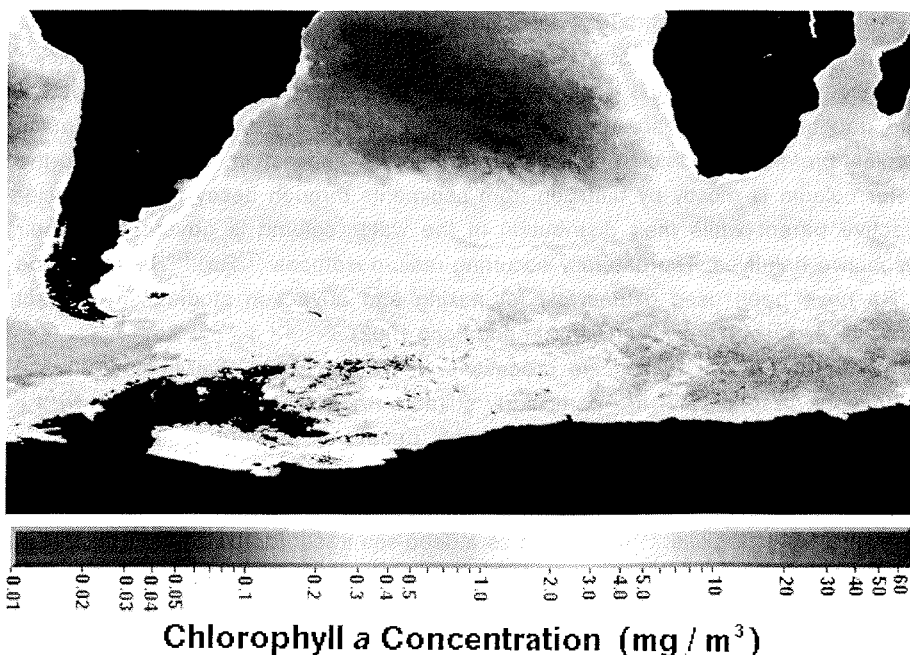


Fig. 1: Averaged distribution of chlorophyll a in the Atlantic sector of the Southern Ocean in 1998 as seen from SeaWiFS. The extremely high concentrations close to the Antarctic continent in the Weddell Sea are probably artefacts caused by cloud cover, ice and light conditions.

The idea that iron might represent an essential micronutrient, today often referred to as the "iron-hypothesis", was first published by Gran (1931), based on observations in coastal waters off Norway (p. 41): "...*indicating that the conditions for a rich growth are satisfied only by a mixture of waters of different origin. The Atlantic water certainly contains enough of nitrates and phosphates, while the coastal (or polar) water may bring either living cells or some stimulating stuff coming from land and lacking in oceanic water.* (...) These considerations gave me the idea that the rich productivity of the coastal waters might be explained by iron-containing humus-compounds drained out from land. (...) If the productivity of the coastal waters is dependent on any factor of a chemical nature acting as a minimum factor, it must be an element which in its circulation does not follow the nitrates and phosphates accumulating in solution in the deep sea and reaching the surface again by vertical circulation of any kind. If such minimum stuffs exist, they must irreversibly go out of circulation in the sea, so that they can only be renewed from land."

Since then, many investigators have tested this concept in the so-called High Nutrient Low Chlorophyll (HNLC) regions, i.e. areas with a sharp contrast in the availability of macronutrients and primary production. Apart from the ice-free Southern Ocean, major open ocean HNLC regimes have been described in both the subarctic and the equatorial eastern Pacific. In recent years, the Southern Ocean has been the focus of many of these investigations as it is believed to have the greatest potential in affecting atmospheric CO₂ concentrations (Sarmiento et al. 1991, Orr et al. in press).

In the contemporary Southern Ocean, iron has a direct influence on the occurrence of intensive plankton blooms along the Polar Front (de Baar et al. 1995), where spring blooms lead to biomass production an order of magnitude higher than in the waters of the southern ACC. In situ fertilization experiments have been conducted south of Tasmania (SOIREE; Abraham et al. 2000, Boyd et al. 2000) and south of Africa (EISENEX; Smetacek et al. 2001) along the respective locations of the Polar Front and confirmed the relationship between iron and primary productivity.

While research programs continue to test the strength of the iron hypothesis, the industrial community hopes to fulfill a part of their Kyoto promises by carbon credits. Ocean fertilization is considered to be one possible way of mitigating man's influence on the climate system, and hitherto purely scientific experiments are being discussed in relation to their applicability. Patents for ocean fertilization have already been issued (e.g. Howard and O'Brien 1999, Markels 2000) and studies are carried out to model large-scale fertilization (Ormerod and Angel 1998). With this as a backdrop, even small-scale scientific experiments should be seen in a different light as they have added a new aspect to climate research and discussion and are about to become a political driving force.

1.2 Transport mechanisms for iron into the Atlantic sector of the Southern Ocean

In view of the many interactions of iron with phytoplankton and its feed-back mechanisms on the climate system, it seems crucial to know more about its natural possible transport paths into the open ocean. Only then can assumptions about e.g. the drop in CO₂ during the last glacial, caused by increased dust-derived iron input be validated (Martin 1990, Sarmiento et al. 1991).

Yet little is known about how the micronutrient iron reaches the productive regions of the Southern Ocean today. Four main transport mechanisms have been proposed for the Atlantic sector (de Baar et al. 1995, Löscher et al. 1997; de Baar and de Jong 2001, Hegner et al. in prep.): upwelling of deep water, input by ice-raftered debris released from melting icebergs, aeolian input of continental detritus from the Antarctic Peninsula and southern South America and shelfwater inputs from their respective shelf areas (Fig. 2). The Argentinean and Antarctic continental shelf areas represent important sources where iron is set free into the overlying water column during diagenetic processes in the shelf sediments (Westerlund and Öhman 1991). However, the relative or regional importance of the respective input mechanisms is still a matter of debate. The need for a better understanding of processes supplying bio-available iron to the euphotic zone was clearly recognized during a round table session at the Southern Ocean JGOFS (Joint Global Ocean Flux Studies) Symposium held in Brest, 8-12th July 2000.

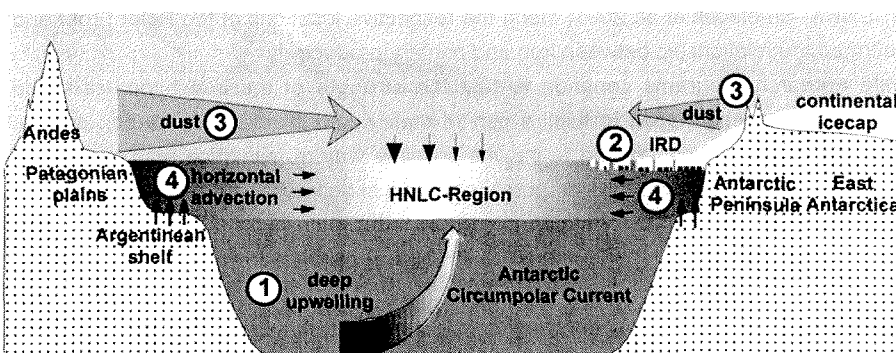


Fig. 2: Schematic view through the Drake Passage towards the east along the Antarctic Circumpolar Current, illustrating the main transport routes and mechanisms for iron into the productive regions of the Atlantic sector of the Southern Ocean: (1) upwelling of deep water; (2) input of shelfwater; (3) aeolian input; (4) input from ice-raftered debris released by melting icebergs. HNLC: High Nutrient Low Chlorophyll.

The iron transport paths can be investigated by means of different geochemical tracers: aluminium and the isotopic composition of neodymium reveal information about terrigenous input - either by dust or by ice-raftered debris (Duce and Tindale 1991, Grousset et al. 1992, Hegner et al. in prep.), ^{227}Ac has been suggested as a tracer for upwelling of deep water (Geibert 2001) and ^{228}Ra will be applied in the present study to investigate the role of shelfwater advection.

1.3 Objectives

Aim of this study is to provide an improved understanding of the sources, distribution and behaviour of the naturally occurring radionuclides ^{226}Ra (half-life 1600 years) and ^{228}Ra (half-life 5.75 years) in the Atlantic sector of the Southern Ocean.

As ^{226}Ra is the most abundant of the radium isotopes in open ocean waters, it is best suited to study the biogeochemistry of radium in the marine environment, i.e. its behaviour as a biointermediate element. Based on the similarities of vertical ^{226}Ra and Si water profiles, radium has often been suggested to take part in the marine Si cycle (e.g. Ku et al. 1970, Ku and Lin 1976).

The questions addressed in this study with respect to ^{226}Ra are:

- What is the relationship between ^{226}Ra and Si in circumpolar waters?
- Which are the processes that control the behaviour of ^{226}Ra as a bio-intermediate element in the water column?

In the context of iron as a growth-limiting factor for phytoplankton in the open South Atlantic, the suitability and strength of ^{228}Ra is tested here as a tracer for advection of shelfwater. To this end, the following questions need to be settled:

- How can ^{228}Ra be measured at extremely low activities and what techniques of sample collection and processing are required?
- What is the distribution of ^{228}Ra in shallow water regions, i.e. its potential source regions, and in the open ocean?

With the objective to answer the main question:

- Which are the main transport mechanisms for shelfwater to reach the open ocean?

In order to obtain a better understanding of the biogeochemistry of radium in the Southern Ocean, a high resolution sampling is performed. As far as sampling strategy is concerned, the main focus is put on ^{228}Ra and its potential to identify shelfwater masses in the open South Atlantic. It was tried to coordinate the sample collection for ^{228}Ra and geochemical tracers for other iron transport paths in order to get a good comparability of the different processes at work.

Effort is also put on the identification of anthropogenic radium sources that could complicate especially the use of ^{228}Ra as a natural tracer for shelfwater advection.

Introduction

The present work has been funded by DFG-project Ru 712/1-3. The investigations are thematically associated with and have been carried out within the framework of CARUSO (Carbon Uptake in the Southern Ocean), a European Community-funded project investigating the processes that are "*regulating the photosynthetic CO₂ fixation of large diatoms and carbon export into deeper Antarctic waters*".

2 HYDROGRAPHY OF THE SAMPLING AREA

The relationship between the sampling locations and the hydrographic regime of the Atlantic sector of the Southern Ocean is the base for the data interpretation in the chapters to follow. The general circulation, special oceanographic features and water mass properties of the sampling area will be presented. Special emphasis is put on the hydrographic situation in the Argentine Basin and south of Africa. Both regions are strongly influenced by the western boundary currents of the subtropical Atlantic and Indian Ocean gyres. It will be shown that physical structures, iron concentration and productivity in the ocean can be related to each other and what hydrographical features exist for the eastward transport of the above-mentioned trace elements.

2.1 General features of the Southern Ocean

Strictly speaking, the Southern Ocean is not an ocean by itself but comprises the southern extensions, i.e. the areas south of approximately 40° S of the Pacific, the Indian and the Atlantic Ocean. Commonly, its northern limit is set at the Subtropical Front line (see chapter 2.2.1) where the permanent thermocline reaches the surface (Tomczak and Godfrey 1994). The Southern Ocean is dominated by the Antarctic Circumpolar Current (ACC), a strong zonal easterly water flow that is mainly driven by the prevailing Westerlies between 40/42° and 70/72° S (Iriondo 2000). The ACC links the three major oceans and isolates the continent Antarctica from subtropical influence, keeping it at freezing temperatures throughout the year. Close to the Antarctic continent, prevailing Easterlies drive the narrow Coastal Current (CC) in the opposite direction.

One of the prevalent characteristics of the ACC are oceanic fronts (Fig. 3) - areas that in a conventional view have simply been regarded as boundaries between water masses that lead to a zonation of the Southern Ocean. Today it is accepted that the nature of these fronts is highly dynamic, involving steep meridional density gradients that lead to high geostrophic velocities. While speeds within in the ACC are rather sluggish, they can exceed 50 cm/s (Strass and Langreder 2000) within restricted bands along the fronts, the so-called frontal jets. The fronts are also known for the frequent formation of meanders and eddies (Veth et al. 1997) which contribute to the meridional exchange of energy and nutrients. The frontal characteristics and the eastward flow of the ACC can be tracked over the whole water column down to the seafloor. Hence, islands and bottom topography have an impact on its eastward flow and are responsible for deviations of the current, convergence of the fronts and areas of intensive meandering.

Hydrography of the sampling area

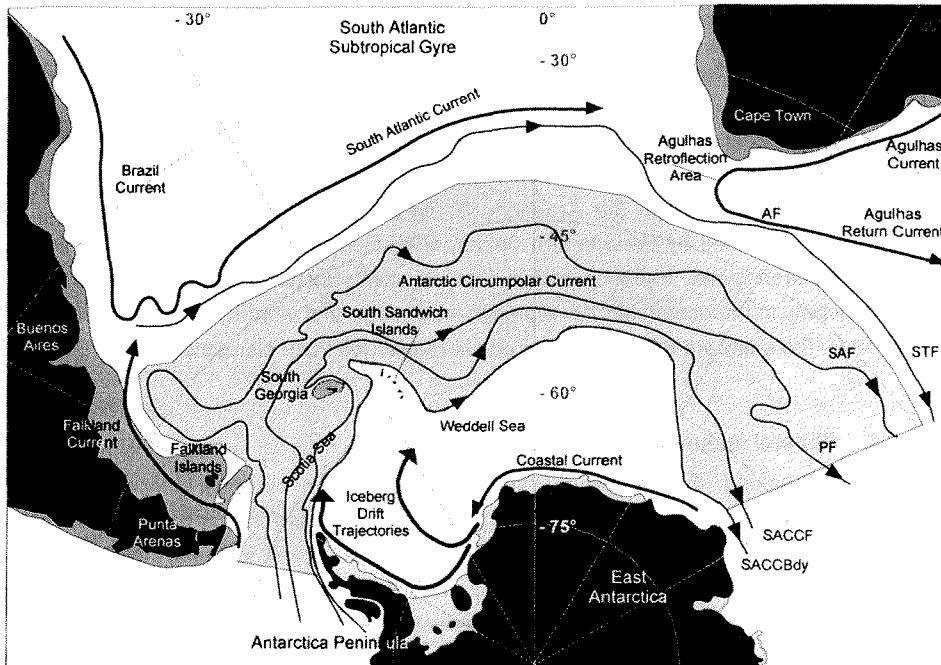


Fig. 3: Atlantic sector of the Southern Ocean. Currents, oceanographic fronts and extent of the Antarctic Circumpolar Current (shaded area) after Peterson and Stramma (1991) and Orsi et al. (1995), iceberg trajectories after Tchernia and Jeannin (1984) and Drinkwater et al. (1999). STF: Subtropical Front; SAF: Subantarctic Front; PF: Polar Front; SACCF: Southern ACC Front; SACCbdy: Southern ACC Boundary.

2.2 Circulation within the South Atlantic

The circulation in the South Atlantic from north to south is broadly as follows (Fig. 3): The South Atlantic Subtropical Gyre covers the region from equatorial to subtropical latitudes and is delineated at its southwestern end by the Brazil Current and the South Atlantic Current. In the region south of Africa, the Agulhas Current is responsible for a leakage of Indian Ocean water masses to the Atlantic Ocean. As part of the Indian Ocean Subtropical Gyre, it is one of the major western boundary currents of the southern hemisphere and enters the Atlantic south of Africa. The source waters of the Agulhas Current are believed to be derived from east of Madagascar and from the Mozambique Channel between Madagascar and Africa (van Leeuwen et al. 2000). A recirculation in a Southwest Indian Ocean subgyre has equally been suggested (Lutjeharms 1996). The Agulhas Current follows tightly the narrow continental shelf and can be found as close as 30 km of the shelf break (Park et al. 2001). It turns eastwards between 20 and 15° E and flows back into the Indian Ocean along about 40° S as the Agulhas Return Current (Fig. 3). This so-called Agulhas Retroflection Area is characterized by extreme mesoscale variability (Lutjeharms 1996).

Hydrography of the sampling area

South of the subtropical gyres lies the broad band of the ACC that encircles the Antarctic continent. Between the ACC and the Antarctic coastline in the Weddell Sea, a cyclonic gyre stretches along a SW-NE-trending axis from the Antarctic Peninsula to 30° E (Schröder and Fahrbach 1999). Park et al. (2001) shift its eastern termination to at least 53° E in the Enderby Basin. At 50° W, the clockwise circulation of the Weddell Gyre joins with waters entering the South Atlantic through the Drake Passage at the Weddell-Scotia-Confluence (WSC; Gordon 1967). The Southern ACC Boundary forms the northern boundary of this Weddell Gyre. At 25° E, the boundary of the Weddell Gyre and the Southern ACC Front converge and form a zone of mesoscale variability (Orsi et al. 1993). Both warm and cold core eddies are shed and move mainly southwestwards (Gouretski and Danilov 1993, Schröder and Fahrbach 1999).

Icebergs that calve from East Antarctica drift westwards in a narrow band close to the coast, driven by the wind and the CC.

They enter the ACC over the South Scotia Ridge along the WSC. Some icebergs have also been observed to move northward in a more narrow loop at approximately 40° W (Tchernia and Jeannin 1984, Drinkwater et al. 1999). Sediment-laden icebergs have been suggested as a possible carrier of iron into the productive regions of the ACC, but were dismissed as a major pathway (Löscher et al. 1997, Smetacek et al. 1997).

2.2.1 *Frontal systems in the South Atlantic*

Taking the Greenwich Meridian as a reference line, four deep-reaching fronts can be depicted of which three are located within the ACC (Whitworth and Nowlin 1987).

Although most of the fronts might be identified by sea surface temperatures alone (Lutjeharms and Valentine 1984), seasonality and air-sea interaction can disguise their true location and extent. Temperature inversions adjacent to mean thermal gradient are a dominant feature of the oceanic fronts, giving sea surface temperature curves often a z-shaped appearance when plotted against latitude (Lutjeharms and Valentine 1984). A more robust positioning of the fronts can be based on subsurface observations including temperature, salinity, and oxygen concentrations. The following paragraphs give a general description of the fronts and their hydrographic properties are summarized in Table 1, based on the definitions given by Orsi et al. (1995).

Subtropical Front

The Subtropical Front (STF) separates the subtropical from the circumpolar regime further south and delineates the northernmost extent of Subantarctic Surface Water (SASW) that is getting subducted underneath the Subtropical Surface Water (STS; Fig. 6). The landmass of South America interrupts the circumpolar flow of the STF, underlining the fact that this front is not part of the ACC proper. As the temperature distribution is more affected by seasonality, the salinity field proves to be more reliable for the detection of the STF (Deacon 1982).

Hydrography of the sampling area

South of South Africa, the STF is part of a wider, highly variable zone that is known for intensive eddy shedding, probably caused by interference with the Agulhas Return Current and influenced by bottom topography (Lutjeharms 1985, Lutjeharms 1999).

Subantarctic Front

The Subantarctic Front (SAF) is characterized by the northward sinking of the Antarctic Intermediate Water (AAIW) which involves the development of a salinity minimum at subsurface levels (Fig. 6). Intensive eddy shedding has been reported for the SAF (Lutjeharms 1985, Ansorge 1999, Park et al. 2001). Waters south of the SAF have been associated with a maximum in chlorophyll a (Allanson et al. 1981).

Table 1: Parameters used for the identification of the oceanic fronts, compiled after Orsi et al. (1995).

Front	Property	Reference depth z (m)	Direction
Subtropical Front	$12^{\circ}\text{C} > T > 10^{\circ}\text{C}$	100	
	$35.0 > S > 34.6$	100	
Subantarctic Front	$S < 34.20$	< 300	southward
	$\theta > 4-5^{\circ}\text{C}$	400	northward
	$O_2 > 7 \text{ ml/l}$	< 200	southward
Polar Front	$\theta < 2^{\circ}\text{C}$ along the θ -minimum	< 200	southward
	θ -minimum	> 200	northward
	$\theta > 2.2^{\circ}\text{C}$ along the θ -maximum	> 800	northward
Southern ACC Front	$\theta > 1.8^{\circ}\text{C}$ along the θ -maximum	> 500	northward
	$\theta < 0^{\circ}\text{C}$ along the θ -minimum	< 150	southward
	$S > 34.73$ along the S -maximum	> 800	northward
	$O_2 < 4.2 \text{ ml/l}$ along the O_2 -minimum	> 500	southward
Southern ACC Boundary	$\theta > 1.5^{\circ}\text{C}$	200	northward
	$S > 34.5$	200	northward

Polar Front

At the Polar Front (PF), Antarctic Surface Water (AASW) gets subducted underneath the SASW and spreads northwards (Naveira Garabato et al. 2001). It is the temperature field of the AASW that defines the position of the PF. The dominant features of the PF are the steep rise of the isotherms and the strong meandering of the jet stream with associated eddy generation (Veth et al. 1997, Ansorge and Lutjeharms 1999, Strass et al. 1999). Increased phytoplankton biomass has been repeatedly reported for the PF (Allanson et al. 1981, Lutjeharms et al. 1985, Bathmann et al. 2000, Strass et al. subm.), a relationship between physical phenomena, increased dissolved iron concentrations and the distribution of chlorophyll a has been described by de Baar et al. (1995), Bathmann et al. (1997), Smetacek et al. (1997) and Strass et al. (subm.). The PF has also been identified as an important foraging ground for higher trophic levels of the Antarctic food-chain (van Franeker 1999).

Southern ACC Front

The third distinctive front within the ACC as evidenced by the density field is the Southern ACC Front (SACCF). In contrast to the SAF and PF, it does not separate different surface water masses as the AASW stretches southward from the PF all the way to the continental zone. The location of the SACCF is determined by the southward extent of the 1.8°C-isotherm of the upwelling Upper Circumpolar Deep Water (UCDW). Topographic features influence the path of the SACCF.

Southern ACC Boundary (Weddell Front)

Orsi et al. (1995) define the poleward limit of the ACC with the southern edge of the shoaling UCDW. This location coincides with a change in geostrophic shear between the circumpolar and the subpolar regime, giving the boundary a frontal feature. In the Scotia Sea, the SACCF and the Southern ACC Boundary are found close to each other. At 25° E, both fronts converge again due to the wedge-shaped structure of the South Indian Ridge (Fig. 3 and Fig. 4). Tynan (1998) has pointed out the ecological importance of the Southern ACC Boundary as a foraging ground for whales.

Frontal systems south of Africa

South of Africa, the retroflection of the Agulhas Current creates a fifth front, the Agulhas Front (AF; Lutjeharms et al. 1981). It separates the incoming warm and saline subtropical Indian waters from the colder and fresher Atlantic waters (Lutjeharms and Valentine 1984; Gordon et al. 1987) and can often be depicted from sea surface temperatures. Occasionally, the southern edge of the Agulhas Return Current coincides with the STF further south, inducing a strong increase of the mean temperature and the frontal intensity. In general, the AF and the STF are clearly separated by about one degree of latitude with the AF showing the steepest thermal gradient of all the fronts present between Africa and Antarctica.

Strong eddy activity, generated by bottom topography is reported for the Agulhas Retroflection Area (Cheney et al. 1983, Lutjeharms and van Ballegooyen 1984). Occlusion of the retroflecting loop regularly generates Agulhas rings that move northwestwards into the Atlantic. Perturbations in the flow of the Agulhas Current lead to the spawning of both cyclonic and anticyclonic eddies (Lutjeharms 1996, Boebel et al. 2001).

Frontal systems in the Drake Passage and the Scotia Sea

The Drake Passage and the Scotia Sea represent a crucial region for the flow of the ACC with respect to the objectives of this work and will therefore be described in more detail.

The Drake Passage separates South America from the Antarctic Peninsula, the northernmost extension of West-Antarctica. The eastern side of South America is bordered by the broad Argentinean shelf with water depths of approximately 200 m. The shelf areas that surround the Antarctic Peninsula have less extension and

Hydrography of the sampling area

generally greater water depths. Water depths within the Drake Passage exceed 3000 m in most places. Further east, the North Scotia Ridge, the islands of South Georgia, the South Sandwich Arc and the South Scotia Ridge form a U-shaped barrier of reduced water depths enclosing the Scotia Sea (Fig. 4).

The hydrography and the location of the oceanic fronts between South America and Antarctica are clearly controlled by the topography. When passing through the narrow gap of the Drake Passage, the ACC is squeezed and, by consequence, accelerates considerably. It then encounters the obstacle of the South Scotia Ridge/South Sandwich Arc and gets deflected to the north to perform a sharp loop east of South America with strong meandering between the Falklands and South Georgia (Peterson and Stramma 1991). The SAF and PF pass between both island groups and are found close to each other between 38° and 40° W. At times, they merge to form a single, powerful jet with surface velocities exceeding 80 cm/s (Peterson and Whitworth 1989). The detrainment of subpolar water is known as being associated with the Falkland Current which forms a confluence zone with the opposing flowing Brazil Current (Fig. 3; Peterson 1992). The confluence of subtropical and subantarctic waters causes turbulent mixing and the generation of eddies (Fig. 5; Peterson and Stramma 1991).

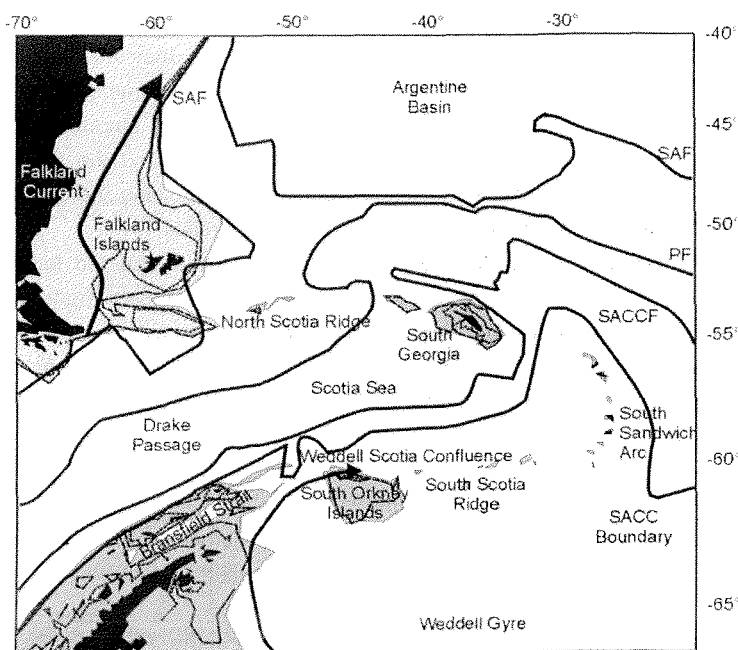


Fig. 4: Location of the oceanic fronts in the Scotia Sea (after Orsi et al. 1993, Arhan et al. 1999). Shaded areas indicate regions shallower than 1000 m. The 500 m (dashed) and 200 m (dotted) isobaths are given as well.

Hydrography of the sampling area

At the Drake Passage itself, three deep-reaching fronts (SAF, PF and SACC) can be depicted from vertical sections within the ACC. In contrast to the region south of Africa, the fronts lie adjacent to each other and especially the SACC and the Southern ACC Boundary can be found as close as 50 km apart (Fig. 4; Orsi et al. 1995). The UCDW is reported to extend regionally over the continental slope up to a depth of 1500 m (Sievers and Nowlin 1988). The Bransfield Strait, an island-bordered passage on the Pacific side of the Antarctic Peninsula, is the source area of cold subsurface waters, the so-called continental slope water (Orsi et al. 1993). On the Atlantic side of the Peninsula, cold waters from the cyclonic Weddell Gyre join the relatively warmer waters passing through the Drake Passage in the Weddell-Scotia-Confluence (Gordon 1967). The admixture of fresher water, which results from ice melting on the continental shelves or downstream of the Antarctic Peninsula is traceable as far as 40° E (Orsi et al. 1993).

Interaction of the ACC and its deep-reaching oceanic fronts with the slope sediments of South America and the subantarctic islands bordering the Scotia Sea as well as the proximity of the Southern ACC Boundary to the Antarctic Peninsula provide favourable conditions for an eastward advection of iron and ^{228}Ra with the ACC into the open South Atlantic.

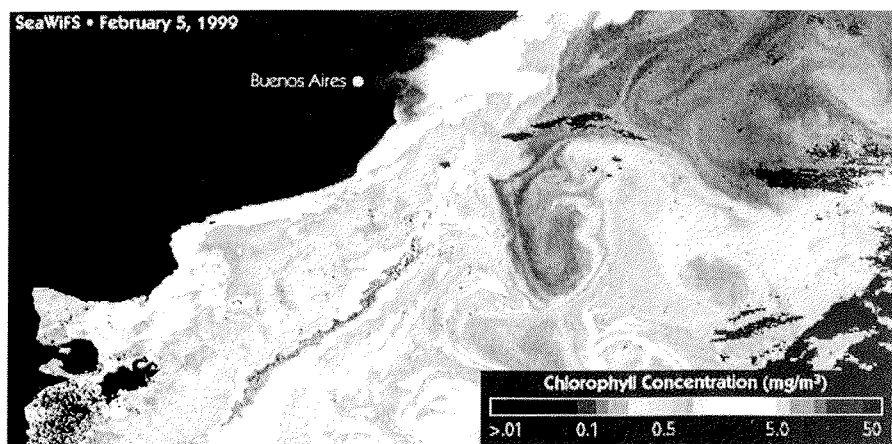


Fig. 5: SeaWiFS image taken on 5.2.1999 offshore of the coast of Argentina. It shows the turbulent region of the confluence of the Brazil/Falkland Currents. The long, narrow band of high productivity stretching parallel to the coast marks the convergence zone between the two currents. Eddy formation is visible east of it.

Hydrography of the sampling area

2.2.2 Water masses of the Atlantic sector of the Southern Ocean

The meridional circulation in the South Atlantic is strongly affected by the formation of downwelling bottom water that must be replaced in other places by waters rising to subsurface levels. Circumpolar Deep Water (CDW) will be presented first because the main water masses in the circumpolar and subpolar regimes are modifications of this water mass. Averaged water mass properties in this section are taken from Orsi et al. (1993, 1995). An overview of water mass circulation on a N-S-transect across the Atlantic sector of the Southern Ocean is given in Fig. 6.

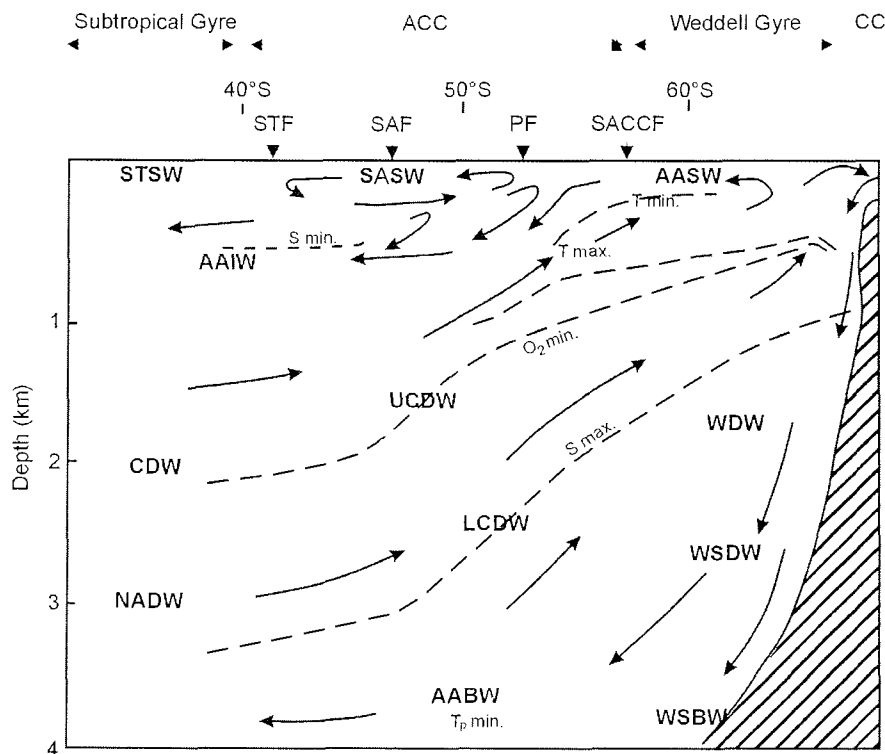


Fig. 6: Schematic representation of oceanic fronts and water masses on a N-S-section in the Atlantic sector of the Southern Ocean (modified after Gordon 1967). ACC: Antarctic Circumpolar Current; CC: Coastal Current; STF: Subtropical Front; SAF: Subantarctic Front; SACC: Southern ACC Front; STSW: Subtropical Surface Water; SASW: Subantarctic Surface Water; AASW: Antarctic Surface Water; AAIW: Antarctic Intermediate Water; U/L CDW: Upper/Lower Circumpolar Deep Water; NADW: North Atlantic Deep Water; WDW: Warm Deep Water; WSDW: Weddell Sea Deep Water; WSBW: Weddell Sea Bottom Water; AABW: Antarctic Bottom Water.

Hydrography of the sampling area

Circumpolar Deep Water

The main water body of the ACC is build up from Circumpolar Deep Water (CDW). It originates from the west Indian Ocean and southeast Pacific (Callahan 1972, Warren 1981). In the Atlantic, further input comes from North Atlantic Deep Water (NADW), a water body sandwiched between the Antarctic Bottom Water (AABW) below and the AAIW above. This relatively warm, saline, oxygen-rich and nutrient-poor water enters the ACC from the north and rises from below 2000 m depth at the STF to less than 200 m at the Southern ACC Boundary. The injection of NADW leads to a further distinction between UCDW and Lower CDW (LCDW; Gordon et al. 1977). UCDW is characterized by an oxygen minimum ($O_2 = 4-5 \text{ ml/l}$) resulting from remineralisation of organic material. Accordingly, the water is rich in nutrients. LCDW has lower nutrient levels and a distinctive salinity maximum ($S > 34.7$), inherited from the admixture of NADW. This water can mix with shelfwaters along the Antarctic continental shelves to form the dense deep and bottom waters that will spread northwards again (Foster and Carmack 1976). Hence, the CDW is subject to permanent alteration during its southward rise. The region of the rising of CDW to subsurface levels has often been described as Antarctic Divergence, a term alluding to the upwelling induced by Ekman pumping. Part of the rising CDW is deflected northwards and stays at the surface as AASW.

Surface and subsurface waters

STS is found north of the STF. SASW covers the area between the STF and the PF. AASW stretches from the continental shelf of Antarctica northward to the PF with relatively uniform properties. It is low in salinity ($S < 34.4$) due to ice melting in summer and precipitation but extremely cold, reaching freezing temperatures in winter (-1.9°C). Owing to its low temperature, AASW is denser than SASW and sinks to greater depths in the subantarctic zone, contributing to the formation of AAIW. The high oxygen content of the AAIW is an imprint of the equilibration between AASW and the atmosphere. The signature of the AAIW is modified by mixing processes with the underlying CDW. South of the PF, cores of Winter Water (WW) persist throughout the austral summer at subsurface levels below the mixed layer as a remnant of sea ice formation during winter.

Bottom water formation

Major bottom water formation occurs in the waters around Antarctica, thereby contributing to the global thermohaline circulation in the world's oceans. In winter time, the surface water is cooled down to freezing temperatures of -1.9°C and gets enriched in salt by ice formation. Intensive mixing and heat loss in both coastal and open ocean polynyas create bodies of dense water that sink to form AABW or, in the Weddell Sea, Weddell Sea Deep Water (WSDW). AABW will ultimately circulate northwards into the three major ocean basins.

Hydrography of the sampling area

Water masses within the Weddell Gyre

Warm Deep Water (WDW) is the main intermediate water mass of the Weddell Gyre. The WDW is derived mainly from LCDW, which enters the Weddell Gyre at its eastern limb in the Enderby Basin. At the submarine elevation of Maud Rise (64° S / 0° E), the inflow splits into a northward and a southwestward facing branch that feed the eastern and the western (also called central) gyre, respectively (Orsi et al. 1993). Modifications due to loss of heat to the atmosphere and ice melting or precipitation lead to the formation of cold, but fresher AASW that constitutes the upper 200 m of the water column. During sea ice formation in the cold season, saline waters sink down the continental slopes to form Weddell Sea Bottom Water (WSBW). Undercooled, but relatively fresh Ice Shelf Water (ISW) forms underneath the Filchner-Ronne and Larsen Shelf Ice (Weppernig et al. 1996). Mixing with the less dense WDW alters the properties and creates WSDW. It is this water mass that forms the major source of AABW. All water masses within the Weddell Gyre are less saline as well as colder than their common source CDW.

3 RADIUM IN THE MARINE ENVIRONMENT

The analysis of radium as well as the subsequent interpretation of the results obtained are related to its chemical properties and its behaviour and distribution in sea water. The physical and (geo-) chemical properties of radium as a radioactive element will be presented. It will be shown that the distribution of an unstable nuclide in sea water is dependent on the half-lives and geochemical behaviour of the mother-daughter pair (e.g. $^{232}\text{Th} - ^{228}\text{Ra}$) it belongs to. ^{228}Th is introduced as the grand-daughter of ^{228}Ra that is sometimes used as an indicator of the ^{228}Ra activity. The distribution of ^{226}Ra and ^{228}Ra in the marine environment is laid out and existing data of ^{228}Ra and ^{228}Th in the Southern Ocean are compiled.

3.1 Physical and chemical properties

Radium (from latin *radius*, "ray") was discovered in 1898 by Marie and Pierre Curie. They separated the highly radioactive substance from the uranium ore pitchblende and precipitated it as $\text{Ba}(\text{Ra})\text{SO}_4$. Succeeding steps of fractional crystallization led to a high degree of radium enrichment. In 1911, Marie Curie and André Debierne achieved the preparation of pure radium by means of electrolytic separation from RaCl_2 with a mercury cathode.

Radium belongs to the alkaline earth group and has an atomic mass of 226.0254 (physical determination; IUPAC 1999) and a chemical valence of +2. The ionization potential of 5.28 eV is the lowest of the alkaline earths. The density of radium is 5.5 g/cm³, melting and boiling point lie at 700° and 1140° C, respectively (Lide 1995). Due to its high electropositive character, radium tends to form strong ionic bonds and oxidizes immediately when exposed to air. Further compounds are known with halogens, carbon, nitrogen, sulfur, selenium and tellurium. $\text{Ra}(\text{OH})_2$ is a strong base. $\text{Ra}(\text{NO}_3)_2$ is soluble in water and RaCO_3 in acids while RaSO_4 is virtually insoluble. Under oxidizing conditions in sea water, the stable dissolved valence of radium is Ra^{2+} (Gmelin 1997).

Because of their position underneath each other in the periodic table, the chemical properties of radium resemble those of barium (atomic numbers 88 and 56, respectively). As will be shown in chapters 3.2 and 4.3.4, these similarities are used for the investigation of marine processes as well as for the analysis of radium. The concentration of radium in natural waters is normally below the threshold for a direct precipitation of RaSO_4 , but in the presence of sufficient Ba^{2+} , Ca^{2+} or Sr^{2+} , radium will be coprecipitated with these ions (Gmelin 1997). Barium in contrast may precipitate in the water column and barite particles are ubiquitous in sea water (Bishop 1988; see chapter 6.1). Both barium and radium are classified as „biointermediate“ elements, indicating that they participate in the biological cycle (Chow and Goldberg 1960, Dehairs et al. 1980, Bishop 1988, Moore and Dymond 1991), but are only partially depleted in surface waters. For barium, depletion can reach as much as 70% compared to deeper waters (Broecker and Peng 1982). Approximately the same value

holds for ^{226}Ra in the Pacific Ocean while the Atlantic Ocean yields a surface to deep water ratio of 0.5 (Broecker et al. 1967).

Four isotopes of radium occur naturally (see Appendix A 6):

Isotope	decays with half-life	by
^{228}Ra	half-life 5.75 years	β -decay
^{226}Ra	half-life 1600 years	α -decay
^{224}Ra	half-life 3.7 days	α -decay
^{223}Ra	half-life 11.4 days	α -decay

While the current knowledge about the general behaviour of radium in the marine environment is largely derived from ^{226}Ra , all four naturally occurring radium isotopes find specific applications according to their half-lives in the study of processes on local, regional or global scales (Elsinger et al. 1982, Elsinger and Moore 1983, Bollinger and Moore 1984, Levy and Moore 1985, Rama et al. 1987, Moore and Astwood 1990, Moore and Todd 1993, Moore and Arnold 1996, Torgensen et al. 1996, Moore 1997, Hancock et al. 2000, Moore 2000; for ^{228}Ra and ^{226}Ra see below). The focus in this study is to provide a better understanding of the distribution and biogeochemistry of ^{228}Ra and ^{226}Ra in the Southern Ocean. In the special context of iron transport mechanisms, ^{228}Ra seems to be a promising tracer to study shelfwater advection into the open South Atlantic.

3.2 Geochemical behaviour of radium

The nuclides of the naturally occurring decay chains (see Appendix A 6) can be grouped into rather adsorption-prone and more soluble elements. The former ones are removed rapidly out of the water column by sinking particles, a process referred to as "scavenging", and accumulate in sea sediments while the latter ones will tend to stay in solution. The different hydrochemical behaviour of a given mother-daughter pair of radionuclides in combination with the vast range of half-lives make the natural decay chains a powerful tool in ocean geochemistry.

Both ^{228}Ra and ^{226}Ra belong to the rather soluble nuclides but have a strongly particle reactive progenitor (^{232}Th and ^{230}Th , respectively). Generally speaking, thorium isotopes get enriched in sediments while radium tends to stay in solution or, if produced through decay in the sediment, escapes back into the water column. The specific distribution of both ^{228}Ra and ^{226}Ra in the water column depends on their respective half-lives as well as the distribution of their parent nuclides in the sediments.

The total amount of radium in the world's oceans is estimated to be 92.5 t (Brown et al. 1989), of which the overwhelming majority consists of ^{226}Ra . Concentrations of naturally occurring radionuclides are normally reported in disintegrations per minute (dpm), normalized to volume or mass. In older publications, ^{226}Ra concentrations are

often given in mol or g (^{226}Ra). The conversion into dpm is done according to the following equations.

$$\frac{\text{dpm}}{100\text{kg}} = 0.204 \times 10^{-16} \frac{\text{mol}}{\text{kg}}$$

$$\frac{\text{dpm}}{100\text{kg}} = 0.461 \times 10^{-14} \frac{\text{g}}{\text{kg}}$$

Note that these specific equations only hold for ^{226}Ra . The general formula of the relationship between activity and concentration of a radionuclide is given in Appendix A 5.

After its discovery in 1898, only ten years had to pass before radium attracted the attention of marine scientists. The first investigations on the marine behaviour of radium were based on ^{226}Ra . It was found that deep sea sediments had higher ^{226}Ra activities than nearshore sediments (Joly 1908). Evans et al. (1938) brought evidence for an increase of ^{226}Ra with depth in water profiles from the Pacific. The development of analytical methods for ^{230}Th proved the source of ^{226}Ra to be in deep sea sediments caused by the removal of ^{230}Th out of the water column by adsorptive processes and subsequent decay to ^{226}Ra . Supportive evidence for this source came from calculations on the riverine input of ^{226}Ra into the oceans that could, in the case of the Atlantic, account for only approximately 1% of the standing stock in near surface waters (Key et al. 1985). The migration of ^{226}Ra from sediments into the overlying water column is directly related to the ^{230}Th content at the sediment-water interface which in turn is a function of the sediment accumulation rate (Francois et al. 1990). Low fluxes have been observed in areas with high accumulation rates (Cochran 1980a). The depth of bioturbation is a further controlling factor for the ^{226}Ra flux. Between 60-70% of the ^{226}Ra produced from the excess¹ ^{230}Th in the sediment escape into the pore water (Cochran and Krishnaswami 1980). Cochran (1980a) reports a relationship between the ^{226}Ra activity in the topmost part of the sediment and its flux into the overlying water column. Geographic variations in the flux are matched by different activities in near-bottom waters.

Koczy (1958) suggested ^{226}Ra as a tracer to study ocean circulation. It seemed ideal due to a half-life in the order of the overturning rate of the world's oceans. Intensive

¹ „Excess“ refers to the activity of a radionuclide that exceeds the activity which would be expected from the radioactive equilibrium between a parent nuclide and one of its shorter-lived descendants. In this example: the ^{234}U content in the sediment maintains a certain ^{230}Th activity. Anything measured that goes beyond this is called excess ^{230}Th . The excess activity is adsorbed on the particles. Diffusion into the pore water is easier for ^{226}Ra produced from adsorbed ^{230}Th than from ^{230}Th bound in the crystal lattice.

efforts to map the distribution of this isotope on a global scale were made during the GEOSECS (Geochemical Ocean Sections) program, a global survey performed between 1972 and 1978 for the investigation of the three-dimensional distribution of various oceanic tracers (Bainbridge 1971). Fig. 7 shows that, except for the Southern Ocean, ^{226}Ra surface activities are about the same in all oceans. The profiles increase constantly with depth with the strongest increase in the Pacific. In fact, the ^{226}Ra content of bottom water progressively increases from the North Atlantic through the Indian Ocean to the northeast Pacific. Here, a fourfold enrichment compared to Atlantic values was reported (Broecker et al. 1967, Chung and Craig 1973, Östlund et al. 1987). Yet it is unclear whether the higher values are the result of the ageing of the

water masses along the conveyor-belt within the oceans or due to a regionally higher ^{226}Ra flux from the sediment (Ku and Luo 1994).

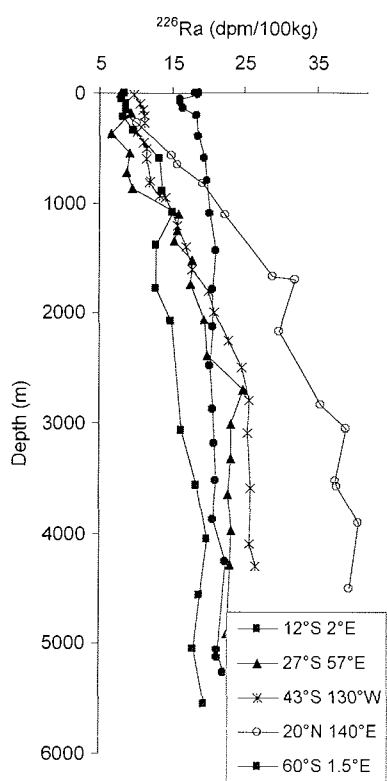


Fig. 7: Water column profiles of ^{226}Ra for the Atlantic (squares; Broecker et al. 1976), Indian (triangles; Chung 1987), Pacific (stars; Ku et al. 1980; open circles; Tsunogai and Harada 1980) and Southern Ocean (closed circles; Ku and Lin 1976).

To correct for the biogenic cycling component in the distribution of ^{226}Ra , Ba had been suggested as a useful stable analogue because of their nearly identical chemistries (Chow and Goldberg 1960, Chan et al. 1976). Various works (Chung 1974, Chan et al. 1976, Chung 1980, Cochran 1980b) have shown that except for the northeast Pacific region, ^{226}Ra and Ba correlate fairly well in the upper and intermediate water columns, best results are reported for circumpolar waters. However, this is not what would be expected from an unstable and a stable isotope with different source functions: While riverine input is negligible for ^{226}Ra , it constitutes a major source for Ba. Hence, the apparent linearity shows that vertical mixing must be fast compared to the decay rate of ^{226}Ra and that the cyclic component more or less obliterates the influx from bottom sediments.

However, problems remained as to the variability of the $^{226}\text{Ra/Ba}$ ratio during biogenic cycling on the one hand and the distinctive regional differences

concerning the strength of sedimentary ^{226}Ra source on the other. As a tracer for ocean circulation, ^{226}Ra got replaced by e.g. tritium (Dreisigacker and Roether 1978; Östlund 1982), chlorofluorocarbons (Gammon et al. 1982, Fogelquist 1985, Wallace et al. 1994), ^{14}C (Stuiver and Östlund 1980) or ^3He (Jenkins and Clarke 1976, Schlosser et al. 1995), but GEOSECS set the stage for a concise understanding of the distribution of ^{226}Ra in the ocean. Recently, a re-examination of the Indian GEOSECS data attested ^{226}Ra a quasi-conservative behaviour over much of the deep ocean, implying its restricted use as a tracer for large-scale ocean mixing in the deep sea (Ku and Luo 1994).

Based on the above observations, radium is grouped as a bio-intermediate element that is partially depleted in surface waters (Broecker and Peng 1982). While the particulate uptake of ^{226}Ra in surface water is apparent from vertical profiles, the (chemical) nature of the particles involved is not quite clear. ^{226}Ra data from this study will be examined in view of possible carrier phases in the southern circumpolar waters (see chapter 6.1).

For the deep East Atlantic, the regeneration of ^{226}Ra and Ba from calcareous shells has been suggested (Rhein et al. 1987) and disproved (Rhein and Schlitzer 1988). Szabo (1967) excluded carbonate particles as a ^{226}Ra carrier because their $^{226}\text{Ra}/\text{Ca}$ ratio does not match the respective difference in concentration between the deep ocean and surface waters. A comparison with vertical nutrient profiles has yielded close similarities between ^{226}Ra and Si (Szabo 1967). Hence, siliceous tests have been suggested as an effective carrier of radium into deeper water layers (Ku et al. 1970). Indeed, certain diatoms like *Chaetoceras* and *Rhizosolenia* are reported to concentrate ^{226}Ra (Shannon and Cherry 1971). Acantharians, a SrSO_4 -building group of organisms, are also ascribed a crucial role in the chemistry of both Ba and radium (Bernstein et al. 1998).

For ^{226}Ra and Si, Ku and Lin (1976) give a correlation of:

$$^{226}\text{Ra} (\text{dpm}/100\text{kg}) = 13 + 0.073 \times \text{Si} (\mu\text{m}/\text{kg})$$

which comprises all depths of circumpolar stations in the Atlantic and Pacific south of the Polar Front. A comparable correlation for the Weddell Sea subsurface waters is given by Chung and Applequist (1980):

$$^{226}\text{Ra} (\text{dpm}/100\text{kg}) = 13 + 0.06 \times \text{Si} (\mu\text{m}/\text{kg})$$

The originally published value for the slope of 0.0007 is most likely a misprint. Departures from a linear relationship between ^{226}Ra and Si have been reported by Chung (1980) and Ku et al. (1980) and results from this study indicate that these relationships do not hold for surface waters (see chapter 6.1).

3.3 Origin of ^{228}Ra in sea water

^{228}Ra is a transient decay product of the ^{232}Th decay chain with a half-life of 5.75 years. In older publications, a value of 6.7 years is reported - called Mesothorium 1 then - (Curie et al. 1931) that was later revised (Gmelin 1997).

In general, the repartitioning of ^{232}Th and ^{228}Ra in the ocean follows the systematics of the $^{230}\text{Th} - ^{226}\text{Ra}$ pair: the parent nuclide is mostly confined to the oceans' sediments while ^{228}Ra diffuses into the water column. ^{232}Th is a non-radiogenic isotope, hence is not produced in the water column but reaches the ocean with continental detritus, either through fluvial or aeolian input. Its distribution is therefore determined primarily by biogenic admixtures, just like in the case of e.g. Al. Data from Walter et al. (1997) show no dependence of the ^{232}Th content in the sediment with the depth of the overlying water column. In contrast to ^{226}Ra with a clear deep sea source, the distribution of ^{232}Th in combination with the half-life of ^{228}Ra leads to elevated activities of ^{228}Ra in shallow waters like shelf regions, reflecting the interaction of the sediment with the overlying water mass (Moore 1969a, Moore 1969b, Li et al. 1980). ^{228}Ra activities are highest in estuaries (Elsinger and Moore 1984), in water masses overlying fine-grained sediment and in regions with restricted water exchange (Moore 1987). In consequence, a water mass that has been in contact with such a ^{228}Ra source shows a decreasing signal of ^{228}Ra with increasing distance from the source due to radioactive decay and mixing (Fig. 8; Moore 1969b, Kaufman et al. 1973, Moore et al. 1980, Moore et al. 1986, Moore 1987, Rutgers van der Loeff et al. 1995). Its half-life of 5.75 years makes ^{228}Ra a suitable tracer for mesoscale oceanographic topics. ^{228}Ra decays to ^{228}Th , which in turn is a particle-reactive nuclide (half-life 1.91 years). Owing to the solubility of ^{228}Ra in sea water and the shorter half-life of ^{228}Th , the latter accumulates through ingrowth and can reach $^{228}\text{Th}/^{228}\text{Ra}$ activity ratios of up to 1.5 once the water mass has lost contact to the bottom-source of ^{228}Ra (Fig. 15; Moore 1969b). In specific cases, ^{228}Th can therefore be used as an analytically attractive analogue for ^{228}Ra (Li et al. 1980, Broecker and Peng 1982, Rutgers van der Loeff 1994). However, in waters rich in particles scavenging will lead to a depletion of ^{228}Th relative to ^{228}Ra (see chapters 5.3 and 6.2).

Techniques for the determination of ^{228}Ra were not as early available as for ^{226}Ra . Koczy et al. (1957) reported an excess of ^{228}Th relative to ^{232}Th in coastal waters, leading to a general interest in the ^{232}Th natural decay series. It was found that the high $^{228}\text{Th}/^{232}\text{Th}$ activity ratio in sea water was caused by an excess of ^{228}Ra relative to ^{232}Th (Koczy et al. 1957, Moore & Sackett 1964, Somayajulu and Goldberg 1966). First determinations of oceanic ^{228}Ra concentrations reported by Moore (1969a, 1969b) confirmed that nearshore waters show high activities of unsupported ^{228}Ra . Advection processes carry the ^{228}Ra signal into the open ocean and lead to measurable concentrations of ^{228}Ra in offshore surface waters. On a vertical scale, concentrations decrease at intermediate water depths below the limit of detection but show an increase towards the bottom. These findings pointed to diffusion from ^{232}Th -bearing

sediments as a source for ^{228}Ra instead of input by river water as it had formerly been suggested by Moore and Sackett (1964).

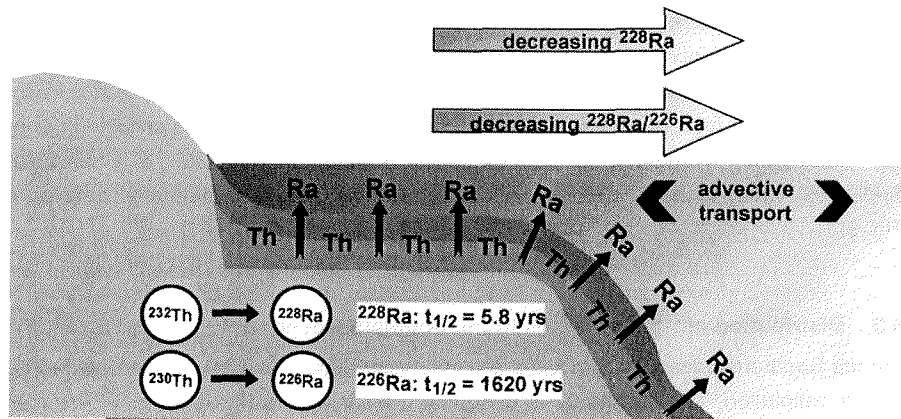


Fig. 8: Simplified process showing the diffusion of radium from thorium-bearing sediments into the overlying water column. High concentrations of ^{228}Ra are found especially in shallow water masses overlying fine-grained sediment.

Once its sources and geochemical properties in the water column were understood, ^{228}Ra became a useful natural tracer for a wealth of oceanic applications. Its half-life of 5.75 years makes it suitable for processes on a timescale between a few months and some decades. ^{228}Ra has been used as a tracer for ocean circulation (Kaufman et al. 1973, Reid et al. 1979, Moore et al. 1986, Moore 1987, Rhein et al. 1987, Rutgers van der Loeff et al. 1995, Turekian et al. 1996, Nozaki et al. 1998), mixing processes between different water bodies (Moore 1972, Sakanoue et al. 1980, Moore et al. 1986, Moore and Todd 1993, Moise et al. 2000) and vertical mixing in the deep ocean (Moore and Santschi 1986), nutrient budgets (Ku et al. 1995, Nozaki and Yamamoto 2001), groundwater discharge (Krest et al. 1999), gulf stream eddies (Orr 1988), sediment resuspension rates (Moore et al. 1996) or bioturbation rates (Hancock et al. 2000).

3.4 Distribution of ^{226}Ra in the Southern Ocean

First measurements of ^{226}Ra activities in the Southern Ocean were performed by Ku et al. (1976) in the Indian Sector. Data for the Pacific sector are provided by Chung (1974). A first concise ^{226}Ra sampling of circumpolar water masses was done during the GEOSECS sampling program that extended into the Antarctic sectors of the world's oceans (Broecker et al. 1976, Ku and Lin 1976, Chung 1981, Chung 1987). In the Atlantic sector, a high resolution transect across the Weddell Sea was collected during the International Weddell Sea Oceanographic Expedition (IWSOE 73; Chung and Applequist 1980). Existing literature values for surface water activities are compiled in Fig. 9.

3.5 Distribution of ^{228}Ra and ^{228}Th in the Southern Ocean

For the Southern Ocean, ^{228}Ra values are very scarce and have never been carried out in high resolution. The first analysis in southern polar waters including a N-S-transect between Australia and Antarctica was done during a five-year global survey for collecting more data on the distribution of ^{228}Ra and its daughter product ^{228}Th in all the major ocean basins (Kaufman et al. 1973). It could be shown that the activities in the surface waters of the Southern Ocean were lower than in any other ocean. ^{228}Ra was measured in all world oceans as part of the GEOSECS program. Sampling in the South Atlantic was done to 62°S but concentrations south of the Polar Front were below the analytical detection limit of $0.1\text{ dpm}/100\text{kg}$ (Li et al. 1980). Rutgers van der Loeff (1994) reports the only transect for ^{228}Ra through the Antarctic Circumpolar Current (ACC) in the Atlantic sector, showing similarly low values for the open waters but high activities close to the Antarctic continent. Moore and Santschi (1986) have determined deep water activities for the Indian Sector of the Southern Ocean. A compilation of the existing literature values for ^{228}Ra in surface waters at latitudes south of 35°S is given in Fig. 10. The data confirm the general picture of distribution of higher ^{228}Ra concentrations close to coastal areas and very low activities in open waters. A transect of ^{228}Th across the Drake Passage (Moore; unpublished data) confirms the general distribution of high activities along the continents of both South America and Antarctica and low values in the open waters (Fig. 10).

For an extensive study of possible inputs of shelfwater into any part of the Southern Ocean, more data about the importance of the shelf areas as possible source regions for ^{228}Ra are necessary as well as high-resolution sampling on transects across the ACC. Especially the frontal regions, which are expected to play a major role for the rapid transport of water masses have hitherto not been subject to extensive investigations.

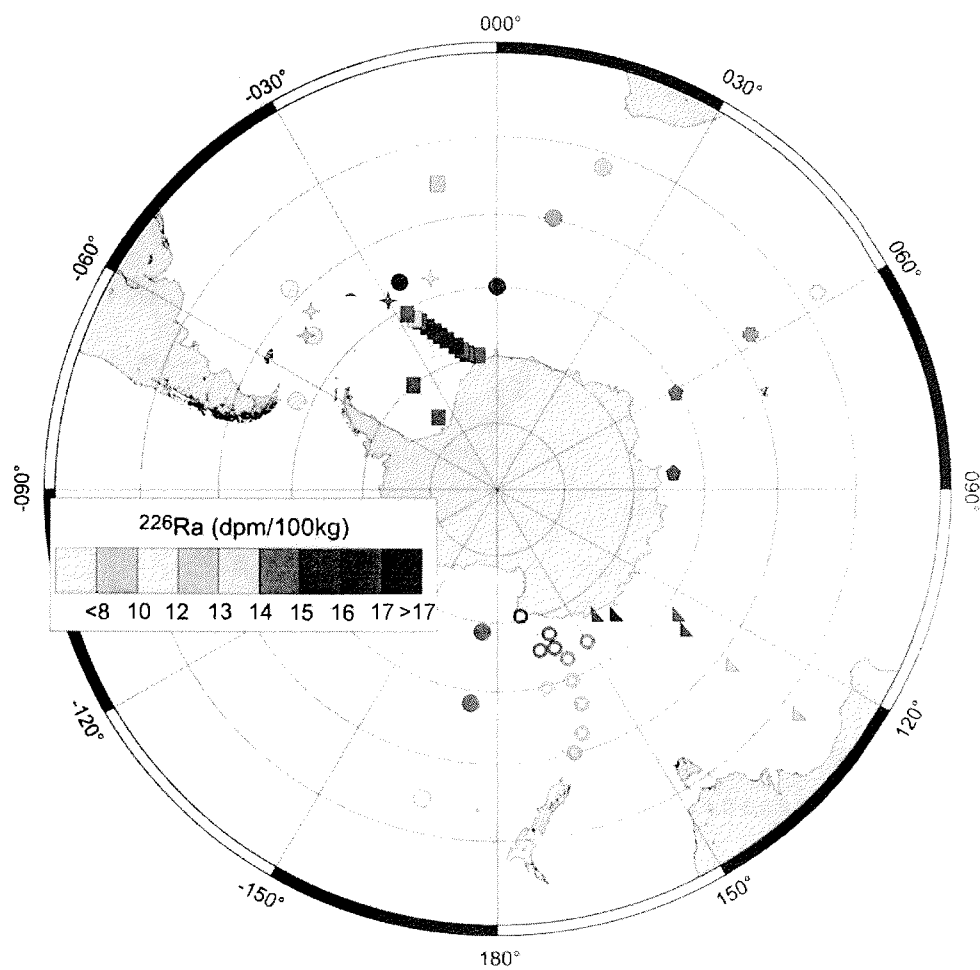


Fig. 9: Surface water activities of ^{226}Ra in the Southern Ocean, compiled after Chung (1974; open circles), Broecker et al. (1976; stars), Ku and Lin (1976; closed circles), Ku et al. (1976; triangles), Chung and Applequist (1980; squares), Chung (1981; pentagons) and Chung (1987; crosses).

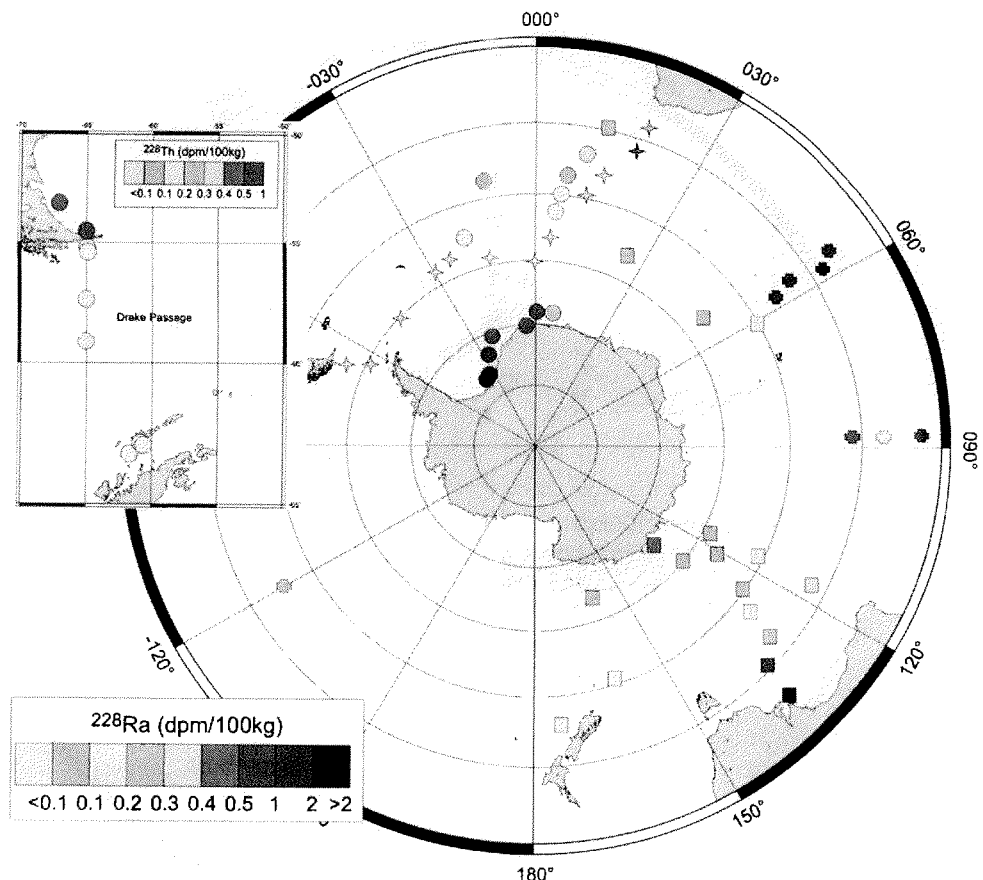


Fig. 10: Surface water activities of ^{228}Ra and ^{228}Th in the Southern Ocean, compiled after Kaufman et al. (1973; squares), Li et al. (1980; stars), Sarmiento (1988; crosses) and Rutgers van der Loeff (1994; circles). All values are given in dpm/100kg. Inlay Drake Passage: Unpublished data from W.S. Moore. Yellow stars are below the detection limit (Li et al. 1980).

4 MATERIAL AND METHODS

The decay modes and the distribution of radium isotopes in sea water as discussed in chapter 3 have a determining influence on the way of collecting and processing the samples. While ^{226}Ra can be measured in 20 l of sea water, the open ocean values of ^{228}Ra in the Southern Ocean are among the lowest ones worldwide (Fig. 10) and require about a hundred times this amount of sample volume for a precise determination. The ideal method for the analysis of this isotope combines large volume water sampling with enrichment of radium in a small sample volume and with a high efficiency.

The sampling technique and the choice of the sampling locations against the background of the objectives of this work will be presented. Different techniques for the determination of the investigated isotopes are expounded in brief. The sample processing and the counting methods applied in this work are described in greater detail. Specifications of the measuring instruments conclude chapter 4.

4.1 Sampling strategy and techniques

Radium sampling was performed during six expeditions to the Atlantic sector of the Southern Ocean in 1998, 1999 and 2000. In the following, expeditions with RV POLARSTERN are uniformly labelled "ANT" and one cruise with the US-research vessel NATHANIEL B. PALMER is given the abbreviation "NBP" (Fig. 11).

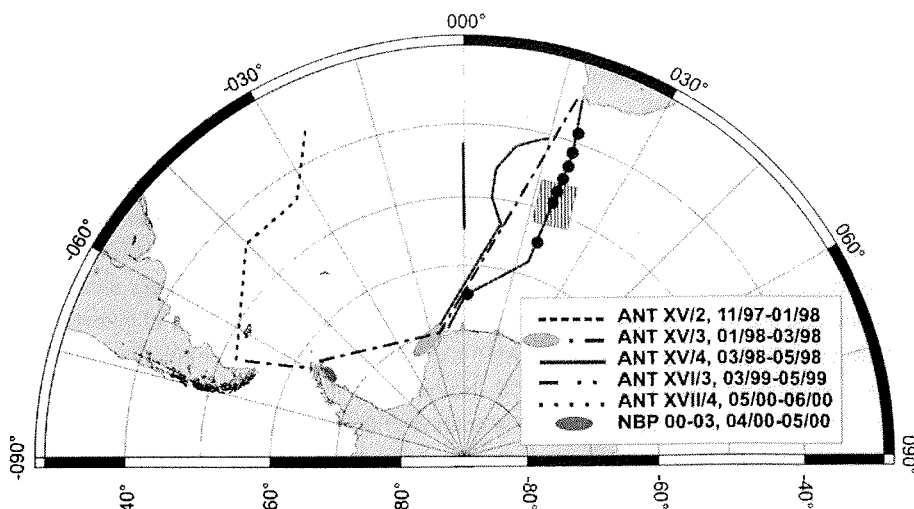


Fig. 11: Map of the Atlantic sector of the Southern Ocean with the sampling tracks for radium during expeditions with RV POLARSTERN (labelled ANT) and the US research vessel NATHANIEL B. PALMER (labelled NBP) from 1998 to 2000. The shaded box indicates a grid survey at the Polar Front at 20° E and dots refer to deep water stations during expedition ANT XVI/3.

Material and methods

A common method for the concentration of radionuclides from a large volume of sea water was followed, using MnO₂-coated cartridge filters. The adsorbing power of MnO₂ had already been observed in the context of trace element abundances in manganese ores (Ljunggren 1955). Radionuclides and a variety of other metals get adsorbed on the MnO₂-coating of the cartridges. Prewound polypropylene filter cartridges (CUNO Micro Wind or Hytrex II) were used with an outer diameter of 65 mm, a hole centered lengthwise and in variable lengths. They had been prepared before the cruises by immersion overnight at 70° C in a bath of a saturated KMnO₄ solution. A detailed description of the coating technique is given in Rutgers van der Loeff and Moore (1999). The cartridges were sealed in plastic bags to keep them wet until they came into use on board the ship.

4.1.1 Surface water sampling for ²²⁸Radium

In order to test whether ²²⁸Ra can indeed originate from either the Argentinean shelf, the shelf regions along the Antarctic Peninsula or the Weddell Sea, surface water sampling for the analysis of ²²⁸Ra has been done in these possible source regions. Five N-S-transects have been sampled through the Antarctic Circumpolar Current (ACC) along different longitudes. As the oceanographic fronts with their high geostrophic velocities seem particularly promising for a rapid transport of shelf signals, a dense sampling of the region between 46° and 52° S along the 20° E meridian was performed during a grid survey of the Polar Front during expedition ANT XVI/3 (Fig. 11).

All surface water samples except those of the expedition NBP 00-03 were taken parallel with a 20 l subsample for the quantitative determination of ²²⁶Ra. This was necessary for the calculation of absolute ²²⁸Ra activities (see chapter 4.3), but provided at the same time valuable information on the distribution and geochemical behaviour of ²²⁶Ra in southern circumpolar waters (see chapter 3.2).

As one of the objectives of this study is the investigation of possible iron transport routes into the South Atlantic, samples of suspended particulate matter have been taken on most ²²⁸Ra surface water locations for the analysis of aluminium and the isotopic composition of neodymium (Hegner et al. in prep.). These tracers should help to illuminate the role and origin of terrigenous input of iron into the area of investigation. ²²⁸Ra sampling during expedition ANT XVI/3 was done in conjunction with iron measurements carried out by the NIOZ (Netherlands Institute for Sea Research). The results for ²²⁸Ra will be discussed in the context of these accompanying measurements and will contribute to a better understanding of the dynamics and processes regulating the iron supply into this part of the Southern Ocean.

The sampling was performed with a filter system connected to the ship's sea water supply with a water intake depth at approximately 8 m. The pumps were active constantly after leaving the harbour and the pipe system was flushed thoroughly before taking the first sample.

Material and methods

A cartridge length of 13 cm has been chosen for surface water sampling as it has proven to be a good compromise between sampling efficiency and further handling of the samples. The water sample was run through an uncoated cartridge used as a prefilter (1 µm) for removing particulate matter, two MnO₂-coated cartridges put in series to concentrate radium and a flowmeter for recording the sample volume. It was tried to filter at least 2000 l of sea water for a good recovery of radium. Except for expedition NBP 00-03, this volume could be attained or, in the case of expedition ANT XVI/3, was largely exceeded. After finishing the sampling, the prefilters were discarded and the MnO₂-coated cartridges either directly sealed or first rinsed with deionized water, dried and then sealed.

As most of the sampling was done on a sailing vessel, the results represent values integrated over as much as 120 km.

4.1.2 Profile sampling for ²²⁸Radium

During expedition ANT XVI/3, a transect of eight deep water stations down to 1000–1800 m was carried out at 20° E in order to get a two-dimensional picture of the distribution of the desired radionuclides. Sampling locations are given in Fig. 11. At each station, a CTD profiler² was run first to determine water mass properties. The sampling was done with four time-programmed pumping units that were loaded with two MnO₂-coated cartridges each. For structural reasons, the length of the cartridges was 25 cm. An integrated flowmeter recorded the sample volume.

No prefilter was used as the first sampling depth was at the bottom of the mixed layer and the suspended particle content of the water very low (Usbeck et al. in press). Any additional filter would increase the resistance of and lower the flow through the pumping system. Under oxic conditions in sea water, radium exists mostly in the dissolved form. By analyzing surface water samples with a generally higher particle loading than deep water samples, it could be shown that the radium activity of the particulate matter is less than 1% of the respective dissolved activity. ²²⁸Ra and ²²⁶Ra are not expected to differ in their behaviour regarding the partitioning between the solid and the fluid phase, however, depending on their source region, particles could carry activity ratios different to the surrounding sea water with them (Legeleux and Reyss 1996). But taking the low particle content in deeper water layers and the weak particulate activities into consideration, the missing prefilter would not affect the results in any significant way.

A surface water sample for ²²⁸Ra was taken from the ship's sea water supply at every deep water station. Apart from station 156, the sampling was done in conjunction with measurements of iron depth profiling done by the NIOZ, but the depth resolution for radium is coarser due to the limited number of pumping units.

² Instrument for the measurement of temperature, electrical conductivity, and under water pressure. Depth and salinity are deduced from these parameters.

Material and methods

4.1.3 Sampling for ^{226}Ra

For a quantitative determination of the ^{226}Ra surface water concentration, 20 l subsamples were taken in conjunction with the large volume MnO_2 -filtering. The water was filtered through an uncoated 1 μm filter cartridge to remove the particulate fraction. If taken during steaming of the ship, the subsample was either collected about midway of the ^{228}Ra -sampling (ANT XV/2+3) or split in three bottling times of each 6-7 l (ANT XVI/3): given an average sampling duration of 6 hours, the three parts of the subsample were taken one, three and five hours after having started the sampling. This procedure was adopted to level out possible local variations in the ^{226}Ra concentrations. Samples from expedition ANT XV/4 and ANT XVII/4 were taken solely during station time. All samples were weighed before further processing. No subsamples are available from expedition NBP 00-03.

A restricted number of 20 l subsamples from intermediate and deeper water layers has been taken with a rosette cast at stations 156, 169, 182, 190 and 207. The samples were not filtered before further treatment because the particle content in these subsurface waters was negligible.

4.2 Measurement techniques for ^{228}Ra and ^{226}Ra

A number of different counting techniques is available for ^{228}Ra and ^{226}Ra that will be briefly presented here.

^{226}Ra can be measured by α -spectrometry but this method presupposes an intensive purification procedure (Hancock and Martin 1991). Otherwise, its peak at 4.78 MeV might interfere with ^{234}U or ^{230}Th , which decay at 4.77 and 4.68 MeV, respectively. Commonly, ^{226}Ra is analyzed either by α -scintillation using the Rn-emanation technique (Broecker 1965, Moore et al. 1985, Mathieu et al. 1988) or by γ -spectrometry via its short-lived grand-daughters (Reyss et al. 1995). In this work, the latter technique has been applied due to the problem-free handling of the samples and because γ -counting time was not a limiting factor (see chapter 4.3.4).

^{228}Ra is a weak β -emitter (0.04 MeV) which makes it difficult to be detected by β -counting. It can be detected via its short-lived daughter ^{228}Ac , a β -emitter itself with stronger decay energies. Complication arises from the short half-life (6.13 hours) and the fact that it is not possible to separate ^{228}Ra and ^{226}Ra by conventional analytical methods. The daughters of the latter, β -emitters themselves, will quickly grow in and mask the activities from ^{228}Ra and ^{228}Ac . Furthermore, β -counting is not energy specific. Apart from ^{40}K , the majority of β -decays in sea water can be attributed to ^{234}Th with an average activity of 240 dpm/100kg (Chen et al. 1986) and a minimum activity of 90 dpm/100kg of sea water (Rutgers van der Loeff, pers. comm.), compared to <0.1 dpm/100kg for ^{228}Ra in the open South Atlantic. Hence, the precise measurement of any other nuclide would demand a complete purification from ^{40}K , ^{234}Th and other disturbing nuclides prior to the β -counting. An alternative method is the analysis of

^{228}Ra via its direct daughter ^{228}Th by measuring the initial ^{228}Th content of a given sample via α -spectrometry. This procedure involves the uncertainty that ^{228}Ra and ^{228}Th might not be in secular equilibrium due to their different geochemical behaviours under marine conditions (Hancock and Martin 1991, this study). Time-controlled ingrowth of ^{228}Th after a complete removal of the initial ^{228}Th content circumvents this problem but requires long storage times (Moore 1972, Trier et al. 1972, Li et al. 1980, Moore et al. 1985). The principle of the determination of both the initial and the ingrown ^{228}Th activity is based on the fact that ^{228}Th is a well measurable α -emitter. Due to the higher sensitivity of α -spectrometry versus γ -spectrometry, ^{228}Th is detectable at lower levels than its parent-nuclide ^{228}Ra . An ingrowth period of several months and repeated measurements are required when ^{228}Ra is determined by delayed coincidence via ^{224}Ra , the short-lived daughter of ^{228}Th (Moore and Arnold 1996). Analogous to ^{226}Ra , ^{228}Ra can also be measured via its direct descendant ^{228}Ac by γ -spectrometry (Moore et al. 1985, Reyss et al. 1995). Both the ^{228}Th -ingrowth method and determination by γ -spectrometry have been used in this study.

Units used in this work for the presentation of radionuclide data are counts per minute (cpm) and disintegrations per minute (dpm). The former represents the count rate that is registered by the detector, the latter applies to the real activity of the measured sample.

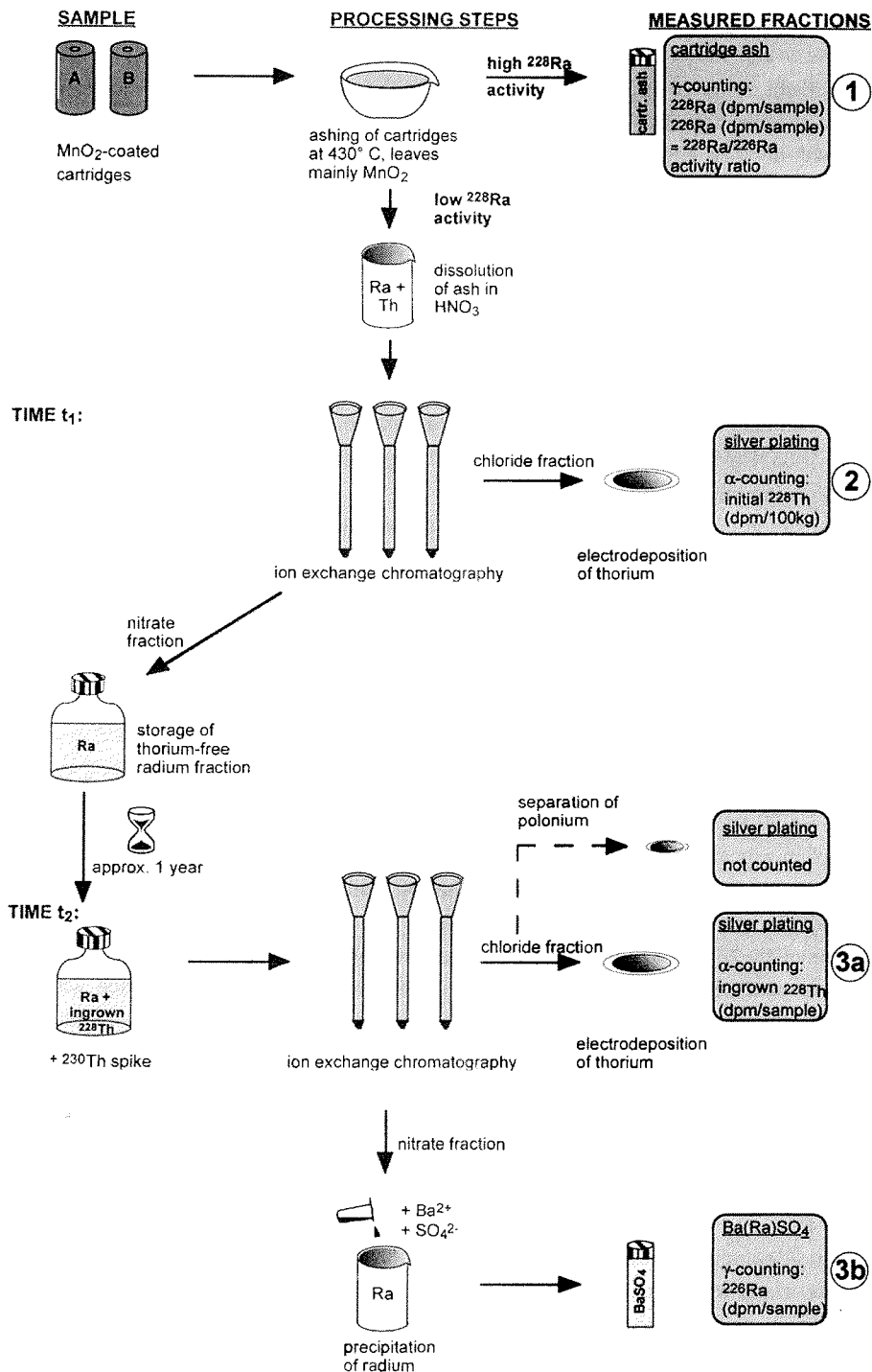
The data in this study will be presented in terms of dpm/100kg as it is the common unit used throughout the marine radium literature (e.g. GEOSECS data). The relationship between dpm and the SI-unit Becquerel (Bq) for radioactivity is 1 Bq = 60 dpm.

4.3 Sample preparation and measurement

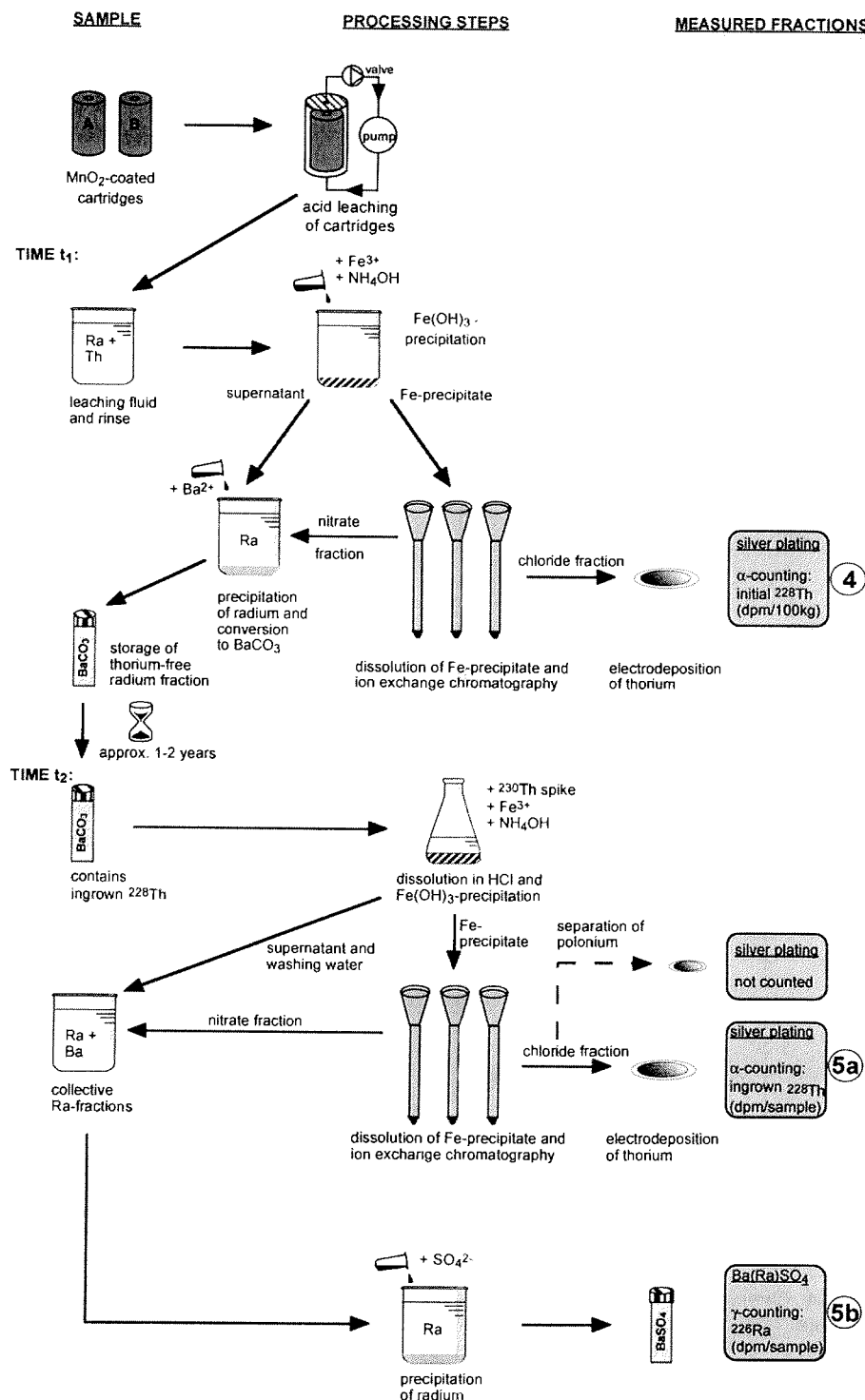
Sampling with MnO_2 -coated cartridges retains ^{228}Ra and ^{226}Ra without a fractionation of the isotopes but constitutes a non-quantitative method that yields results in terms of $^{228}\text{Ra}/^{226}\text{Ra}$ activity ratios only. The conversion into absolute ^{228}Ra activities is done by means of the 20 l subsamples that provide quantitative activities for ^{226}Ra .

The counting techniques for ^{228}Ra used in this work varied in accordance with the expected activities. While samples from continental shelf regions were measurable by γ -spectrometry on the cartridge ash (see chapter 4.3.1), open ocean water samples had to be processed following the ^{228}Th -ingrowth method (Moore 1972, Trier et al. 1972, Li et al. 1980, Moore et al. 1985; see chapter 4.3.2). In this case, the $^{228}\text{Ra}/^{226}\text{Ra}$ activity ratio is attained in two steps: ^{228}Ra is back-calculated from the analysis of a time-controlled ingrowth of ^{228}Th while the respective ^{226}Ra fraction is measured separately by γ -spectrometry on a BaSO_4 precipitate. The laboratory procedure for all cartridge samples can be read from Fig. 12 and Fig. 13 and has been chosen as to assure a way of counting ^{228}Ra with a maximum efficiency. Fig. 14 expounds how the $^{228}\text{Ra}/^{226}\text{Ra}$ activity ratios are converted to absolute ^{228}Ra activities by means of the 20 l subsamples.

Material and methods



Material and methods



Material and methods

Fig. 12 (page before previous page): Flow diagram showing the analytical procedure of surface water samples for the measurement of ^{228}Ra adsorbed on MnO_2 -coated cartridges from expeditions ANT XV/3+4, ANT XVI/3, ANT XVII/4 and NBP 00-03. The conversion of the results from the different radionuclide fractions (labelled 1, 3a and 3b) into ^{228}Ra in dpm/100kg of sea water is illustrated in Fig. 14.

Fig. 13: (previous page): Flow diagram showing the analytical procedure for the measurement of ^{228}Ra adsorbed on MnO_2 -coated cartridges from expeditions ANT XV/2 (surface water) and ANT XVI/3 (deep-water stations). The conversion of the results from the different radionuclide fractions (labelled 5a and 5b) into ^{228}Ra in dpm/100kg of sea water is shown in Fig. 14.

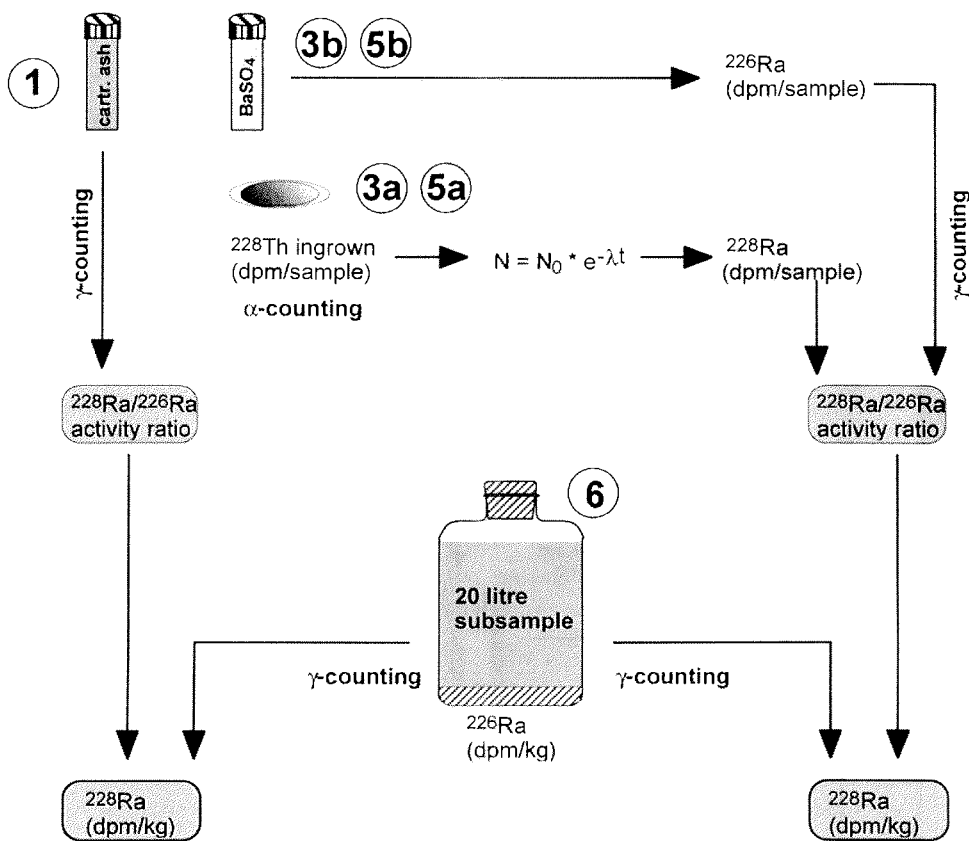


Fig. 14: Overview of the analytical steps to convert $^{228}\text{Ra}/^{226}\text{Ra}$ activity ratios into absolute ^{228}Ra activities (dpm/mass) by means of the 20 l subsamples. ^{226}Ra can be determined quantitatively on these. Numbering of the radionuclide fractions according to Fig. 12 and Fig. 13.

4.3.1 Direct determination of $^{228}\text{Radium}$ on cartridge ash by γ -spectrometry

If not done directly on the ship, the cartridges were rinsed with deionized water to remove all salt. To check for possible loss of radium, a precipitation of $\text{Ba}(\text{Ra})\text{SO}_4$ was made from the washing water (see chapter 4.3.4) which yielded no measurable radium. It could be shown that washing the cartridge ash instead of the cartridges itself led to a considerable loss of activity. The cartridges were then dried and melted to be ashed in a muffle furnace at 430° for 6 to 8 hours (Cochran et al. 1987, Fleer and Bacon 1991, Buesseler et al. 1992, Baskaran et al. 1993). Subsequently, the temperature was increased to 620° for at least 2 hours to remove all remaining organic substances. It should be noted that ashing polypropylene of this order produces large amounts of harmful gases such as polycyclic aromatic hydrocarbons and should only be performed in a fume hood with strong ventilation. To keep the environmental impact as low as possible, the fumes leaving the furnace were sucked through a set of canisters filled with water and charcoal which retained most of the exhaust fumes. Still, a resinous hydrocarbon mass started leaking at the connecting parts after a few ashing sessions. The material used to set up this cleaning system, the charcoal and consumer goods like gloves etc. were disposed of by high-temperature incineration after the sample processing had been finished.

Further processing of the samples depended on their expected ^{228}Ra activities (Fig. 12 and Fig. 13).

Ashed samples from shelf regions were filled in plastic tubes fitting the bore-hole of a γ -detector (fraction 1, Fig. 14), sealed and aged for three weeks to allow the establishment of an equilibrium between ^{226}Ra and its short-lived daughters ^{214}Pb and ^{214}Bi . Loss of radon through the seal was checked by the radon emanation technique after Moore et al. (1985) and found to be within the counting error of ^{226}Ra . After this time, the ash was counted by γ -spectrometry. The results are given as the activity ratio $^{228}\text{Ra}/^{226}\text{Ra}$ and, for samples where a 20 l subsample had been taken and hence a quantitative determination of ^{226}Ra is available, as absolute activities of ^{228}Ra (Fig. 14).

4.3.2 Indirect determination of $^{228}\text{Radium}$ via the $^{228}\text{Thorium-ingrowth}$ method

Counting experiments on the ash from samples with an expected low activity showed that ^{228}Ra was not detectable by conventional γ -spectrometry. The processing of these samples had to follow the so-called $^{228}\text{Th-ingrowth}$ method (Moore 1972, Trier et al. 1972, Li et al. 1980, Moore et al. 1985): The samples have first to be cleaned from all initial ^{228}Th to obtain a pure radium fraction which is set aside to allow a new generation of ^{228}Th to grow. After one year of storage time, ^{228}Th has grown in to 29% of the initial ^{228}Ra activity. The ingrown ^{228}Th is separated chemically in the presence of a yield tracer and counted by α -spectrometry. Knowing the exact time when the sample was set to zero with respect to ^{228}Th , the amount of the ingrown ^{228}Th is used to calculate back on the initial ^{228}Ra content via the laws of radioactive decay (Fig. 15). The equations used for the decay-correction are as follows:

Material and methods

- Calculation of the activity of the parent nuclide from the successive daughter nuclide, e.g. the activity of ^{228}Ra from the activity of ^{228}Th after ingrowth from T_2 to T_1 (Fig. 15).

The amount of atoms of the mother nuclide present at T_1 is calculated after Faure (1986):

$$A_1 = \frac{A_2}{e^{-\lambda_1 t} - e^{-\lambda_2 t}} \frac{\lambda_2 - \lambda_1}{\lambda_1}$$

A_1 : activity of atoms of parent nuclide at time T_1
 A_2 : activity of atoms of daughter nuclide at time T_2
 λ_1 : decay constant of parent nuclide
 λ_2 : decay constant of daughter nuclide
 t : time interval T_2-T_1

- Simple decay of a radionuclide during sample processing, e.g. the decay of ^{228}Ra from T_0 to T_1 (Fig. 15):

$$A_0 = \frac{A_1}{e^{-\lambda t}} = A_1 e^{\lambda t}$$

A_0 : activity of radionuclide at time T_0
 A_1 : activity of radionuclide at time T_1
 λ : decay constant of radionuclide
 t : time interval T_1-T_0

The outline of the chemical methods will be restricted to the most important steps and to modifications from known procedures. A comprehensive and detailed instruction to radionuclide methodology is given in Ivanovitch and Harmon (1992) and Rutgers van der Loeff and Moore (1999) which is the main literature reference for this chapter if not quoted otherwise. The numbering of the measured radionuclide fractions in the following paragraphs refers to Fig. 12, Fig. 13 and Fig. 14.

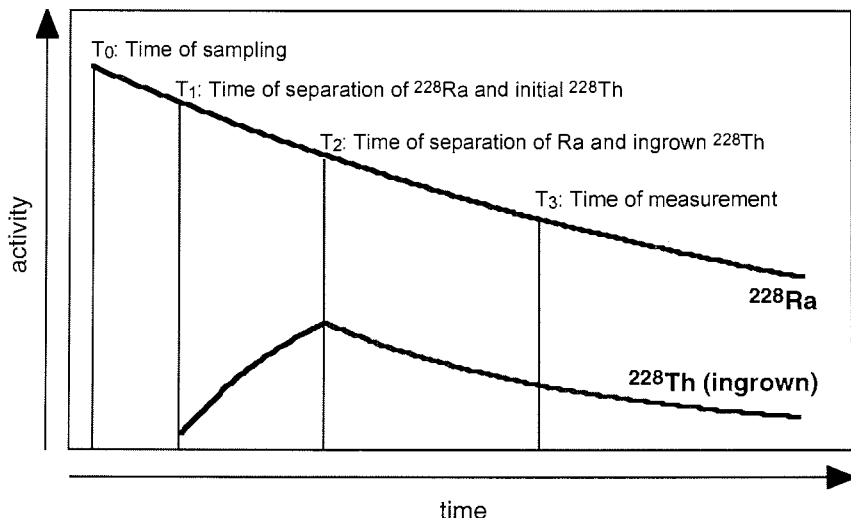


Fig. 15: Decay scheme of the ^{228}Ra - ^{228}Th -system during sample processing following the ^{228}Th -ingrowth method. The back-calculation of ^{228}Ra after ingrowth of ^{228}Th during time period T_2-T_1 and the decay corrections for ^{228}Th for the time interval (T_3-T_2) and for ^{228}Ra for the time interval (T_1-T_0) , are done by means of the equations given in chapter 4.3.2.

Samples from expedition ANT XV/3 and ANT XVI/3

The cartridge ash (fraction 1, Fig. 12) was first transferred with concentrated HNO_3 into teflon beakers, covered with a lid and heated overnight. The remaining MnO_2 was reduced with H_2O_2 to obtain a clear, yellow solution. Further separation of the isotopes was done in several steps by ion exchange chromatography, using BioRad AG1-X8 as a resin. Two consecutive HNO_3 -columns were run to ensure a complete separation of radium and thorium isotopes. While the former passes in the first column rinse with 8 N HNO_3 (nitrate fraction), the latter is collected in a second rinse with 9 N HCl (chloride fraction). For the samples of the expedition ANT XV/2 and ANT XVI/3, the chloride fraction has been electroplated to determine the initial thorium content of the sample, using ^{234}Th as a natural yield tracer (fraction 2, Fig. 12 and fraction 4, Fig. 13). ^{234}Th determinations were done separately (Walter et al. 2001, Usbeck et al. in press). Being the direct daughter of ^{228}Ra , the activity of ^{228}Th can be used as a first indication of ^{228}Ra . Differences in the results will be presented and discussed in chapters 5.3 and 6.2.

After about one to two years of ingrowth, the nitrate fraction was milked for ^{228}Th (fraction 3a, Fig. 12). The solution and a ^{230}Th spike were rinsed into a teflon beaker and set aside for some hours to allow the establishment of an isotopic equilibrium between the sample and the spike. A further set of two HNO_3 -columns was applied to perfectly separate the ingrown thorium and the yield tracer from the radium isotopes. It turned out that the chloride fraction could contain considerable amounts of ^{210}Po ,

Material and methods

causing interference with the ^{228}Th peak in the α -spectrum because the decay activities of both nuclides overlap each other. ^{210}Po and its grandmother ^{210}Pb are members of the ^{238}U decay chain and originate in sea water from the decay of ^{226}Ra . During the separation procedure with ion exchange chromatography, lead behaves similar to radium and both elements will end up in the nitrate fraction to be stored for the ingrowth of ^{228}Th . Taking an average ingrowth time of 15 months, ^{210}Po with a half-life of 138.4 days has enough time to grow in to approximately 90% of the ^{210}Pb activity. Although the successive nitrate columns should retain any polonium, a small fraction apparently slips through into the chloride fraction when rinsing thorium from the columns. In view of the closeness of the peaks of ^{210}Po (5.31 MeV) and ^{228}Th (5.34 and 5.42 MeV) in the α -spectrum and the low activities of ^{228}Th , even a very small amount of ^{210}Po is sufficient to produce interference problems. Therefore, a cleaning step for polonium had to be inserted before the electrodeposition of thorium from the ingrown samples. A silver planchet was left in a weak HCl solution for at least one day to make sure that any traces of polonium are removed. The exact method for polonium plating is described by Fleer and Bacon (1984) or Friedrich (1997). As this procedure is highly specific for polonium (Flynn 1968, Fleer and Bacon 1984), the disappearance of the interference is considered proof that it was indeed ^{210}Po .

Unlike the ingrown ^{228}Th activity, the plating and measurement of the initial ^{228}Th content of a sample occurred directly after the sample processing in a way that initial ^{210}Po was retained on the columns and new ^{210}Po did not have time to grow in.

The nitrate fraction of the columns at the time of milking was saved to quantitatively precipitate radium as $\text{Ba}(\text{Ra})\text{SO}_4$ by the addition of a pre-weighed aliquot of BaCl_2 and sulfate ions (fraction 3b, Fig. 12). Analysis of this precipitate was similar to the 20 l subsamples and is given in detail in chapter 4.3.4. Together with the back-calculated value of ^{228}Ra it yields a $^{228}\text{Ra}/^{226}\text{Ra}$ activity ratio for any given sample. Absolute ^{228}Ra activities can be computed by means of the respective 20 l subsample (fraction 6) as sketched in Fig. 14.

Samples from expedition ANT XV/2

This sample set could not be processed for ingrown ^{228}Th as described above by using the cartridge ash because other analyses had been performed previously (Walter et al. 2001), leaving an initially thorium-free radium fraction as BaSO_4 that had been converted to BaCO_3 following the description given by Moore et al. (1985) and stored for two years. The sample processing done in this work started at time t_2 as indicated in Fig. 13.

Separation of the ingrown ^{228}Th had to be done other than by nitrate column chemistry. The carbonate precipitate could not be dissolved directly in 8N HNO_3 as was done with MnO_2 , but the barium had to be removed first as otherwise insoluble $\text{Ba}(\text{NO}_3)_2$ would form. Therefore, the carbonate precipitate was washed thoroughly with Milli-Q and the supernatant stored. The precipitate was dissolved in 2 N HCl, ^{230}Th added as a yield-tracer and the solution set aside overnight. Addition of a FeCl_3 solution and subsequent

precipitation with NH_4OH as $\text{Fe}(\text{OH})_3$ at pH 8.5 concentrated thorium in the precipitate and radium in the supernatant. The iron precipitate was washed several times to remove any remaining radium and the washing water was united with previous supernatants.

For the analysis of ^{228}Th (fraction 5a, Fig. 13), the iron precipitate got dissolved in concentrated HCl. A HCl-column followed to remove iron. Further processing, including HNO_3 -column chemistry, separation of polonium and electroplating was similar to the general procedure given above. For a complete recovery of radium, the nitrate fraction of the HNO_3 column was saved and combined with the respective supernatants. Only then this fraction was re-precipitated quantitatively as $\text{Ba}(\text{Ra})\text{SO}_4$ for the determination of ^{226}Ra in the sample by the addition of excess SO_4^{2-} , using a solution made from MgSO_4 (fraction 5b, Fig. 13). Again, absolute ^{228}Ra activities are deduced from the combination of back-calculated $^{228}\text{Ra}/^{226}\text{Ra}$ activity ratios and 20 l subsample values (fraction 6, Fig. 14).

4.3.3 Determination of initial $^{228}\text{Thorium}$ on vertical water profiles

On the vertical water profiles along the 20° E meridian, only the initial ^{228}Th content was determined (fraction 4, Fig. 13). The main literature references for sample processing are Ivanovitch and Harmon (1992) and Rutgers van der Loeff and Moore (1999).

The sample processing had to deviate from the ashing procedure described for surface water samples (see chapter 4.3.2) because longer cartridges were deployed in the pumping units that were not suitable for combustion. Instead, the cartridges were leached with a combination of hydroxylamine hydrochloride as a reducing agent and 6 N HCl to desorb the radionuclides and keep them in solution (Fig. 13). The acid was circulated in a closed system by means of a small aquarium pump for one hour and the liquid transferred to a plastic beaker. The procedure was followed by a second extraction step and subsequent rinsing with Milli-Q. All liquid was combined in the beaker. To remove thorium quantitatively from the solution, a precipitation with 1 ml of FeCl_3 at pH 8.5 was done by adding NH_4OH solution. While all thorium isotopes get concentrated in the precipitate, radium isotopes will stay mostly in solution. In regard to the separation of radium and thorium, this step is analogous to the HNO_3 -column described above and sets the remaining supernatant to zero with respect to thorium. The precipitation was allowed to settle overnight before recovery by centrifugation. It was then washed three times with Milli-Q and the rinse combined with the remaining solution. A precipitation of $\text{Ba}(\text{Ra})\text{SO}_4$ was done by adding a pre-weighed aliquot of BaCl_2 and sulfate ions to concentrate radium for storage. As a prerequisite to ensure a later analysis of the ingrown ^{228}Th in the sulfate fraction (not done during this work), care must be taken not to entrain part of the precipitated $\text{Fe}(\text{OH})_3$ into the $\text{Ba}(\text{Ra})\text{SO}_4$ fraction.

The $\text{Fe}(\text{OH})_3$ precipitate was dissolved in 1 ml of concentrated HCl, followed by a HCl column to remove all iron. Thorium is collected with the eluate. The column rinse was

Material and methods

dried to a spot and re-dissolved in 8 N HNO₃ for further purification of thorium by a HNO₃ column. Thorium was electroplated and counted by α -spectrometry (fraction 4, Fig. 13).

No yield tracer for thorium was added during sample processing because ²³⁰Th, which is often used, is a natural component of sea water and would necessitate overspiking of the sample with ²³⁰Th which in turn can cause contamination problems. The artificial isotope ²²⁹Th, equally used as a yield tracer, increases significantly the background of the detectors, especially over the long counting period that is necessary for the measurement of low activities of ²²⁸Th. It was thus planned to use ²³⁴Th (half-life 24 days) as a natural yield tracer because its activity in sea water is well known and easily measured by β -counting. However, it was found that the initial ²³⁴Th activity on the cartridges was masked to more than 90% by ²³⁴Th that had grown during transport and storage of the samples from ²³⁸U which was co-adsorbed in small amounts on the MnO₂ cartridges. A separation of initial and ingrown ²³⁴Th was no longer possible for most of the samples. Results of the initial ²²⁸Th content for the vertical water profiles will therefore be reported as ²²⁸Th/²³⁰Th activity ratios.

4.3.4 Determination of ²²⁶Radium

Determination of the ²²⁶Ra concentration on 20 l subsamples (fraction 6, Fig. 14) follows closely the procedure described by Reyss et al. (1995) and Rutgers van der Loeff and Moore (1999), taking advantage of the low solubility product of BaSO₄ (1.07×10^{-10} mol²/l² at 25° C) that allows a gravimetric determination of the radium recovery when precipitated as Ba(Ra)SO₄.

Pre-weighed aliquots (100 ml) of a BaCl₂-solution had been prepared before the cruises from BaCO₃, each containing about 0.35 g Ba²⁺ ions. One aliquot was added under constant stirring to every 20 l water sample to precipitate radium as Ba(Ra)SO₄, making use of the natural sulfate content in sea water. After at least one hour of further mixing on the magnetic stirrer, the crystals were recovered by decantation and centrifugation, washed several times to remove any interfering ions and dried. The chemical yield was calculated from gravimetric determination of the recovery as BaSO₄. About 0.55 g Ba(Ra)SO₄ were precipitated from one aliquot of BaCl₂. Recoveries of the BaSO₄ carrier generally reached more than 95%. The precipitate was filled in appropriate tubes, sealed and set aside for about three weeks to allow the short-lived daughters ²¹⁴Pb and ²¹⁴Bi to grow into equilibrium with their parent ²²⁶Ra (see chapter 4.4.3). After establishment of a secular equilibrium, the sample was counted by γ -spectrometry.

The same procedure has been applied to fraction 3b (Fig. 12) and fraction 5b (Fig. 13) but here, both a pre-weighed BaCl₂-solution and SO₄²⁻ ions in form of H₂SO₄ have been added to precipitate radium as Ba(Ra)SO₄. This method is quantitative for all radium isotopes, but due to the low concentrations of ²²⁸Ra in the Southern Ocean, in most of the cases only ²²⁶Ra can be determined in a reasonable counting time.

4.3.5 Blank determination

All calculations have been background-corrected. Sample blinds were run parallel to the normal sample processing and reflect the possible contamination of a sample during the laboratory procedure. The detectors contribute a second source of background count rate, as they register a certain amount of counts that do not originate in the sample. All detectors were run empty over several weeks and with the sample blinds for a precise quantification of the background. Both laboratory and detector background were then subtracted from the measured results.

α -Spectrometry

For α -spectrometry, the overall background count rate amounts to 0.005 cpm for ^{228}Th and 0.002 cpm for ^{230}Th that had been added as a yield tracer. As most of the specific detector backgrounds are at least one order of magnitude lower, these values can be taken as the laboratory backgrounds. They represent a general background of < 7% (maximum 20%) for ^{228}Th and a consistently low value of 0.6 % for ^{230}Th of the final result.

γ -Spectrometry

Neither of the γ -detectors yielded a measurable blank activity for ^{226}Ra or ^{228}Ra , hence any background contribution must originate from the sample processing or the chemicals involved in the procedure.

A major source of contamination for the BaSO_4 samples is the ^{226}Ra present in BaCO_3 that was used to make the yield tracer solution (see chapter 4.3.4). It contributes an activity of approximately 0.13 dpm/g of barium. The average amount of recovered barium in a BaSO_4 sample is 0.34 g which equals a blank contribution of 0.04 dpm from the BaCO_3 . Total backgrounds for the 20 l subsamples are generally around 2% and never exceed 10% of the total ^{226}Ra activity. Between 80 and 93% of the blanks can be ascribed to the BaCO_3 -yield tracer. There is no measurable ^{228}Ra contamination.

The precipitated radium fractions of the ingrown cartridge solutions have relatively lower background values (consistently less than 2% of the sample activity) but seem to include a second source of contamination as the BaCO_3 does not account for more than 15% of the blanks. MgSO_4 , that has been added as a supply of SO_4^{2-} ions to the solution, has been checked but was not found to carry radium. The longer laboratory procedure might play a role as well as imperfect cleaning of labware. As the overall activities in this type of samples are about one to two orders of magnitude higher than in the subsamples, a tiny contamination can show in the background determination but has nevertheless little impact on the sample activity.

Although no measurable radium activity was found in the KMnO_4 utilized for the coating bath (see chapter 4.1.1), ashed cartridges might have been contaminated with radium during the coating procedure or handling in the laboratory. The ashed cartridge blanks give a maximum activity of 0.13 dpm/g of cartridge ash for ^{226}Ra . This equals a

Material and methods

background contribution of < 1% per sample. ^{228}Ra contamination could not be detected by γ -spectrometry.

4.3.6 Error determination

All radioactive decay processes are subject to statistical uncertainties that find their way into the error associated with the measuring result. A detailed outline of the statistical treatment of nuclear data and numerous calculation examples are given in Simon (1974), Ivanovich and Harmon (1992), Tsoulianidis (1995) or Gilmore and Hemingway (1996). In this chapter only the main principles will be expounded.

The radioactive decay of an atom or, in other words, the emission of a particle, is described by the laws of probability. The decay follows the Poisson distribution but with a sufficiently high number ($n > 25$) of incidents, the Poisson approaches the Gaussian distribution, i.e. the distribution becomes symmetric around the mean.

For measurements with a number of counts $n \geq 100$, the standard deviation is given by

$$\sigma = \pm \sqrt{n}$$

It should be noted that the standard deviation is calculated from a single counting and not from the mean of a series of measurements.

The relative standard error σ_n of the measurement decreases with an increasing number of recorded incidents and is reported as

$$\sigma_n = \frac{\sqrt{n}}{n} = \frac{1}{\sqrt{n}}$$

For the ^{226}Ra measurements of the 20 l subsamples by γ -spectrometry, a count number of $n \geq 1000$ could be achieved in a maximum counting time of 3-4 days. Disregarding the background correction, this yields an associated standard error of $\sigma_n < 3.2\%$. For the low activities of ^{228}Th , all samples with 400 or more counts ($\sigma_n = 5\%$) before background subtraction were taken into account, still this did involve extremely long counting times of several weeks. Although variable from one cruise to another due to different sample volumes, the detection limit for ^{228}Th can be drawn at approximately 0.01 dpm/100kg. The counting error associated with the background determination has been calculated after Ivanovich and Harmon (1992):

$$S = s \pm \sqrt{(s/T_s + b/T_s + b/T_b)}$$

S: best estimate of net count rate

s: background-corrected count-rate of the sample (cpm)

Material and methods

- b: count-rate of the background (cpm)
T_s: measuring time of the sample (min)
T_b: measuring time of the background (min)

Uncertainties in association with the sample preparation, processing and efficiency calculation further contribute to the overall error. For γ -spectrometry, this includes the determination of the factor E as a calibration factor (see chapter 4.4.3), weighing uncertainties in connection with the preparation of the yield tracer, the determination of the recovery and the weight of the sample. Errors attributed to the laboratory balance have a negligible contribution in relation to the remaining factors and have therefore been omitted. Determination of the sample size has even in rough seas been accurate to approximately 100 g which equals 0.5% for 20 kg. For α -spectrometry, the error associated with the activity of the yield tracer has to be taken into account.

The total error of the activity of a specific isotope in dpm in a given sample has been determined by propagation of errors. In detail, the following parameters have been considered for the overall error calculation (based on the 1σ counting error) of the different radionuclide fractions. Percentages in brackets indicate the relative errors associated with the single factors:

- ^{226}Ra 20 l subsamples (BaSO_4):
 - uncertainty associated with the activity of the standard (1.23%)
 - statistical error of the calibration factor (< 1%)
 - weighing uncertainty for 20 l sea water on board the ship (0.5%)
 - statistical error of the γ -counting (< 3.2%)
 - statistical error of the background measurement (7%)
- $^{228}\text{Ra}/^{226}\text{Ra}$ activity ratios (cartridge ash):
 - uncertainty associated with the activity of the standard (0.67%)
 - statistical error of the calibration factor (^{226}Ra : 0.5%; ^{228}Ra : 2%)
 - statistical error of the γ -counting (^{226}Ra : < 1%; ^{228}Ra : < 6%)
 - statistical error of the background measurement (^{226}Ra : < 20%;)
- ^{228}Th initial:
 - statistical error of the β -counting of ^{234}Th (< 3%)
 - total error associated with quantitative ^{234}Th determination used as a natural yield tracer (< 10%)
 - statistical error of the α -counting (< 4%)
 - statistical error of the background measurement (13%)
- ^{228}Th ingrown:
 - uncertainty associated with the activity of ^{230}Th used as a yield tracer (2.1%)
 - statistical error of the α -counting (^{230}Th : < 6%; ^{228}Th : < 5%, one value 16%)

Material and methods

- statistical error of the background measurement (^{230}Th : 14%; ^{228}Th : 22%)
- ^{226}Ra fraction from ^{228}Th -ingrowth method (BaSO_4):
 - uncertainty associated with the activity of the standard (1.23%)
 - statistical error of the calibration factor (< 1%)
 - statistical error of the γ -counting (< 3.2%)
 - statistical error of the background measurement < 8%)
- $^{228}\text{Th}/^{230}\text{Th}$ activities ratios (deep water stations):
 - statistical error of the α -counting (^{230}Th : < 5%, one value 11%; ^{228}Th : < 4%, one value 7%)
 - statistical error of the background measurement (^{230}Th : 14%; ^{228}Th : 12%)

4.3.7 Comparison of different measuring techniques

According to their expected ^{228}Ra activities, the samples have been prepared for and measured by different counting techniques. The question might thus arise, to what degree these results are comparable.

The ^{228}Ra activity of sample R 2 was determined by both direct γ -counting of the cartridge ash and the ^{228}Th -ingrowth method and gave values of 0.70 ± 0.04 and 0.67 ± 0.04 , respectively.

A few of the samples processed by the ^{228}Th -ingrowth method had ^{228}Ra activities high enough to be detected by γ -spectrometry. Therefore, the need of measuring the ^{226}Ra content of the cartridges (fraction 3a, Fig. 12) provides a good possibility for a reproducibility check of the determination of the ^{228}Ra activity as these samples yielded $^{226}\text{Ra}/^{228}\text{Ra}$ activity ratios. The calibration of these samples followed the same principle as for ^{226}Ra and is laid out in chapter 4.4.3. A plot of the results obtained by α -spectrometry versus the results obtained by γ -spectrometry on the respective BaSO_4 fractions shows a very good agreement between both techniques (Fig. 16).

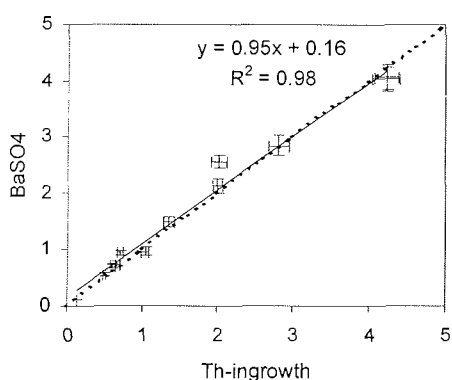


Fig. 16: Comparison of the ^{228}Ra activity determined by the Th-ingrowth method vs. a determination by γ -spectrometry on the $\text{Ba}(\text{Ra})\text{SO}_4$ precipitate of the same samples (i.e. fraction 3a vs. 3b, Fig. 12). Solid line: regression fit, dashed line: 1:1 relation.

4.4 Spectroscopic instruments for the detection of radiation

The principle behind the measurement of nuclear radiation is the interaction of particles with the material of the detector, resulting in a pulse in the counter that is, in the case of α - and γ -spectrometry, proportional to the amount of energy deposited by the incoming particle. In the case of α -spectrometry, this particle will be a ${}^4\text{He}$ -nucleus (α -particle) whereas in γ -spectrometry photons are recorded. The general assemblage of radiation instruments normally consists of a detector with a high-voltage power supply, connected in series to a preamplifier, an amplifier, an analog-to-digital converter (ADC), a multichannel analyzer (MCA) and a computer for data processing and graphical presentation.

4.4.1 α -Spectrometer

α -spectrometry is generally characterized by its low background levels and an energy-independent detector efficiency. These advantages contrast with the high requirement of time needed for sample preparation and purification. The detectors used in α -spectrometry are semiconductors. As α -particles are prone to collide with anything in their path, the chambers are operated under vacuum to avoid energy loss in air and to ensure best efficiencies.

All measurements of ${}^{228}\text{Th}$ were performed with an α -spectroscopic system from EG&G ORTEC, containing a total of 40 detection chambers. Each chamber includes a circular ion implanted silicon detector (EG&G ORTEC or CANBERRA) with an active area of 450 mm^2 that was operated in a selected energy range of 3 to 8 MeV. The warranted α -resolution of the detectors is 20 keV Full line Width at Half Maximum (FWHM), representing the detector's ability to separate between lines of different energies. The applied vacuum was $< 7 \text{ Pa}$. The silver planchets were placed on sample trays underneath the detector in a distance varying between 2 and 5 mm. Fig. 17 is a view into a detection chamber of an α -spectrometer.

4.4.2 γ -Spectrometer

γ -spectrometry is a non-destructive method to quantify radiation but, in contrast to α -spectrometry, has a much smaller efficiency, which furthermore varies with the energy of the emitted photons and the geometry of the measured sample. For small sample volumes, well-type detectors made from high-purity germanium have proven to be the best choice in terms of counting efficiency. A cylinder with a bore-hole situated at the centre of the crystal ensures that the sample is surrounded by germanium from nearly all sides. The disadvantage of a somewhat reduced energy resolution for these detectors (compared with coaxial detectors for example) can be neglected when analyzing spectra with defined, clearly separated lines of energy.

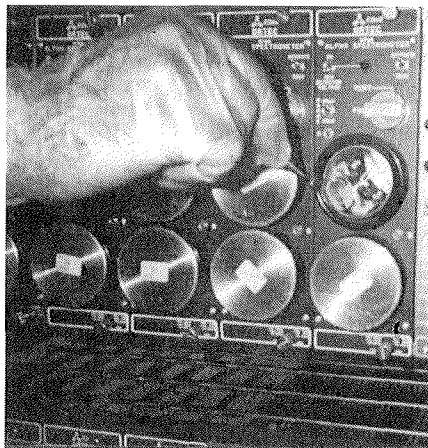


Fig. 17: Placing a silver planchet underneath a silicon detector in a vacuum chamber for α -spectrometry.



Fig. 18: Insertion of a sample in the borehole detector of a γ -spectrometer. The detector is surrounded by a lead shield from all sides to reduce the background radiation.

In order to minimize the detector leakage current (thermal noise), germanium detectors are cooled with liquid nitrogen. The detector itself is held under constant vacuum to be protected from dirt or condensation of vapour and to avoid any electrical discharges. A lead shield surrounding the detector reduces the influence of cosmic rays on the spectral background (Fig. 18).

Table 2: Technical specifications of the AWI-detectors for γ -spectrometry.

	Detector 1	Detector 2
useful hole diameter	12 mm	12 mm
useful depth of hole	57 mm	70 mm
sensitive volume of Ge-crystal	126 cm ³	155cm ³
measured absolute efficiency at 122 keV	76.9%	79.4%
measured resolution at 122 keV	1.25 keV	1.39 keV
measured resolution at 1332 keV	2.05 keV	2.12 keV
measured peak-to-Compton-ratio at 662 keV	75	126
thickness of lead shield	15 cm	10 cm
thickness of old lead shield thereof	2 cm	—

Determinations for ^{228}Ra and ^{226}Ra on cartridge ash and BaSO_4 have been done with two well-type germanium detectors from EURISYS (formerly INTERTECHNIQUE). Detector 2 has also been operated on board RV POLARSTERN during the expedition

ANT XVI/3. The technical properties of both detectors as specified by the manufacturer are presented in Table 2. The energy resolution of the detector system is given in terms of the FWHM. The peak-to-Compton-ratio indicates to what degree low-energy peaks will be identified by the detector in the presence of stronger high-energy peaks. The calibration curves for both detectors, using DL-1a uranium-thorium reference ore as a standard (Steger and Bowman 1980), are given in Fig. 19.

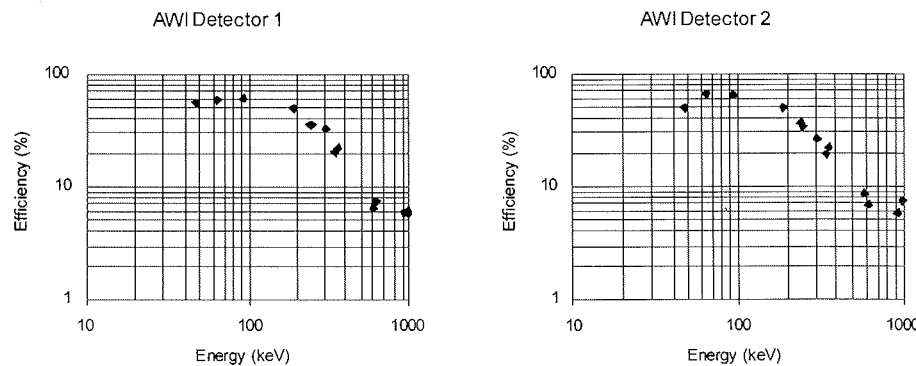


Fig. 19: Efficiency curves of both AWI detectors, calculated from the measurement of DL-1a uranium-thorium reference ore in counting tubes, filled up to 5 mm.

4.4.3 Preparation of standards for γ -spectrometry and spectrum analysis

Well-type detectors cannot be calibrated with a linear efficiency calibration curve (Reyss et al. 1995). Commonly, standards are prepared that yield a conversion factor E for each measured energy line, thus allowing the direct comparison of the samples with the standard. E includes the γ -intensity, detector efficiency and self-adsorption (Moore 1984, Reyss et al. 1995). It relates to the counts at a given energy by:

$$E = \frac{cpm}{dpm}$$

Table 3 gives the value of factor E for all energies used for the determination of ^{226}Ra and ^{228}Ra .

Care has to be taken that dimensions, matrix and weight of the standard resemble those of the samples as otherwise the self-adsorption inside the sample might be different. For cartridge ash samples, a calibration source was made from a mixture of blank cartridge ash and 0.48 g of DL-1a uranium-thorium reference ore (Steger and Bowman 1980). DL-1a is certified for ^{226}Ra and ^{232}Th but not for ^{228}Ra . As it yields a $^{232}\text{Th}/^{228}\text{Th}$ activity ratio of 0.99 between ^{232}Th and ^{228}Th , thus indicating a high degree

Material and methods

of secular equilibrium between both thorium isotopes (Steger and Bowman 1980), it can be used as a calibration standard for ^{228}Ra as well.

For the calibration of BaSO_4 , two different types of standards were produced that yielded similar factors of E . For the first type, about 1 g of DL-1a was weighed and digested with a combination of HF, HClO_4 and HNO_3 . The solution was precipitated as BaSO_4 . Both ^{226}Ra and ^{228}Ra can be calibrated with this standard. The second type was prepared by weighing about 1 ml of a liquid ^{226}Ra standard (Amersham), composed of 0.5 N HCl with BaCl_2 as the carrier phase, followed by subsequent precipitation as $\text{Ba}(\text{Ra})\text{SO}_4$.

Table 3: γ -emission lines and counting efficiencies (E ; including γ -intensities and detector efficiencies) of the γ -detectors at AWI. Emission energies and γ -intensities taken from Erdmann and Soyka (1979).

Nuclid	Measured via	Emission energy(keV)	γ -Intensity (%)	E (%) detector 1	E (%) detector 2
^{226}Ra	^{214}Pb	295.2	19.2	ash: 6.01 ± 0.06 BaSO_4 : 5.69 ± 0.01	BaSO_4 : 5.44 ± 0.01
	^{214}Pb	351.9	37.1	ash: 9.62 ± 0.08 BaSO_4 : 9.08 ± 0.02	BaSO_4 : 8.69 ± 0.02
	^{214}Bi	609.3	46.0	ash: 3.47 ± 0.04 BaSO_4 : 3.33 ± 0.01	BaSO_4 : 3.19 ± 0.01
			sum:	ash: 19.1 ± 0.1 BaSO_4 : 18.10 ± 0.02	BaSO_4 : 17.33 ± 0.02
^{228}Ra	^{228}Ac	338.4	12.0	ash: 2.8 ± 0.07	BaSO_4 : 2.31 ± 0.03
	^{228}Ac	911.0	29.0	ash: 1.98 ± 0.06	BaSO_4 : 1.84 ± 0.03
	^{228}Ac	968.9	17.4	ash: 1.14 ± 0.04	BaSO_4 : 1.01 ± 0.02
			sum:	ash: 5.93 ± 0.1	BaSO_4 : 5.17 ± 0.08

Both ^{226}Ra and ^{228}Ra are measured using their short-lived descendants which are stronger γ -emitters than their respective parents. ^{226}Ra is analysed using the prominent energy lines from the emissions of ^{214}Pb (295 and 352 keV) and ^{214}Bi (609 keV). Equilibrium between the mother and its daughters is reached after about three weeks. The successive decay steps include the noble gas radon. In order to preserve a closed system with regard to the decay chain, the tube containing the precipitate must be firmly sealed to prevent any escape of radon. Moore and Dymond (1991) showed that BaSO_4 itself retains the radon very efficiently as radium is part of the crystal lattice. For the cartridge ash samples, radon loss was checked with the Rn-emission technique

Material and methods

after Moore et al. (1985; see chapter 4.3.1). ^{228}Ra is measured via ^{228}Ac (338, 911 and 969 keV). The spectrum analysis, i.e. the background calculation and the identification of peak areas, was done with INTERWINNER software from EURISYS. Typical γ -spectra are given in Appendix A 2 and A 3.

5 DISTRIBUTION OF ^{226}Ra AND ^{228}Ra IN THE SOUTH ATLANTIC

The results obtained for ^{226}Ra , ^{228}Ra and ^{228}Th are presented and compared to the existing literature values. A compilation of the latter is given in Fig. 9 and Fig. 10. It will be shown to what extent the initial ^{228}Th activity and the $^{228}\text{Th}/^{230}\text{Th}$ activity ratio (AR) can serve as indicators of the ^{228}Ra distribution.

Samples that are mentioned specifically in the text are annotated in the respective figures. A complete list of all results is tabulated in Appendices A 7 and A 8. The geographical presentation of the data has been performed with PanMap (Pangaea 1997) and Ocean Data View (Schlitzer 2001). For the sake of simplicity, labelling of the deep water stations within the text will be restricted to the last three digits (e.g. station PS 53-156 will become station 156).

5.1 Surface water activities of ^{226}Ra

^{226}Ra has for the first time been sampled on a high-resolution scale in southern polar surface waters. The samples cover a range from 5.45 to 18.04 dpm/100kg with the lowest values in Subantarctic Surface Water (SASW) north of the Polar Front (PF) and the highest value in Antarctic Surface Water (AASW).

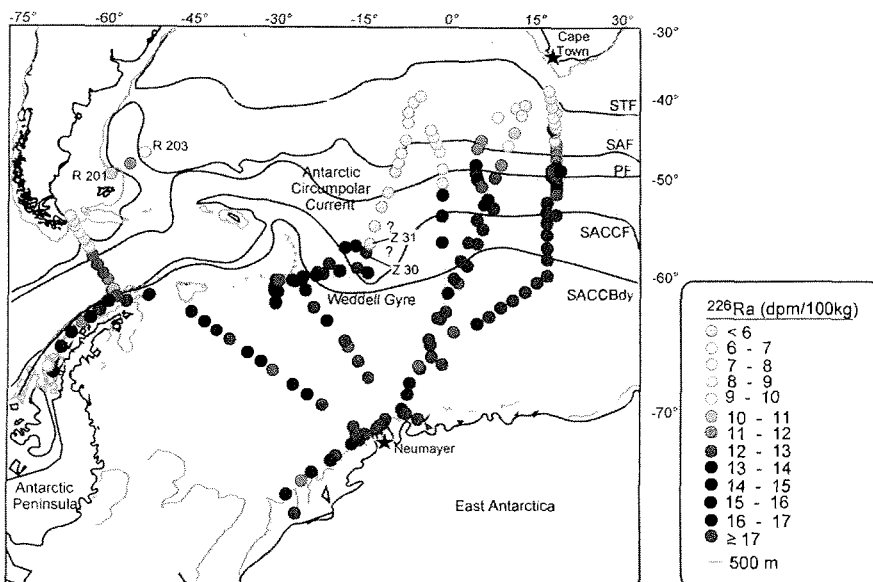


Fig. 20: Surface water activities of ^{226}Ra (dpm/100kg) in the Atlantic sector of the Southern Ocean. The sharp decrease from sample Z 30 to Z 31 is most likely due to analytical reasons. Approximate positions of the oceanic fronts after Orsi et al. (1995). STF: Subtropical Front; SAF: Subantarctic Front; PF: Polar Front; SACCF: Southern ACC Front; SACCBdy: Southern ACC Boundary.

Altogether, 186 surface water samples from five cruises have been analyzed for their ^{226}Ra activity (Fig. 20). The most salient feature in the distribution of ^{226}Ra is a strong southward increase from approximate 8 dpm/100kg north of the PF to about twice as much in the Weddell Gyre with a mean activity in the southern waters of the Antarctic Circumpolar Current (ACC) and within the Weddell Gyre of about 15.5 dpm/100kg. This gradual increase of the ^{226}Ra activity is closely related to a drop in temperature and displays the effect of upwelling of deeper waters (see also chapter 2.2.2). It can be observed on all transects although the gradients differ in intensity. The steepest one in combination with a southward dislocation in comparison to the other transects occurs at 15° W between samples Z 30 and Z 31. However, and there is no indication from hydrographical and nutrient data that this feature is real and the activities of Z 31 and north of it are much lower than anything reported in the literature for this region (Broecker et al. 1976, Ku and Lin 1976, Chung and Applequist 1980). In the absence of confirmation by other parameters analytical problems must be assumed as the main cause, e.g. a non-quantitative precipitation of radium with BaSO_4 . The sharp contrast between ^{226}Ra concentrations in subantarctic and antarctic waters is also maintained in the northward bending loop of the ACC east of South America, covered by samples R 201 – R 203.

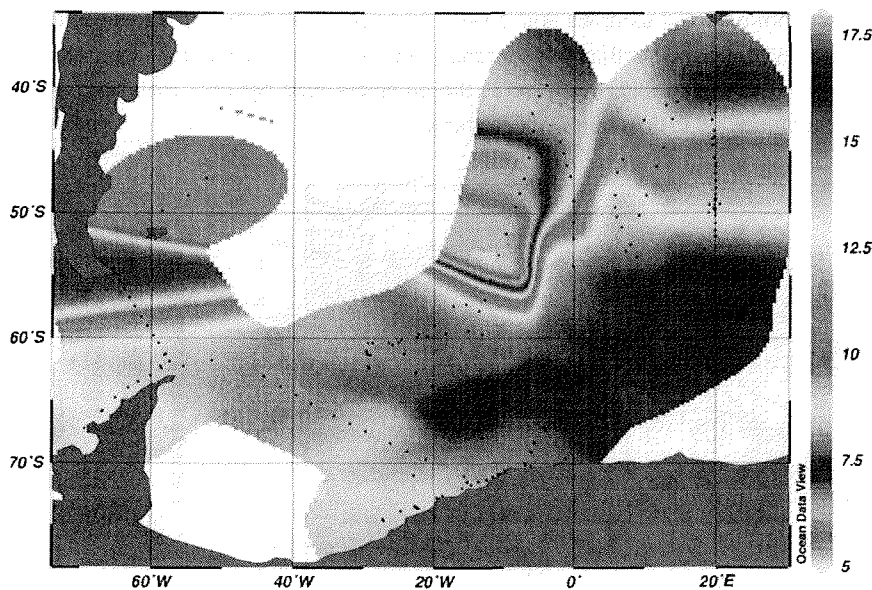


Fig. 21: Contour plot of ^{226}Ra (dpm/100kg) surface water activities in the Atlantic sector of the Southern Ocean. The sharp gradient and the extremely low values at 58° S / 15° W are most likely the result of an analytical problem.

A contour plot reveals a strong surface maximum in the southeastern corner of the Weddell Gyre that stretches westwards at approximately 65° S into the central gyre (Fig. 21). This pattern can be ascribed to the upwelling of Circumpolar Deep Water (CDW) which enters the Weddell Gyre in the East (Orsi et al. 1993, Schröder and Fahrbach 1999).

Although subject to regional variations, the data set is in good agreement with existing literature values. Ku and Lin (1976) report a ^{226}Ra activity of 8 dpm/100kg for SASW in the South Atlantic while Antarctic Surface Water (AASW) has been described with activities ranging from 13 to 19 dpm/100kg with a mean of 17 dpm/100kg (Chung and Applequist 1980, Chung 1981).

5.2 Surface water activities of ^{228}Ra

The present data set constitutes a considerable extension of existing ^{228}Ra in the Atlantic sector of the Southern Ocean. Both sides of the Antarctic Peninsula, the southern Argentinean shelf, the central Weddell Gyre and the Agulhas (Return) Current have for the first time been sampled for ^{228}Ra . A discrete 20 l subsample could not be taken with every sample (see chapter 4.1.3). In this case, the ^{226}Ra concentration of these samples has been calculated on the basis of existing literature values or estimated from adjacent samples and is listed in Appendix A 7. The ^{228}Ra values in the area of investigation fall within a wide range with activities from below the detection limit to 4.37 dpm/100kg. Fig. 22 presents the complete data set of ^{228}Ra activities that has been determined in the course of this study.

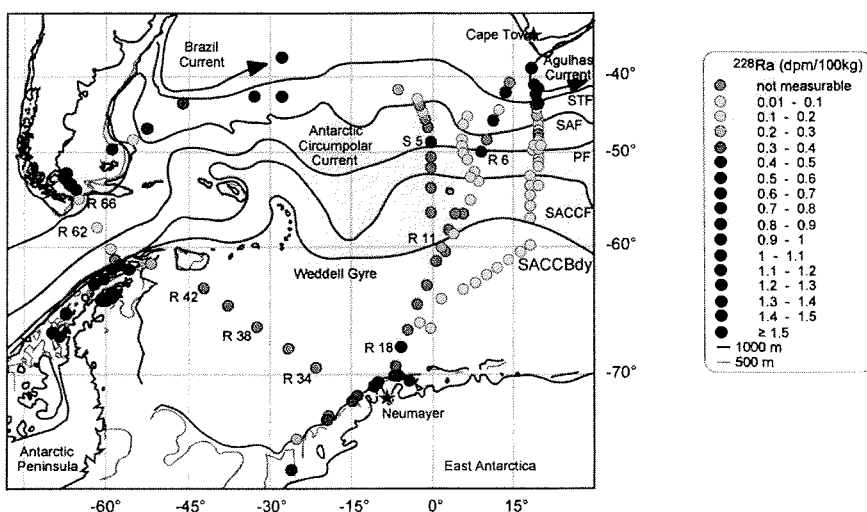


Fig. 22: Surface water activities of ^{228}Ra (dpm/100kg) determined in this study in the Atlantic sector of the Southern Ocean. Approximate positions of the oceanic fronts after Orsi et al. (1995). For abbreviations see Fig. 20.

5.2.1 Shelf regions

Literature values for ^{228}Ra shelfwater activities have so far only been available for the East Antarctic coastline (Kaufman et al. 1973, Rutgers van der Loeff 1994). The ^{228}Ra activity has been determined in hitherto unsampled areas like the southern Argentinean shelf, the Larsen shelf and the Bransfield Strait and covers for the first time all landmasses that border the Atlantic sector of the Southern Ocean. In the following, the Pacific side of the Antarctic Peninsula will be treated as part of the South Atlantic due to the direct link maintained between both by the ACC.

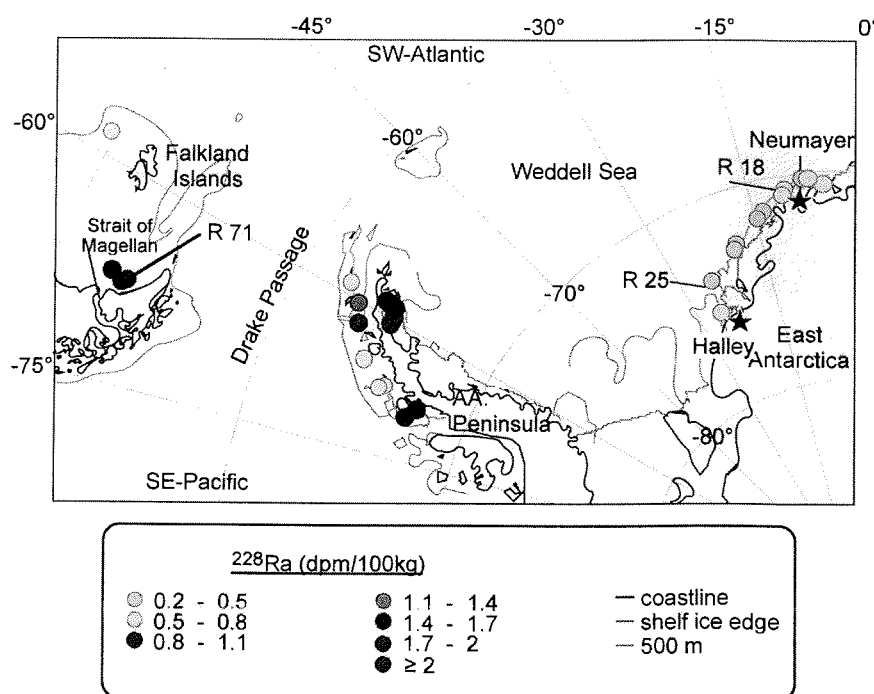


Fig. 23: Surface water activities of ^{228}Ra (dpm/100kg) of the shelf regions of the Atlantic sector of the Southern Ocean. Results obtained along the Antarctic Peninsula are enlarged in Fig. 24.

Any significant open ocean signal of ^{228}Ra requires a strong nearshore source that allows an accumulation of high activities in the water mass before being advected away from coastal regions. A screening of the shelf regions was meant to prove that these shallow water regions could indeed act as a source for ^{228}Ra . Fig. 23 shows the surface water activities of ^{228}Ra for the shelf areas of southern South America, the Antarctic Peninsula and East Antarctica. They cover a range from 0.23 to 3.7 dpm/100kg with the lowest values on the East Antarctic (R 25) and the highest on the Argentinean shelf (R 71). All sampled shelf regions bordering the Atlantic sector of the Southern Ocean

yield clearly elevated, well measurable ^{228}Ra activities up to 3.7 dpm/100kg and can thus be considered as source regions for this isotope.

The mean activity at the entrance to the Strait of Magellan where three samples have been taken is 2.78 dpm/100kg. Another measurement north of the Falkland Islands at the continental shelf edge yields 1.57 dpm/100kg.

Along the East Antarctic coast between Neumayer Base and Halley Base, eleven samples have been determined for their ^{228}Ra content and gave activities between 0.23 and 0.71 dpm/100kg with a mean of 0.49 dpm/100kg. North of 73° S, these values agree well with previous measurements by Rutgers van der Loeff (1994) who reported ^{228}Ra activities of about 0.6 dpm/100kg for this area³. Further south, his activities³ increase to 2.17 dpm/100kg.

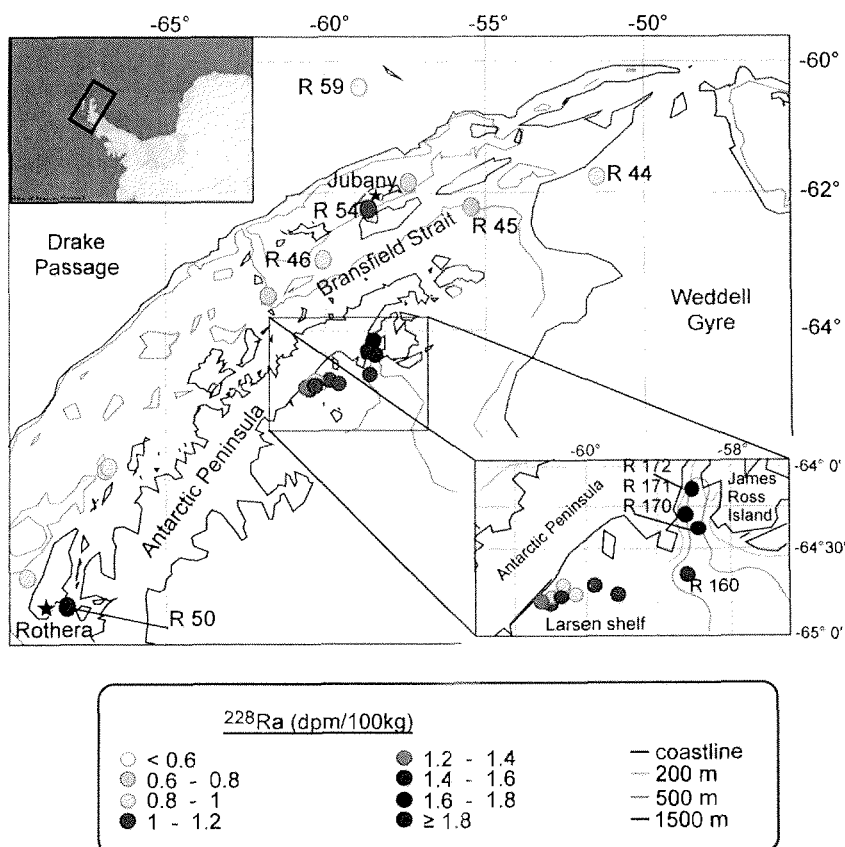


Fig. 24: Surface water activities of ^{228}Ra (dpm/100kg) along the Antarctic Peninsula. The box gives an enlargement of the activities on the Atlantic side with the Larsen shelf.

³ The unity in the original literature is dpm/m³. For means of comparison, this value has been converted to dpm/100kg by assuming an average weight of sea water of 1.033 kg/l.

A more detailed view of samples collected along the Antarctic Peninsula is given in Fig. 24. They are characterized by generally higher ^{228}Ra activities than those along the East Antarctic coast.

On the whole, 23 samples have been collected along the Peninsula's coast line. Within this set of data, the eastern (Atlantic) side of the Peninsula displays generally higher values than the western (Pacific) side. On the latter, ^{228}Ra activities in the Bransfield Strait and its southward extension are very uniform with a mean of 0.79 dpm/100kg. Two clearly elevated exceptions have been measured in sheltered bays of Adelaide Island in the vicinity of the Rothera Base (R 50) and in the Potter Cove next to Jubany (R 54), with values of 1.99 dpm/100kg and 1.12 dpm/100kg, respectively. Activities on the Atlantic side of the Peninsula range from 0.59 to 1.77 dpm/100kg with a mean of 1.16 dpm/100kg. In the restricted bay between James Ross Island and the main land, activities double between sample R 160 and R 172 (enlargement of Fig. 24). The elevated ^{228}Ra concentrations are closely centred around the Antarctic Peninsula and decrease rapidly beyond: at sample R 44, located close to the Weddell-Scotia-Confluence (WSC), the activity drops to 0.23 dpm/100kg. On the northeastern side, R 59 (0.07 dpm/100kg) displays background levels that are typical for the Drake Passage.

The values on the shelves of the Peninsula are congruent with other Antarctic shelf regions (Kaufman et al. 1973, Rutgers van der Loeff 1994).

5.2.2 Open ocean waters

The waters entering the South Atlantic through the Drake Passage have not been in contact with ^{232}Th -bearing sediments for a long time, so one would expect very low ^{228}Ra activities. Both R 59 and R 62 have a low, but still distinctive activity of 0.07 and 0.02 dpm/100kg, respectively (Fig. 25). A northward increase can be observed between R 66 which is situated at the northern rim of the Drake Passage and R 71 that was taken on the Argentinean shelf.

A SW-NE-transect (R 200 – R 207) at subtropical latitudes through the Argentine Basin yields increased ^{228}Ra activities in the western open South Atlantic (Fig. 25). Activities are lower than on the Argentinean shelf but, with the exception of R 202, stay an order of magnitude higher than open ocean values of the ACC (see below). R 207 comes closest to shelf activities and is expected to display the influence of the Brazil Current. The northward steering of the ACC is mirrored in the ^{228}Ra activities as could already be shown for ^{226}Ra . A plot of both ^{226}Ra and ^{228}Ra activities together with sea surface temperatures locates R 202 in the core of the north-directed loop of the ACC (Fig. 25 and Fig. 26). It is characterized by a sharp drop in temperature while ^{226}Ra and ^{228}Ra concentrations show an opposite pattern: the loop entrains subpolar waters with a higher ^{226}Ra signal, gained from the upwelling of CDW within the ACC. In contrast, the enveloping waters carry the imprint of the Argentinean shelf and slope, indicated by an about similar enrichment in ^{228}Ra east and west of R 202. ^{228}Ra activities along the

Distribution of radium in the South Atlantic

whole transect cover a range from 0.09 to 1.57 dpm/100kg and are comparable to the values published by Li et al. (1980).

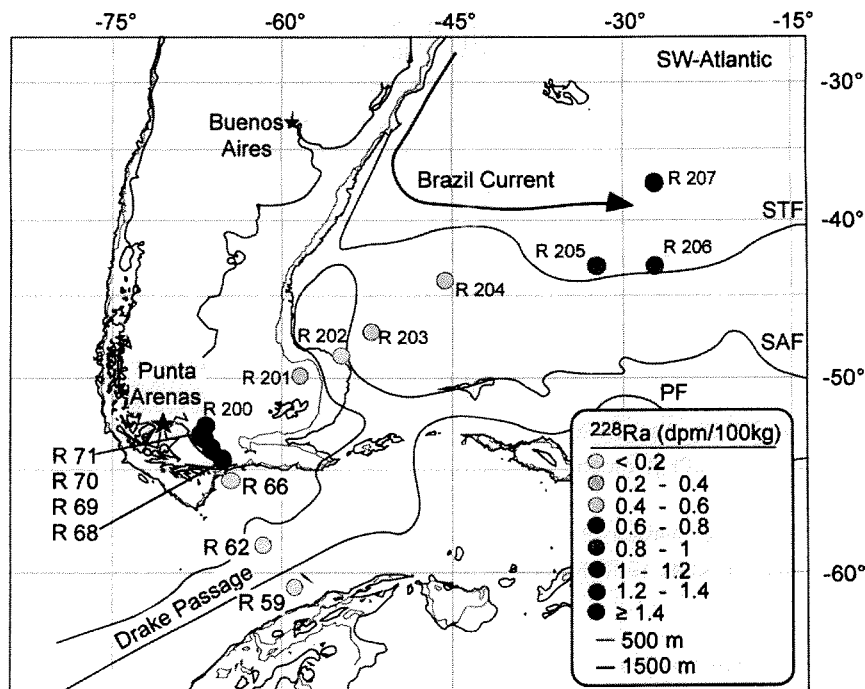


Fig. 25: Surface water activities of ^{228}Ra (dpm/100kg) in the Drake Passage and in the western South Atlantic. Approximate positions of the oceanic fronts after Orsi et al. (1995). For abbreviations see Fig. 20.

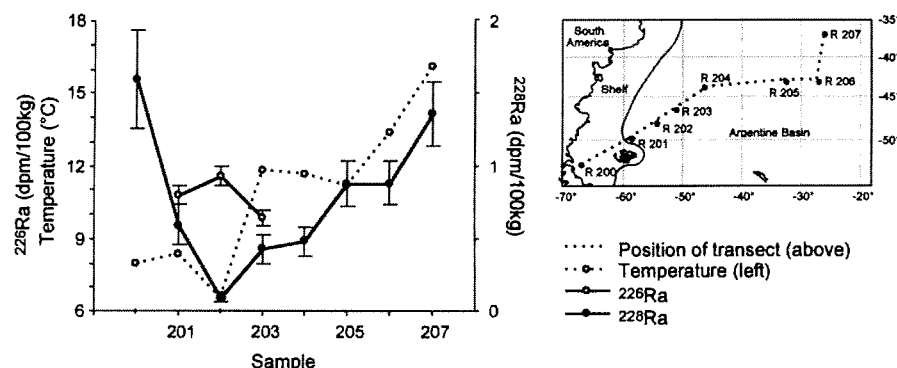


Fig. 26: Left: Surface water activities of ^{226}Ra and ^{228}Ra and sea surface temperature on a SW-NE-transect (samples R 200 – R 207) in the Argentine Basin. Right: Geographical position of the transect.

N-S-transects from South Africa to the Antarctica are characterized by high ^{228}Ra activities at their northern end. An enlargement of the situation south of Africa is given in Fig. 27. Between the continent and the Subtropical Front (STF), sampling points are influenced by the Agulhas and Agulhas Return Current that are responsible for activities as high as 4.23 dpm/100kg (R 151). South of the STF, activities drop back to an average of 0.2 dpm/100kg. Kaufman et al. (1973) report an activity of 0.3 dpm/100kg east of the Agulhas retroreflection area while values for the Agulhas regime proper have hitherto not been published. High subtropical activities up to 2.1 dpm/100kg at 60° E in the Indian Ocean (Fig. 10; Sarmiento 1988) are likely to originate from the Agulhas Return Current.

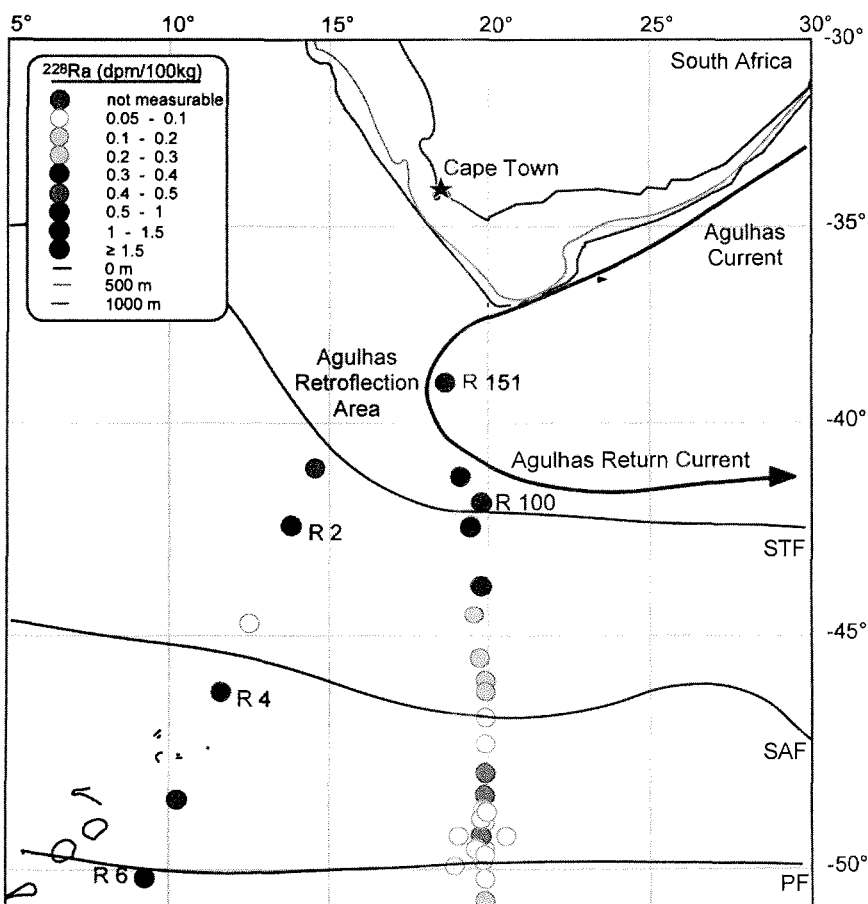


Fig. 27: Surface water activities of ^{228}Ra (dpm/100kg) south of Africa at subtropical and subpolar latitudes. Approximate positions of the oceanic fronts after Orsi et al. (1995). For abbreviations see Fig. 20.

In the open ACC waters (Fig. 22), concentrations are uniformly low with activities generally less than 0.1 dpm/100kg but some higher values can be seen. It must be stressed that the sampling volume during the ANT XV expeditions was lower than during ANT XVI/3 (20° E transect) which probably explains the higher number of samples below the detection limit in the former transects. The most conspicuous feature in the ACC are samples S 5 and R 6 that besides sample R 151 exhibit the highest ^{228}Ra activities determined in this study (4.37 and 4.23 dpm/100kg, respectively). Both correspond with the approximate position of the Polar Front (PF) in the respective cruises. At 60° S, sample R 11 has a clearly elevated activity (0.22 dpm/100kg) while the adjacent samples are below the detection limit. The signal coincides approximately with the Weddell Gyre Boundary. A pronounced maximum (R 16) is detectable at 68° S with 2.65 dpm/100kg. Rutgers van der Loeff (1994) reports activities up to 0.8 dpm/100kg for a position six degrees further east than R 16 which represents equally an enrichment compared to his own neighbouring concentrations.

Disregarding samples R 11 and R 16, ^{228}Ra activities in the Weddell Gyre (Fig. 22) are comparably low like in the open ACC waters which is in agreement with findings by Li et al. (1980) who reported all GEOSECS measurements south of the PF to be less than 0.1 dpm/100kg. All samples on a transect through the central part of the gyre (R 34 – R 42) were below the detection limit, indicating that horizontal mixing from the shelf towards the open ocean must be slow compared to the half-life of ^{228}Ra . Rutgers van der Loeff (1994) pointed out that the shelfwater influence in this region could not be traced far offshore. However, it should be noted that from samples R 38 and R 42 only the first cartridge was processed so that the overall efficiency of these two samples was considerably lower than usually. Based on the measurements in this study, the central Weddell Gyre represents a region with the lowest ^{228}Ra activities worldwide.

5.3 Surface water activities of ^{228}Th

In addition to the ^{228}Ra activity, the initial⁴ dissolved ^{228}Th content was determined on selected samples from expeditions ANT XV/2 and ANT XVI/3. The $^{228}\text{Th}/^{228}\text{Ra}$ (activity ratio) AR has been used for the determination of scavenging rates in the ocean (Moore 1969a, Broecker et al. 1973, Li et al. 1980). In the view of the ^{228}Th -ingrowth method that requires long storage times before final ^{228}Ra activities become available, it might be useful to examine whether ^{228}Th can serve as a more rapidly-available indicator of the ^{228}Ra activity. The $^{228}\text{Th}/^{228}\text{Ra}$ AR in a water mass that is in contact with a ^{228}Ra source should be close to unity as long as scavenging processes can be neglected. Once the water mass is cut off from its source, both radionuclides decline with their respective half-lives. After about 15 years, the $^{228}\text{Th}/^{228}\text{Ra}$ AR reaches a transient equilibrium of about 1.5. In the surface ocean, in coastal waters or close to bottom

⁴ In this context, "initial" refers to the in situ ^{228}Th activity of a sample and is used to avoid confusion with the ^{228}Th activity determined after ingrowth from ^{228}Ra (see chapter 4.3.2).

sediments, where scavenging becomes important, the $^{228}\text{Th}/^{228}\text{Ra}$ ratio is always far below unity (Broecker and Peng 1982). Rutgers van der Loeff (1994) has shown that indeed ^{228}Ra can be measured through its granddaughter ^{228}Th in intermediate circumpolar waters. The question arises to what extent the initial ^{228}Th content in open ocean surface waters, can be used as an indication for ^{228}Ra activities.

Fig. 28 and Fig. 29 show the activities of both nuclides in the dissolved fraction between 45 and 70° S determined on expeditions ANT XV/2 and ANT XVI/3. The highest values within the Agulhas regime have been omitted for a better presentation of differences within the lower activities. With two exceptions, the ^{228}Th activity in both sections is consistently lower than the respective ^{228}Ra activity which is what would be expected from a particle reactive element. Accordingly, the $^{228}\text{Th}/^{228}\text{Ra}$ AR are well below unity. A similar finding is reported for the $^{234}\text{Th}/^{238}\text{U}$ AR which also consists of a mobile parent and a particle reactive daughter (Usbeck et al. in press).

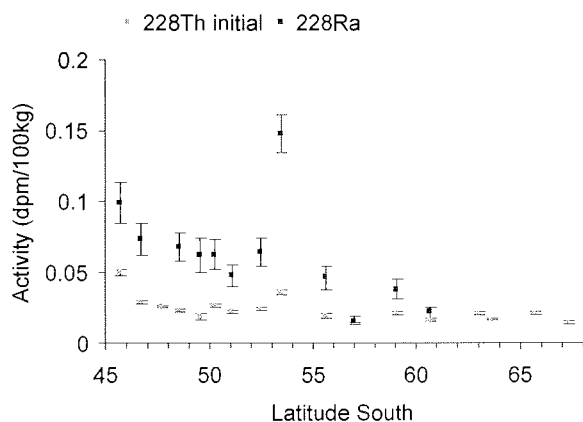


Fig. 28: Activities of ^{228}Ra and of the initial dissolved ^{228}Th content during expedition ANT XV/2. ^{228}Ra activities are not available for the whole transect.

The general features of the ^{228}Ra distribution with increased activities in the vicinity of the African and the Antarctic continent and uniformly low activities in between are nevertheless maintained in the ^{228}Th concentrations. If plotted against each other, it can be shown that on both expeditions higher ^{228}Ra coincide with higher ^{228}Th activities (Fig. 30) and that a qualitative relationship between both radionuclides exists in surface waters of the Southern Ocean. Hence, in principle, ^{228}Th can be used as a qualitative indicator of the ^{228}Ra activity. As a strongly particle-reactive nuclide, it is, however, subject to scavenging processes that in turn can vary widely in a given area. The effect will be looked closer at in chapter 6.2.

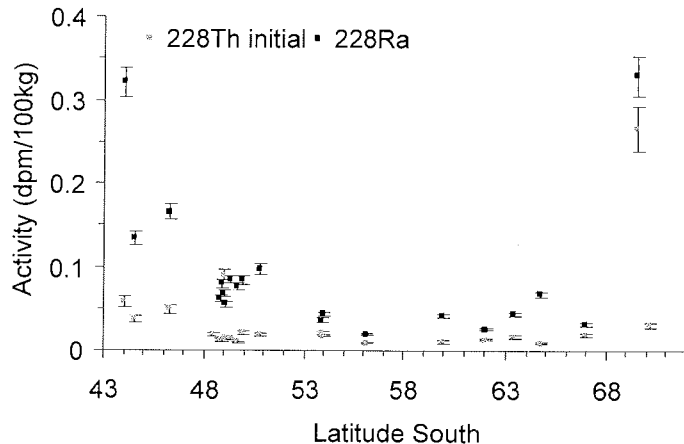


Fig. 29: Activities of ^{228}Ra and of the initial dissolved ^{228}Th content during expedition ANT XVI/3. High values north of 44° S have been omitted to ensure a better resolution but are included in Fig. 30.

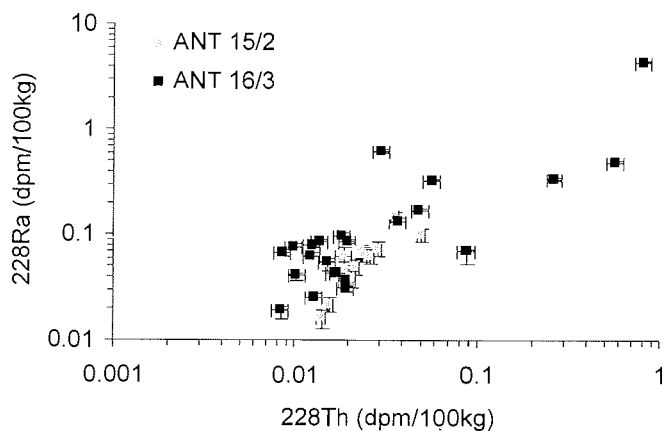


Fig. 30: Surface water activities of ^{228}Ra plotted against initial dissolved ^{228}Th activities for all samples collected during expeditions ANT XV/2 and ANT XVI/3.

5.4 Vertical distribution of ^{226}Ra and ^{228}Th within the ACC and the Weddell Gyre

A vertical section with a total of eight stations covering the upper 1000-1800 m of the water column has been sampled at 20° E during expedition ANT XVI/3. The hydrographic situation between 44° and 60° S during that cruise is displayed in Fig. 32. The oceanic fronts of the ACC cause a crowding of the isotherms north of 50° S while the downwelling Antarctic Intermediate Water (AAIW) is illustrated by a salinity

minimum at about 500 m. The upwelling of CDW is illustrated by the southward shoaling of the isohalines.

^{226}Ra activities from intermediate and deep waters have been determined on twelve samples of this N-S-transect through the ACC. The values range from 8.85 to 18.45 dpm/100kg and are sorted by water masses in Table 4. All results are in good agreement with ^{226}Ra activities from GEOSECS stations 89, 91 and 93 (Ku and Lin 1976). Subsurface activities in the SASW and AASW display a north-to-south enrichment and are consistent with the surface activities presented in chapter 5.1 and Fig. 20. The intermediate water masses mirror the thermohaline circulation in the South Atlantic with higher values in deeper waters. Highest concentrations averaging 18 dpm/100kg are found in the CDW and the derived Warm Deep Water (WDW) in the Weddell Gyre. The vertical distribution of ^{226}Ra (not shown due to paucity of data points) is in support of the observed surface water maximum in the southeastern part of the Weddell Gyre (Fig. 21).

Table 4: ^{226}Ra activities from intermediate and deep waters compared with GEOSECS stations (Ku and Lin 1976). Circumpolar Deep Water comprises also the Warm Deep Water in the Weddell Gyre.

Water mass	^{226}Ra activity this study (dpm/100kg)	^{226}Ra activity GEOSECS (dpm/100kg)
Subantarctic Surface Water	8.85, 10.85	8.1 – 10.6
Antarctic Surface Water	16.43	14.9 – 18.6
Antarctic Intermediate Water	11.78 – 15.47	15.7 – 16.8
Circumpolar Deep Water	15.98 – 18.45	16.6 – 19.7

^{228}Ra activities are not yet available for the deep water stations. The samples have been set to zero with respect to thorium and are currently stored to allow the ingrowth of a new generation of ^{228}Th that will allow the calculation of the ^{228}Ra activity which will be published elsewhere when available. Absolute concentrations of ^{228}Th are also not available due to the lack of a suitable yield tracer (see chapter 4.3.3). Instead, ^{230}Th is used as a qualitative reference for ^{228}Th . Therefore, the activities determined in the course of this study are reported as total $^{228}\text{Th}/^{230}\text{Th}$ AR. The following considerations will show to what extent the $^{228}\text{Th}/^{230}\text{Th}$ AR is suitable for a qualitative assessment of the ^{228}Ra distribution.

^{230}Th is produced at well-known rates in the water column through decay of ^{238}U . Its total concentration generally increases with depth (Bacon and Anderson 1982). Within the upper 1000 m, the increase is approximately by a factor of two (Rutgers van der Loeff and Berger 1993, Walter et al. 1997). $^{228}\text{Th}/^{230}\text{Th}$ AR determined in this work in contrast decrease by a factor of 2.6-13.5 over the same vertical distance. Hence, decreasing $^{228}\text{Th}/^{230}\text{Th}$ AR are in part due to the known increase in ^{230}Th . The remaining ^{228}Th signal accounts for a 1.3 to 5.5-fold decrease with depth.

Reported ^{230}Th activities also increase threefold at a given depth from north to south across the ACC into the Weddell Sea (Walter et al. 1997, Walter et al. 2001). At

subsurface levels, measured $^{228}\text{Th}/^{230}\text{Th}$ AR decrease by a factor of 0.5-3.6 from north to south which is less or about the same as the expected increase in ^{230}Th . Only in surface waters is the $^{228}\text{Th}/^{230}\text{Th}$ AR clearly dominated by the ^{228}Th activity: within the ACC, the ratio decreases by a factor of twelve from north to south.

In summary it can be said that the $^{228}\text{Th}/^{230}\text{Th}$ AR is a valuable indicator of ^{228}Th activity changes on a vertical scale but less useful for the detection of latitudinal changes between different profiles. As a qualitative indicator of the ^{228}Ra activity, the $^{228}\text{Th}/^{230}\text{Th}$ AR can safely be used when the variation in $^{228}\text{Th}/^{230}\text{Th}$ AR is greater than the expected variation in ^{230}Th activity. This is the case here within given profiles but not always between different profiles. However, while awaiting the ingrowth of ^{228}Th in the stored samples, preliminary information about the vertical distribution of the tracer ^{228}Ra can be drawn from the $^{228}\text{Th}/^{230}\text{Th}$ AR.

A plot of all stations from a vertical section at 20° E down to a water depth of 1800 m shows that the main differences in the AR are located in the upper 500 m (Fig. 31). Two groups can be distinguished on the grounds of their $^{228}\text{Th}/^{230}\text{Th}$ AR in the top 500 m: stations 169, 190 and 197 south of the PF have $^{228}\text{Th}/^{230}\text{Th}$ AR of less than 2. Stations 206, 156 and 161, located at and north of the PF, display high AR between 3 and 6. The difference between both groups matches well with the north to south increase of ^{230}Th ; however, this cannot be seen below 500 m where both groups have a mean $^{228}\text{Th}/^{230}\text{Th}$ AR of 0.6. Stations 207 and 182, the northern- and southernmost stations of the transect, are distinctive from both groups. Station 207 yields an extremely high AR in the upper 200 m and station 182 displays a subsurface maximum. For station 182, the hydrographical data evidenced a mixed layer down to 600 m due to recent ice formation.

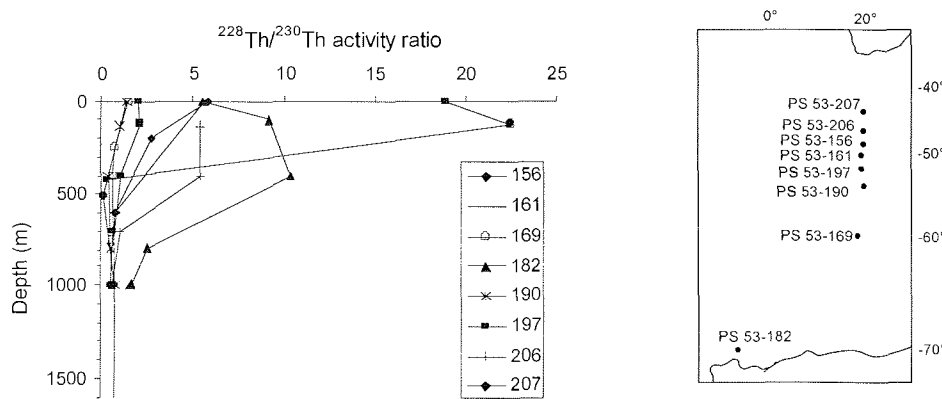


Fig. 31: Left: Vertical profiles of $^{228}\text{Th}/^{230}\text{Th}$ activity ratios on a N-S-transect across the ACC at 20°. Right: Position of stations during expedition ANT XVI/3.

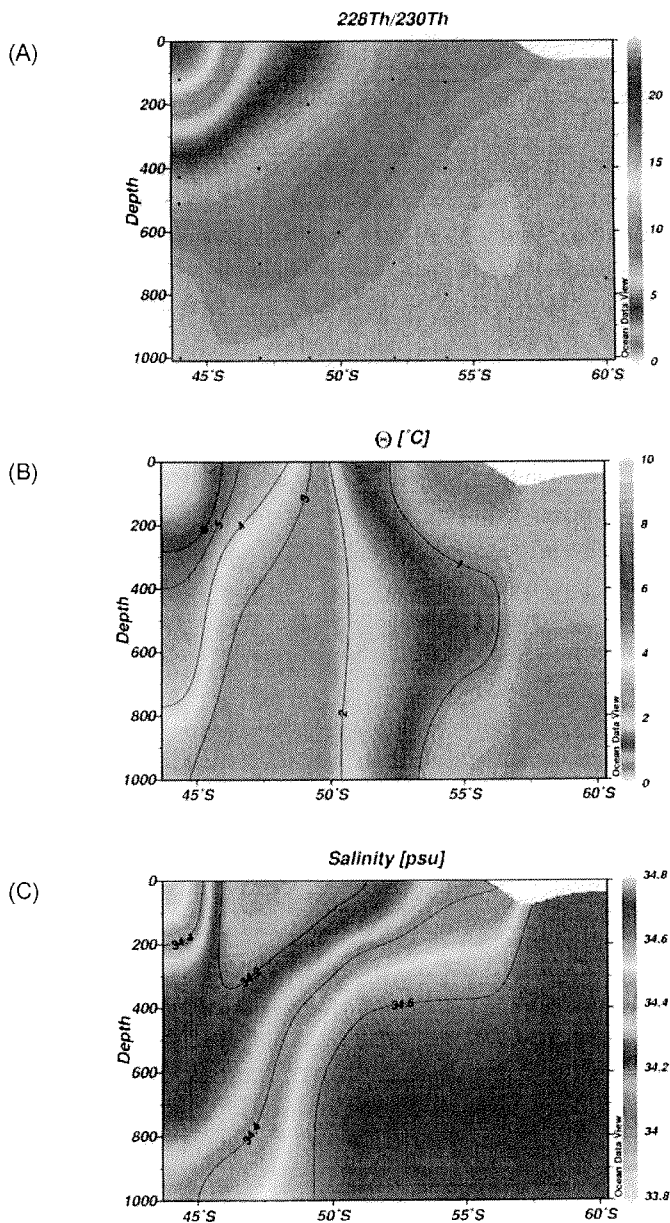


Fig. 32: Vertical section of the upper 1800 m water layer at 20° E sampled during expedition ANT XVI/3. (a) $^{228}\text{Th}/^{230}\text{Th}$ activity ratios. (b) Potential temperature. (c) Salinity. T-S-data kindly provided by Dr. V.Strass, AWI.

Between 40° and 60° S, a contour plot against depth shows the highest values for the $^{228}\text{Th}/^{230}\text{Th}$ AR north of the PF (Fig. 32a).

As discussed above, the distribution of the $^{228}\text{Th}/^{230}\text{Th}$ AR is used as a qualitative indication of the distribution of ^{228}Ra , under consideration of the uncertainty associated with the variable natural ^{230}Th activity.

The distribution pattern of the AR in surface waters agrees with the measured distribution of ^{228}Ra with highest concentrations north of 50° S (see chapter 5.2.2). The mean decrease of the $^{228}\text{Th}/^{230}\text{Th}$ AR with depth by a factor 8 must be considered a lower estimate for decrease of ^{228}Ra activities with depth because a stronger depletion of ^{228}Th due to scavenging has to be expected in surface waters compared to deep waters (Usbeck et al. in press).

Thus, the large variations in the $^{228}\text{Th}/^{230}\text{Th}$ AR with depth allow the conclusion that the enhanced ^{228}Ra concentrations found at the sea surface north of the PF (see chapter 5.2.2) are limited to shallow water masses. This observation confirms the expectation that ^{228}Ra is indeed supplied by a shallow source, like continental shelves are. In contrast, ^{226}Ra was found highest in upwelling CDW, thus underlining the deep sea source of this isotope.

6 BIOGEOCHEMISTRY OF RADIUM AND THORIUM IN THE SOUTH ATLANTIC

6.1 Bio-intermediate behaviour of radium in the upper ocean

^{226}Ra has been considered as a water mass tracer with a nutrient-like distribution due to its participation in the biogeochemical cycle (Broecker et al. 1967; see also chapter 3.2).

Based on the similarity of vertical water column profiles of ^{226}Ra and Si, it has been hypothesised that siliceous tests act as a main carrier phase for ^{226}Ra (Edmond 1970, Ku et al. 1970, Ku and Lin 1976). However, direct evidence for incorporation of ^{226}Ra by silicate-forming plankton is very scanty and yields ambiguous results. Szabo (1970) gives a list of ^{226}Ra activities in different plankton samples and shows that radium is preferred by plankton with respect to calcium. The associated discrimination factor D:

$$D_{\text{Ca}}^{\text{Ra}} = \frac{\left(\frac{\text{Ra}}{\text{Ca}}\right)_{\text{pl}}}{\left(\frac{\text{Ra}}{\text{Ca}}\right)_{\text{sw}}}$$

pl: plankton

sw: sea water

is highest for a diatom sample. Shannon and Cherry (1971) report an enrichment of ^{226}Ra in the diatoms *Rhizosolenia* and *Chaetoceras*. In contrast, a controlled tank experiment performed with the diatom *Thalassiosira pseudonana* did not indicate any significant bioaccumulation of ^{226}Ra (Fisher and Teyssié 1987).

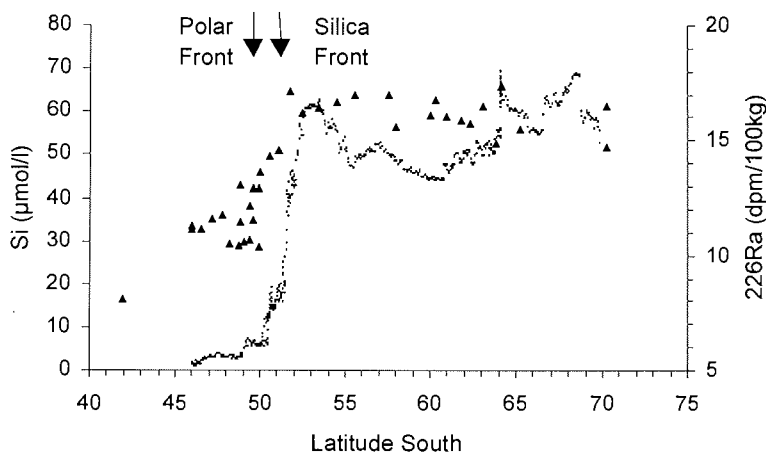
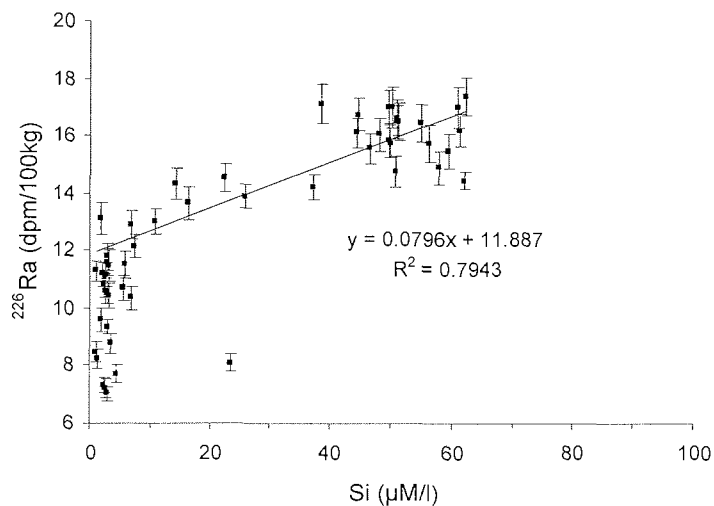


Fig. 33: Concentrations of Si ($\mu\text{mol/l}$; dots) and ^{226}Ra (dpm/100kg; triangles) in surface waters on a N-S-transect across the ACC in austral summer during expedition ANT XVI/3. The broad range of Si values at 64° S is caused by a W-E-section in the cruise track. Si data kindly provided by C.Hartmann, AWI.

Correlations between ^{226}Ra and Si have been given by various authors but are all characterized by a large scatter of the data (Broecker et al. 1976, Ku and Lin 1976, Chung 1980, Chung and Applequist 1980, Chung 1987). The weakest relationships are reported for surface waters. In the following, the ^{226}Ra -Si-relationship will be examined for samples of the present study.

The concentrations of Si and ^{226}Ra in surface waters across the Antarctic Circumpolar Current (ACC) on the southward transect during expedition ANT XVI/3 are given in Fig. 33. Both elements covary in a sense that they show a clear N-S-gradient with highest values in the south. The main increase in ^{226}Ra concentration occurs about 2° of latitude further north than that of Si. The sharp gradient in Si has also been referred to as the "Silica Front" (van Bennekom et al. 1988) and is found 200-300 km south of the oceanic Polar Front (PF). Local variations in the Si concentrations are not mirrored by ^{226}Ra and indicate a decoupling between diatom productivity and ^{226}Ra distribution in the Southern Ocean. It should be noted that Si has been determined on discrete samples while most of the ^{226}Ra activities come from mixed-water samples that were bottled over approximately 6 hours steaming time (see chapter 4.1.3).



more apparent. Concentration of both ^{226}Ra and Si in surface waters are affected by biological uptake which does not happen in a constant ratio over a given transect (see also chapter 6.1.1). Hence, a relatively poor relationship is what would be expected. The correlation given in Fig. 34 is calculated for samples with a ^{226}Ra activity of 11 dpm/100kg or more which is about the activity in the subantarctic zone.

Samples taken below the mixed layer exhibit a better correlation between both parameters (Fig. 35). In the upwelling regime of the Circumpolar Deep Water (CDW), ^{226}Ra and Si can be considered as quasi-conservative as biological cycling is shallow (Usbeck et al. in press) and the loss of ^{226}Ra by radioactive decay negligible compared to the upwelling velocity.

A slope of 0.073 dpm/100kg/ $\mu\text{mol/l}$ of the correlation in Fig. 35 indicates an increase of 1.2×10^{-11} g of ^{226}Ra for every gram of Si which is identical to the slope given by Ku and Lin (1976).

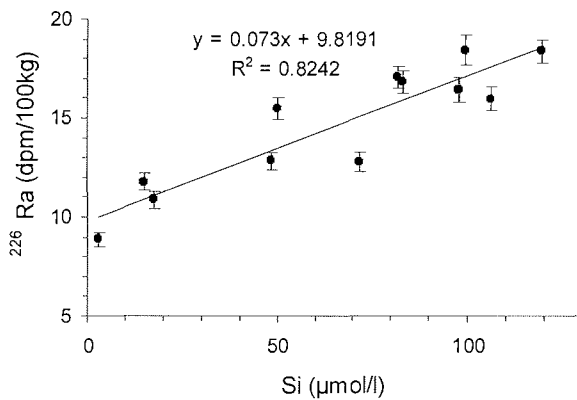


Fig. 35: ^{226}Ra (dpm/100kg) versus Si ($\mu\text{mol/l}$) from intermediate and deep water samples taken during expedition ANT XVI/3.

The surface water plots indicate that the relationship between ^{226}Ra and Si turns out to be much poorer than previously thought and that different factors must control their distribution in circumpolar waters. A mechanism of incorporation of radium ions into siliceous tests has never been described in detail. Looking at the size of the respective ions, 0.4 Å for Si^{4+} and 1.5 Å for Ra^{2+} , there are reasons for the assumption that incorporation of radium into siliceous tests and hence a direct influence of diatom productivity on the radium distribution plays a rather minor role. Adsorption like for thorium isotopes can be excluded due to the low particle-reactivity of radium. More promising in terms of similar ion radii are Sr^{2+} and Ba^{2+} with 1.1 and 1.3 Å, respectively. Frequently occurring substances in the marine environment built from these elements are celestite (SrSO_4) and barite (BaSO_4).

In this context, the relationships for ^{226}Ra -Ba are much more convincing than those for ^{226}Ra -Si (Li et al. 1973, Chan et al. 1976). Biogenic barite formation has been proposed as an important parameter in the marine radium cycle. As the upper ocean is mostly undersaturated with respect to barite (Monnin et al. 1999), its formation is thought to take place in organic-rich microenvironments (Chow and Goldberg 1960, Dehairs et al. 1980, Bishop 1988). The similarity of vertical particulate Ba profiles and O₂-consumption rates underlines the importance of decaying organic matter in the process of barite formation at mesopelagic depths (Dehairs et al. 1997).

6.1.1 The role of acantharians for the biogeochemistry of radium

Recently, the investigation of acantharians, SrSO₄-forming radiolarians, has shed new light on the biogeochemistry of Ba (Bernstein et al. 1998). Acantharians are abundant in the oceans and frequently outnumber radiolarians and foraminifera (Beers et al. 1975, Michaels 1988, Michaels et al. 1995). In plankton studies, acantharians are often underestimated or even overlooked due to sampling techniques that do not assure a preservation of their easily dissolvable SrSO₄ skeletons or cysts (Bernstein and Betzer 1991). Most of the sampled acantharians are found in the upper 400 m of the water column, a finding that is matched by lower Sr/Cl ratios as compared to greater water depths (Bernstein et al. 1992). The celestite contains considerable amounts of Ba with distribution coefficients D_{Sr}^{Ba} between celestite and sea water

$$D_{\text{Sr}}^{\text{Ba}} = \frac{(\frac{\text{Ba}}{\text{Sr}})_{\text{cl}}}{(\frac{\text{Ba}}{\text{Sr}})_{\text{sw}}}$$

cl: celestite

sw: sea water

well above unity and has been ascribed a major role in the depletion of Ba from the upper water column (Bernstein et al. 1992, Bernstein et al. 1998). Upon dilution of the skeletons and cysts, Sr is quickly recycled as seen from vertical water profiles. Microenvironments seem to favour a reprecipitation of Ba as barite, e.g. after ingestion of celestite by zooplankton. This is supported by the observation that barite is a frequent component of fecal pellets while celestite is completely absent (Bernstein et al. 1992). The mineralization-dissolution-mineralization process of celestite and barite enhances the relative enrichment of Ba in particles with respect to ambient sea water concentrations. On the basis of these observations and the fact, that radium is commonly coprecipitated with BaSO₄, it can be inferred that the biogeochemistry of radium is equally affected by acantharians. Considering the solubility products of SrSO₄ ($\log K_{\text{SP}} = -6.5$), BaSO₄ ($\log K_{\text{SP}} = -10.0$) and RaSO₄, ($\log K_{\text{SP}} = -10.4$), the distribution coefficient of radium D_{Sr}^{Ra} with respect to Sr should be about equally large as that for Ba. For thermodynamical reasons, precipitation in a solid-solution-aqueous-solution

system will lead to an enrichment of the less soluble element in the precipitate. However, no direct determination of $D_{\text{Sr}}^{\text{Ra}}$ has hitherto been reported for acantharians that could corroborate these theoretical considerations.

Acantharian cysts have been described in the Weddell Sea by Spindler and Beyer (1990) with an associated distribution coefficient $D_{\text{Sr}}^{\text{Ba}}$ of 2.3 (Bernstein et al. 1998). For the open ACC, their abundance ranges from 1000 to 30000 individuals per m³ (Henjes pers. comm. 2001). General distribution patterns indicate an increase of acantharians from the polar to the temperate ocean (Bernstein et al. 1999). Hence, north of the PF, acantharians must be assumed to gain importance in the marine productivity cycle and could be responsible for the continuing depletion of ²²⁶Ra after the exhaustion of Si.

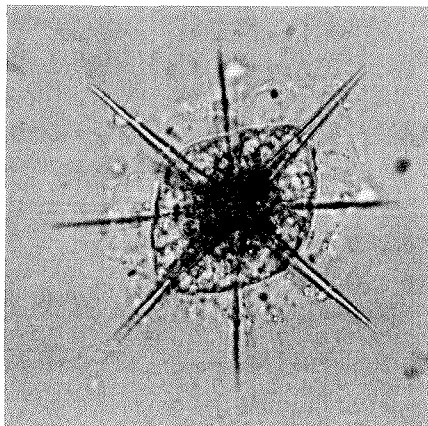


Fig. 36: Acantharia from the Southern Ocean. Radial spicules are clearly visible. Picture taken by U. Freier, AWI.

The conclusion put forth here is that the distribution of ²²⁶Ra and Si are decoupled in circumpolar surface waters. Formation of barite from decaying biogenic debris and biomineralization of SrSO₄ by acantharians seem to be a more favourable explanation for a radium depletion in the upper water column than a direct link with diatom productivity. The fact that microenvironments, where biogenic barite formation takes place, are often created and controlled by decomposing diatom aggregates (Dehairs et al. 1980, Bishop 1988, Dehairs et al. 1997) might feign a linear relationship between ²²⁶Ra and Si concentrations. High resolution sampling across the ACC has shown that the main concentration gradients of both elements are separated by about 2° of latitude and that their covariance is rather qualitative.

6.1.2. Implications for radium analytics

From an analytical point of view, the question arises to what extent ²²⁶Ra can be estimated from Si concentrations. Based on the relationships established in Fig. 34 and Fig. 35, ²²⁶Ra activities have been calculated from Si concentrations and compared

with measured activities. For surface water samples, the measured activities deviate by up to 75% from the calculated activities. (Fig. 37). Largest uncertainties are found for samples north of the PF where the calculated activities tend to overestimate. Within the Weddell Sea, errors are at about 15% and are less biased. The errors associated with samples from intermediate and deeper waters (not shown) range between 1 and 15%. The errors associated with ^{226}Ra by inference from Si concentrations will propagate and cause equally large errors for the ^{228}Ra when $^{228}\text{Ra}/^{226}\text{Ra}$ activity ratios are converted into absolute ^{228}Ra activities.

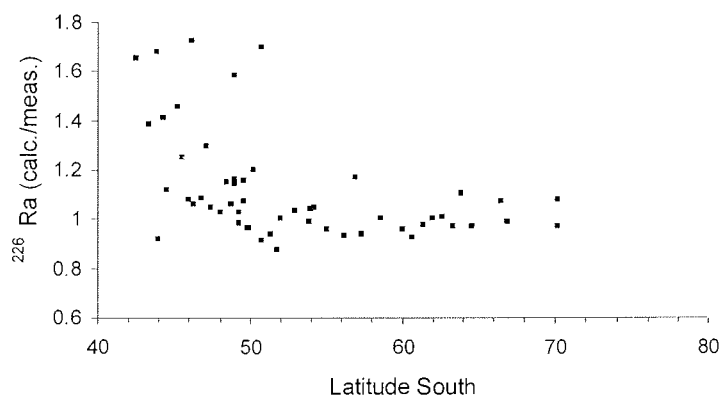


Fig. 37: Comparison of ^{226}Ra activities calculated from Si concentrations with measured ^{226}Ra activities for surface water samples.

6.2 Removal of ^{228}Th from surface waters

Surface water activities of ^{228}Ra in the open Southern Ocean are particularly low and require an investigation by the ^{228}Th -ingrowth method which is sensitive but time-consuming (see chapter 4.3.2). In chapter 5.3 it was shown on a qualitative basis that in principle ^{228}Th can be used as a more rapidly available indicator of the ^{228}Ra activity. Bearing in mind that thorium is a highly particle-reactive element, the relationship between both merits some more attention.

Dissolved (1 μm filtered) ^{228}Th activities have been determined during expeditions ANT XV/2 and ANT XVI/3 and represent the austral spring and autumn situation. The particulate fraction has not been analyzed separately but the percentage of thorium on particles generally increases with the half-life of the respective isotope. For ^{234}Th (half-life 24.1 days), the fraction adsorbed onto particles averages between 10 and 20% but can reach up to 50% during a bloom situation (Rutgers van der Loeff et al. 1997, Usbeck et al. in press). Particulate fractions of ^{230}Th in surface waters (half-life 75000 years) range from 20 to 40% (Rutgers van der Loeff and Berger 1993, Geibert unpublished data; no corresponding data available for bloom situation). According to its

intermediate half-life of 1.91 years, the particulate fraction of ^{228}Th can be expected to be somewhere in-between.

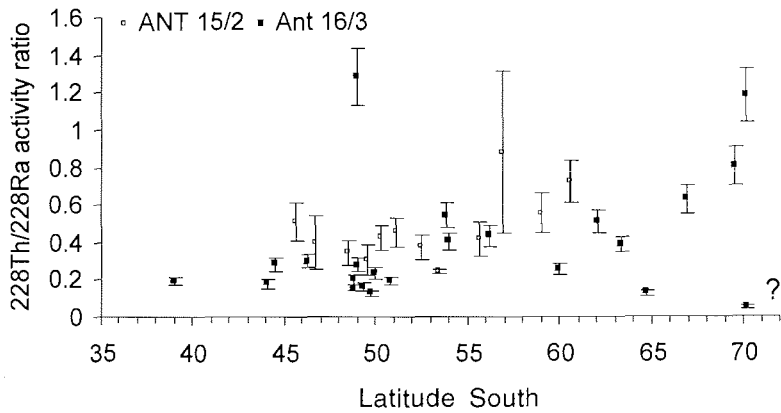


Fig. 38: Plot of dissolved $^{228}\text{Th}/^{228}\text{Ra}$ activity ratios against latitude for austral spring (ANT XV/2; open symbols) and austral autumn (ANT XVI/3; closed symbols).

Scavenging processes in the upper ocean occurring on time scales of weeks to months have been studied extensively with the ^{238}U - ^{234}Th isotope couple (Broecker and Peng 1982). The activity of ^{234}Th is expressed as ratio to its parent nuclide ^{238}U . In the absence of export processes, the sum of dissolved and particulate ^{234}Th activities should be in equilibrium with ^{238}U , i.e. their activity ratio (AR) close to unity. This is indeed the case for the winter situation in the Southern Ocean, when primary productivity reaches a minimum due to light-limitation, indicating that scavenging by terrigenous material has little impact. With the onset of spring productivity, the $^{234}\text{Th}/^{238}\text{U}$ AR start decreasing (Rutgers van der Loeff et al. 1997).

On the transects during ANT XV/2 and ANT XVI/3, $^{234}\text{Th}/^{238}\text{U}$ AR have been determined in surface waters (Usbeck et al. in press, Geibert unpublished data). The information related to scavenging processes as deduced from the $^{234}\text{Th}/^{238}\text{U}$ AR can be used to evaluate where the $^{228}\text{Th}/^{228}\text{Ra}$ AR should be affected, too.

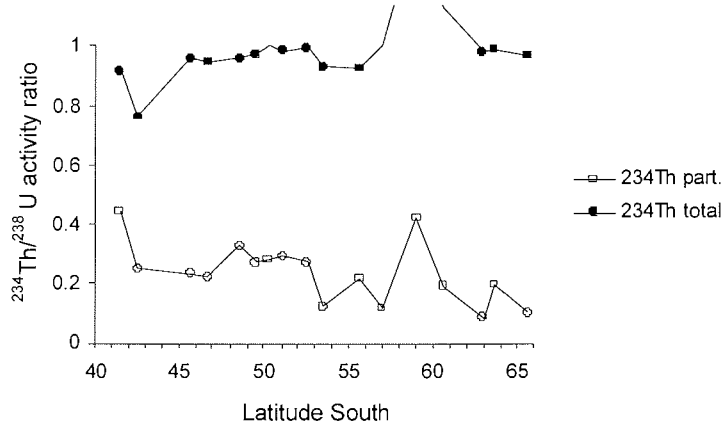


Fig. 39: $^{234}\text{Th}/^{238}\text{U}$ activity ratios for the spring transect (ANT XV/2) across the ACC. Open symbols: particulate ^{234}Th activity; closed symbols: particulate and dissolved ^{234}Th activity. Total activities below unity indicate depletion by scavenging. Data point at 59° S is questionable due to contamination by krill. Data kindly provided by Dr. W. Geibert, AWI.

Fig. 39 shows that $^{234}\text{Th}/^{238}\text{U}$ AR during ANT XV/2 are mostly at equilibrium with significant export occurring only at the approximate position of the Subtropical Front (STF). For ANT XVI/3, distinctive depletion of ^{234}Th is observed along the STF, Subantarctic Front, just south of the PF and in a region between 50 and 55° S. The Weddell Gyre is characterized by a uniform depletion of approximately 15%, while towards the Antarctic coast ^{234}Th is close to equilibrium with ^{238}U (Usbeck et al. in press).

Looking at the dissolved $^{228}\text{Th}/^{228}\text{Ra}$ AR, the mean spring ratio is 0.47 ± 0.04 which should about equal the ratio for the total activities as deduced from $^{234}\text{Th}/^{238}\text{U}$ AR. The values are then at the upper end of surface water ratios measured in the world's ocean. Reported mean ratios are around 0.2 (Broecker and Peng 1982). During the autumn transect, $^{228}\text{Th}/^{228}\text{Ra}$ AR north of the PF have decreased to about 0.21 ± 0.01 , thus displaying the depletion of ^{228}Th throughout the productive season while in southern ACC waters and the Weddell Gyre, the mean ratio remains at 0.45 ± 0.02 . This is qualitatively supported by the $^{234}\text{Th}/^{238}\text{U}$ AR that indicate only weak export production in this region as compared to the northern ACC waters. As the Antarctic coast is approached, $^{228}\text{Th}/^{228}\text{Ra}$ AR rise to about 0.8, in consistence with the observed low particle content within the Coastal Current. Against this background, one ratio at 70° S seems unrealistically low.

Two values, close to the PF and one on the Antarctic shelf, are higher than unity. Although unusual, they are not inconceivable as the $^{228}\text{Th}/^{228}\text{Ra}$ AR can theoretically reach 1.5 (see chapter 7.1.2).

Based on these observations, the use of ^{228}Th as an indicator for ^{228}Ra can be refined. For waters around and north of the PF, ongoing export of ^{228}Th during plankton blooms impairs its potential to mirror ^{228}Ra activities and best results can be expected early in the season. In contrast, the low thorium export in the Antarctic zone makes ^{228}Th here a useful analogue for ^{228}Ra . Its absolute value may be off by about 50%, but the relatively homogenous AR should allow to trace horizontal gradients and the extension of shelfwater signals before recurring to the ^{228}Th -ingrowth method.

7 ²²⁸RADIUM AS A TRACER FOR IRON INPUT INTO THE OPEN SOUTH ATLANTIC

Possible transport mechanisms for iron into the productive regions of the South Atlantic are advection of shelfwater, aeolian input, input from ice-raftered debris by melting icebergs and upwelling of deep water (de Baar et al. 1995, Lüscher et al. 1997). The use of different geochemical tracers offers the possibility to distinguish between these input paths: the role of shelfwater is investigated with ²²⁸Ra in this study. Aluminium (Al) and the isotopic composition of neodymium (ϵ_{Nd}) are indicators of terrigenous input (Hegner et al. in prep.) and ²²⁷Ac has been proposed as an indicator for upwelling of deep waters (Geibert 2001).

The continental shelves bordering the Atlantic sector of the Southern Ocean will be examined in view of their potential to release iron and ²²⁸Ra. The results will be discussed with regard to the possible mechanisms of spreading shelfwater within the South Atlantic and the implications set in context to other transport mechanisms for iron as deduced from their respective tracers. An estimation of the regional importance of aeolian input, input of shelfwater, input via ice rafted debris from melting icebergs and upwelling of deep water summarizes these considerations.

7.1 The continental shelves as source regions for ²²⁸Ra and iron

7.1.1 Iron distribution in coastal waters of the Southern Ocean

The open Southern Ocean represents the largest High Nutrient Low Chlorophyll (HNLC) region worldwide where iron is deficient in surface waters and has been shown to be a growth-limiting factor for primary productivity (Martin et al. 1990, de Baar et al. 1995). Knowledge of the transport paths by which this micronutrient reaches the productive regions is crucial for the understanding of the working of the biological pump today and in the past as well as for future predictions of e.g. what kind of feedback mechanisms climate change might trigger in the Southern Ocean.

While iron is the fourth most common element in the earth's crust, only traces are found in the present ocean with higher concentrations near the continental margins. The mostly oxidizing sea water quickly transforms ferrous iron (Fe^{2+}) into insoluble oxyhydroxides, keeping the dissolved iron concentrations very low. A speciation of this fraction indicates that up to 99% are bound to organic complexing ligands (van den Berg 1995).

Indication for enrichment of iron in Southern Ocean coastal waters comes from direct measurements and indirect observations. Table 5 gives a list of iron determinations performed in coastal waters of the Subantarctic and Antarctic regions. Time series measurements show the great variability of this trace element in the upper water column (Grott et al. 2001, Sanudo-Wilhelmy in press). In contrast to nearshore concentrations, iron in waters of the open Antarctic Circumpolar Current (ACC) and the

Weddell Gyre is mostly present at subnanomolar levels (Martin et al. 1990, Westerlund and Öhman 1991, de Baar et al. 1995).

The subantarctic islands are known for increased primary production during the austral summer with chlorophyll a levels well increased over off-shore stations. Respective observations have been reported from Bouvet Island, the South Sandwich Islands (Perisinotto et al. 1992) and the Crozet Plateau (Pollard et al. 2000). In the latter case, the waxing and waning of the phytoplankton bloom has been observed in several successive years. Iron derived from the shallow water sediments around these islands and submarine plateaus has been suggested to be the triggering factor. De Baar et al. (1995) showed an eastward decrease of iron between two stations downstream of the South Shetland Islands.

Table 5: Iron concentrations on shelves of Antarctica and subantarctic islands in the Southern Ocean. If not stated otherwise, samples have been collected in surface waters. Total concentrations refer to unfiltered, acid-leached samples.

Location	Fe, diss. (nM)	Fe, total (nM)	Reference
Signy Island	66		Nolting et al. (1991)
Deception Island	31.0		Sanudo-Wilhelmy et al. (in press)
Palmer Station	4.5-6.2		Sanudo-Wilhelmy et al. (in press)
Antarctic Sound (Peninsula)	10.1		Sanudo-Wilhelmy et al. (in press)
Antarctic Peninsula	0.9-1.4		Sanudo-Wilhelmy et al. (in press)
Filchner Shelf (100 m)	15.45	17.64	Westerlund and Öhman (1991)
Rijsel-Larsen Shelf (400 m)	2.46	10.74	Westerlund and Öhman (1991)
Terra Nova Bay, Ross Sea	0.7-4.1		Grott et al. (2001)
Kerguelen Archipelago	8.8-12.6		Bucciarelli et al. (2001)

As to the origins of iron enrichment in coastal waters, different mechanisms have been suggested: Diffusion of dissolved iron from sediments, known as reductive dissolution and governed by the redox chemistry of iron, is probably the major source term (de Baar and de Jong 2001). To produce a large flux, the production of dissolved iron must occur close to the sediment-water interface. Rapid oxidation at the interface counteracts this process (Martin 1985). Resuspension of particles into the benthic boundary layer seems to play an important role in upwelling regions (Johnson et al. 1999). Upwelling in the vicinity of islands caused by a deflected current has been demonstrated for the Galapagos Islands (Gordon et al. 1998). Input of lithogenic material and soil by rivers as well as wet and dry deposition of dust from ice-free landmasses is reported for the Kerguelen Archipelago (Bucciarelli et al. 2001).

For the Weddell Sea, mobilization of fine-grained suspended material from the shelves represents an important source term for iron (Nolting et al. 1991, Westerlund and Öhman 1991). Two recent studies have pointed out the importance of iron release by melting of pack ice for the Weddell Sea (Sanudo-Wilhelmy et al. in press) and for Terra Nova Bay in the western Ross Sea (Grott et al. 2001).

7.1.2 Shelf regions as sources for ²²⁸Ra

²²⁸Ra has been introduced as a tracer for spreading of shelfwater into the open ocean in chapter 3.3. It is liberated to the water column from ²³²Th-bearing sediments (Moore 1969a, Moore 1969b). Owing to its relatively short half-life of 5.75 years, it accumulates to higher activities in shallow water regions. Knowledge of the South Atlantic shelf regions in terms of their potential as a ²²⁸Ra source was hitherto very scanty, single values are reported by Kaufman et al. (1973) and Rutgers van der Loeff (1994). In chapter 5.2.1 it was shown that all shelf regions that were sampled in the course of this study are characterized by an enrichment of ²²⁸Ra in surface waters. Yet, the measured activities differed significantly from one region to another; a fact that will be looked closer at in this chapter.

Assuming comparable flux rates for ²²⁸Ra out of the sediment and disregarding the effects of currents, tidal mixing or water column stratification, one would expect an inverse correlation between water depth and ²²⁸Ra activity. It is obvious that these conditions are not met, moreover, the activities are lower than would be expected without exchange, implying that movement of water masses is likely to have an important influence on the accumulation of ²²⁸Ra in the water column.

Apart from the residence time of the water body on the shelf, the ²²⁸Ra flux from the sediment is a further controlling factor that fosters or inhibits an effective accumulation of ²²⁸Ra in the water column. The flux is dependent on the sediments' ²³²Th activity and the bioturbation rate, both terms that are not well defined for the Antarctic continental margins. In a first approximation, the extent of water mass movement by e.g. currents should be the main difference in the environmental conditions reigning on the Antarctic shelf areas. The residence time τ can be calculated according to Rutgers van der Loeff (1994):

$$\tau = \frac{1}{\frac{F}{C_s H} - \lambda}$$

- F: flux of ²²⁸Ra from the sediment into the water column
C_s: ²²⁸Ra concentration in surface water on continental shelf
H: depth of water column
 λ : decay constant for ²²⁸Ra

The equation holds for regions where offshore waters, thought to be in exchange with the water on the shelf, have an activity of or close to zero – a condition that is met in the waters of the Drake Passage and the Weddell Sea (Fig. 22).

Li et al. (1980) calculate a mean ²²⁸Ra flux of 6000 dpm/m²/year for shelves in the Atlantic Ocean. However, this value can be subject to large variations. On the basis of a model developed by Cochran and Krishnaswami (1980), Geibert (2001) calculated ²²⁸Ra fluxes between 540 and 3260 dpm/m²/year for shelf regions in general, based on

a ^{232}Th activity in the sediment of 2 dpm/g. Comparable concentrations have been determined for the Argentine Basin and the adjacent shelf (Niemann pers. comm. 2001). ^{232}Th activities determined for sediments in the Weddell Sea range between 3 and 5 dpm/100kg (Rutgers van der Loeff 1994, Walter et al. 1997). In the following considerations for the Antarctic shelves, the value of 6000 dpm/m²/year will be adopted. A decrease in the flux out of the sediment involves an about proportional increase in the residence time and vice versa to produce the same activities. A prerequisite for the calculation of residence times is a homogenous water column with about similar ^{228}Ra activities at all depths. Especially for greater water depths like those encountered on the Larsen shelf this remains questionable and calculated residence times are to be treated with caution.

Fig. 40 is a plot of the ^{228}Ra activity in surface waters against the water depth at the sampling location.

The East Antarctic coastline is influenced by the strong Coastal Current (CC) that inhibits the build-up of high ^{228}Ra activities. Calculated residence times are between two and five months which is well in accordance with previously calculated values (Rutgers van der Loeff 1994). A wedge of shelfwater with mean activities of 0.5 dpm/100kg stretches over the continental slope into the Weddell Sea.

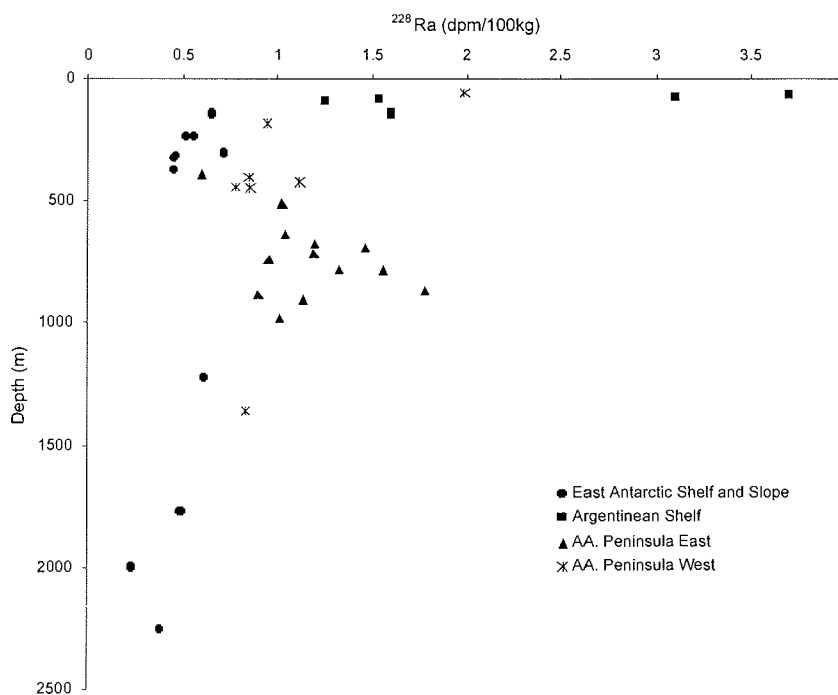


Fig. 40: Plot of ^{228}Ra activity (dpm/100kg) in surface water against the maximum water depth at the sampling location for samples taken on continental shelves and over the East Antarctic continental slope. Sample points are about the size of the error bars.

Samples taken along the Antarctic Peninsula cluster in two distinctive groups indicating that different processes govern the Pacific and the Atlantic side of this landmass. The situation on the eastern side allows the accumulation of significant higher activities despite larger water depths than along both the East Antarctic coast and the Pacific side of the Peninsula. This might be due to a combination of a more sheltered position and the admixture of Ice Shelf Water (ISW). The large inlet of the Larsen shelf weakens the influence of the CC to some extent, allowing longer residence times in this area. Samples with the highest activities have been taken in the narrow Prince Gustav Channel between James Ross Island and the Peninsula where water exchange is assumed to be naturally restricted. Assuming the same flux as on the East Antarctic shelf, residence times range from four months to nearly three years. However, bearing in mind the mean water depth of 730 m in this region, it is doubtful if the surface water activities are purely the result of an in situ accumulation in the water column which is difficult to judge in absence of subsurface water activities. Given the proximity of the, though retreating, Larsen B ice shelf, the ²²⁸Ra activities can to some extent originate from an accumulation underneath the floating shelf ice. The residence time for ISW underneath the Filchner ice shelf has been estimated from tritium concentrations to be in the order of four to seven years (Bayer and Schlosser 1991), thus allowing the build-up of high ²²⁸Ra activities. Mixing of the ISW with the shelf water could account for the higher activities. Considerable ISW fractions have been found in the deep waters close to the Larsen ice shelf (Weppernig et al. 1996).

The northwestern side of the Peninsula does not exhibit extensive ice shelves, thereby excluding this source of higher ²²⁸Ra activities. The nearby passing ACC prevents the accumulation of activities as high as on the eastern side. Two runaway points exist in this group of samples: the highest activity coincides with a water depth of only 55 m, conditions that are otherwise only met on the Argentinean shelf. The Bransfield Strait includes three deep basins where stratification in bottom waters is significant and convection takes place on the time scale of decades (Gordon and Nowlin 1978). Sample R 46 that was taken over the central basin yields a similar ²²⁸Ra activity as samples from shallower regions (Fig. 24), indicating that advection is an important factor. Calculated residence times for shelf samples of the Pacific side of the Peninsula are in the order of two to ten months.

Samples on the Argentinean shelf display a wide range of ²²⁸Ra activities for water depths between 50 and 150 m. Assuming a flux of 3000 dpm/m²/year due to lower ²³²Th sediment activities, associated residence times vary between five and ten months. This is equal to the west Peninsula coast but causes the build up of up to sixfold higher activities.

The enrichment of ²²⁸Ra in the coastal waters of the Atlantic sector of the Southern Ocean makes it a suitable tracer to study the advection of iron-enriched shelfwaters into the open Southern Ocean. While biological activity rapidly decreases the concentration of iron in surface waters (de Baar et al. 1995, Grotti et al. 2001), radium

is much less affected by uptake through plankton (see chapter 6.1). Mixing and decay are therefore the determining factors for ²²⁸Ra activities in the open ocean.

7.2 Transport mechanisms for shelfwater signals into the open South Atlantic

As a working hypothesis, transport of shelfwater and hence iron into the open South Atlantic has been suggested to be accomplished by the fast flowing frontal jets of the ACC. On the basis of the ²²⁸Ra distribution determined in this work, different processes can be distinguished.

7.2.1 Subtropical eddies

The subantarctic zone south of Africa yields high ²²⁸Ra activities in surface waters which have been, in a general approach, attributed to the influence of the Agulhas Current and the Agulhas Return Current (Fig. 27). Yet, the high variability in activities from sample to sample and cruise to cruise demands for a more detailed interpretation.

The subtropical waters north of the ACC carry a clear ²²⁸Ra signal (Li et al. 1980, this study) which originates mainly from two boundary currents: In the western South Atlantic, the Brazil Current gets enriched in ²²⁸Ra from the South American slope sediments before separating from the coast in the Brazil/Falkland Current confluence zone.

The Agulhas Retroflection region south of Africa is supplied by the Agulhas Current, which carries a strong ²²⁸Ra signal from the Indian Ocean (Kaufman et al. 1973) that is enhanced during its flow along the continental shelf edge of southern Africa. Both regions exhibit intense eddy activity (Cheney et al. 1983, Lutjeharms and van Ballegooyen 1984, Fu et al. 1988, Gordon 1988). Around southern Africa, the generation and shedding of both cyclonic and anticyclonic eddies represents important cross-frontal transport mechanisms for water of different origins (Boebel et al. 2001). Anticyclones are typical for subtropical intrusions into the subantarctic regime. Their southward propagation in direction of the ACC leads at the same time to a northward entrainment of subantarctic water. These intrusions -both south- and northwards- are not necessarily detectable from sea surface temperatures alone, as the uppermost water layer will adapt quickly to the ambient atmospheric temperatures.

Reliable evidence for the variety of water masses that are brought together in the Agulhas Retroflection region comes from satellite altimetry and drifter data. Anticyclones are associated with a positive sea surface height anomaly whereas cyclones produce a negative anomaly. It should therefore be possible to identify the origin of the water mass in which the surface water samples for ²²⁸Ra have been taken by backtracking of eddies. Based on the above mentioned observations, one would expect higher ²²⁸Ra activities in anticyclones and lower ones in cyclones.

The formation of eddies and their movement south of Africa have been tracked with satellite altimetry and drifters from 1997 to 1999 as part of the KADEX program (Boebel

et al. 1997; Cape of Good Hope Experiments). Fig. 41 shows two maps of MODAS (Modular Ocean Data Assimilation System) sea surface steric heights with superimposed float trajectories. They represent snapshots for a specific day during expeditions ANT XV/3 and ANT XVI/3. Radium samples that have been collected in this time (± 1 day of snapshot) are indicated with their mean position.

Besides a general higher eddy activity during the 1999 cruise track, the 1998 track seems to be less affected by eddy activity owing to its more westerly position. Fig. 41A reveals an anticyclonic Agulhas Ring centred around 41° S / 16° E whose occlusion from the Agulhas Retroflection area occurred in November 1997. Sample R 2 gained its ²²⁸Ra activity most likely from this ring. Sample R 4 can be associated with a subtropical anticyclone coming from further west as deduced from backtracking of the associated drifter. Situated in-between both is sample R 3 with a very low ²²⁸Ra but higher ²²⁶Ra activity (10.57 dpm/100kg) that are both typical for waters further south. Its mean sampling position coincides with a negative anomaly and displays the effect of subantarctic water being entrained northwards caused by an anticyclone nearby. It is not possible to identify the origin or direction of the water mass that causes the high ²²⁸Ra activity measured with sample R 6 at 50° S.

For the 1999 samples, a similar clear relationship can be established between the ²²⁸Ra activity of the displayed samples and steric sea surface height (Fig. 41B). The anticyclones associated with samples R 100, R 143 and R 145-R 148 can all be traced back to the Agulhas Current system. Activities of R 146 and R 148 are the same as they have been taken in the southern and northern rim of the same anticyclone, respectively, which is nicely mirrored by the equally consistent ²²⁶Ra activities of 7.20 and 7.31 dpm/100kg. Subantarctic influence is reflected in sample R 149, indicated by a drop in ²²⁸Ra activity that can be associated with a negative height anomaly. In this context, the low ²²⁶Ra activity of 5.45 dpm/100kg must be questioned. Sample R 151 has been collected in the outer rim of an Agulhas ring that is about to cut off from the Agulhas Retroflection Area. It yields a sort of end member value for ²²⁸Ra activities within the Agulhas Current.

Sample R 100 was sampled for radium on 20.3.1999 on the southbound journey during ANT XVI/3. The eddy had moved westwards by 4-5° of longitude when the region was revisited seven weeks later, indicated by the sequence of dashed circles in the same snapshot. This example displays the durability of eddies and their persistence in this area.

It should be noted that apart from R 145 all samples that are discussed in this chapter have been collected on a sailing vessel. Hence, reported ²²⁸Ra activities represent mixed values for as much as 100 km, a distance that can cover completely different water masses as shown in Fig. 41. Stationary sampling in accordance with the main hydrographic features would most likely have yielded even larger differences in activity between samples located in anticyclonic and cyclonic eddies.

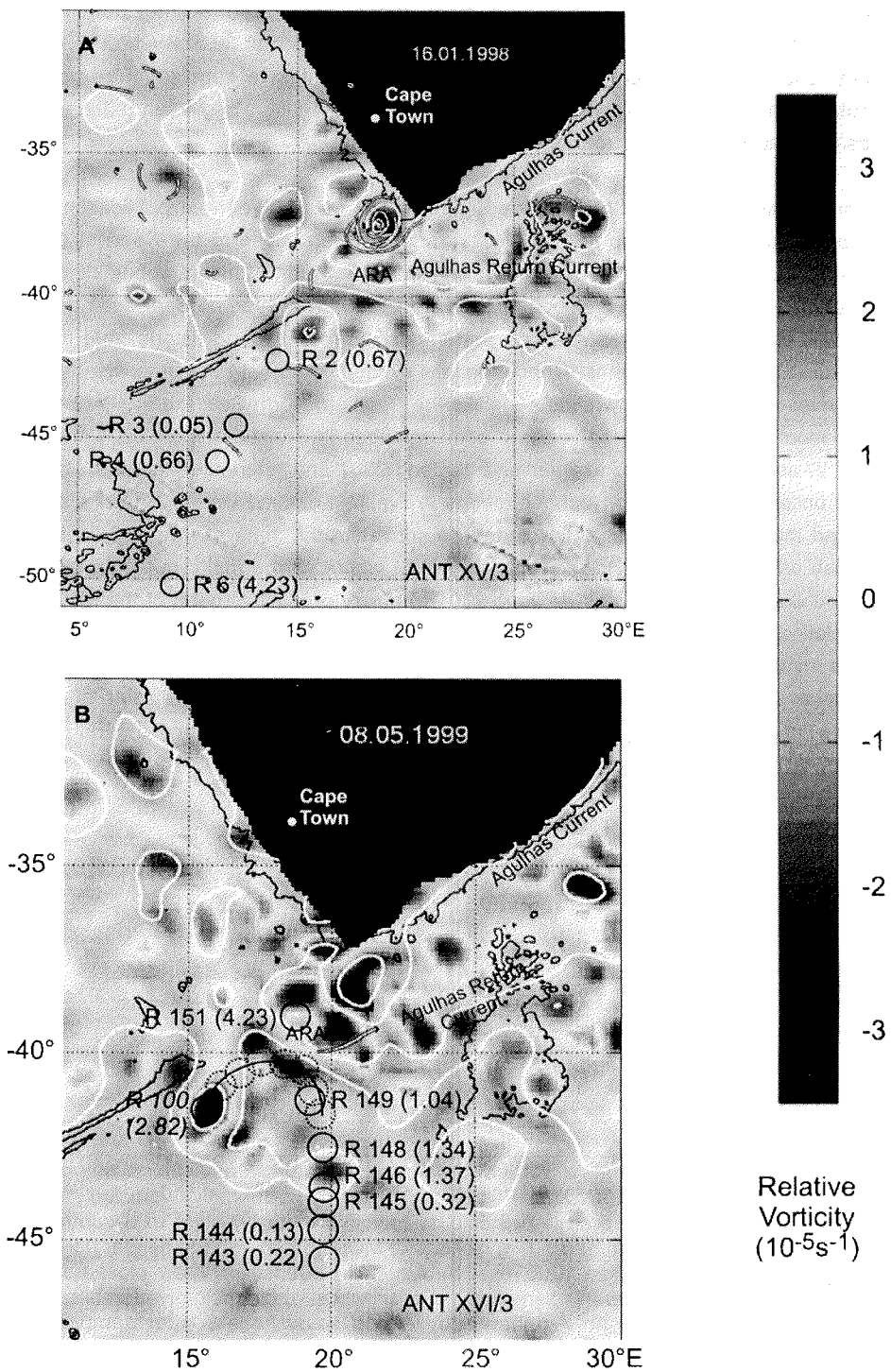
The example of two cruises shows that ²²⁸Ra activities in the subtropical and subantarctic region south of Africa are controlled by ring and eddy formation at the

Agulhas Retroflection. Concluding from these observations, the activity of 0.3 dpm/100kg given by Kaufman et al. (1973) for a position at 39.5° S / 12.2° E does not reflect a pure subtropical signature but must contain a substantial portion of subantarctic water. Subtropical intrusions of Atlantic or Agulhas origin can reach as far as 45° S as inferred from satellite altimetry data.

Iron measurements off South Africa are restricted to a 35-year-old publication that reports concentrations up to 230 nM for surface waters close to the Cape of Good Hope, said to be influenced by upwelling inshore water. Concentrations 60 miles offshore are about 18 nM (Leisegang and Orren 1966). However, de Baar and de Jong (2001) consider iron determinations performed before 1981 as "historic" due to the manifold analytical problems. Concentrations exceeding 100 nM are otherwise typical for river-influenced shallow shelf seas like the Southern North Sea, the Laptev Sea or the IndoPacific Shelf. Dissolved iron concentrations in Atlantic subtropical waters at 40° W are about 1.3 nM (de Baar and de Jong 2001 and references therein). Beside the uncertainty of the iron concentrations in Agulhas-derived water, it must also be noted that the subtropical anticyclones do not reach the zone of true iron limitation which only starts at the Polar Front (ca. 50° S) where all the major nutrients exist in plentiful supply (de Baar and de Jong 2001). Primary production north of the PF faces depletion of the macronutrients.

In summary it can be said that, regardless of the true iron concentrations within the Agulhas Current, the interaction of subtropical and subantarctic waters south of Africa does not account for an efficient iron supply into the HNLC-region south of the PF.

Fig. 41 (next page): Relative vorticity from MODAS sea surface steric height and superimposed tracks of KADEX RAFOS floats. Blue colours (negative vorticity) indicate subantarctic origin while orange-red colours (positive vorticity) point to a subtropical influence. White lines: 1 m and 1.5 m isolines of MODAS sea surface height; dark blue area: regions shallower than 1000 m; ARA: Agulhas Retroflection Area; closed circles: position of ²²⁸Ra surface water samples (²²⁸Ra activity in dpm/100kg given in brackets); dashed circles: track of an Agulhas eddy during seven weeks after sampling. A: expedition ANT XV/3, snapshot for 16.1.1998. B: expedition ANT XVI/3, snapshot for 8.5.1999. Satellite altimetry data kindly provided and interpreted by Dr. O. Boebel, AWI.



7.2.2 Oceanographic fronts

Elevated iron levels in the Polar Frontal Region and along the Weddell-Scotia-Confluence (WSC) have lead to the suggestion that oceanic fronts act as effective transport mechanisms of iron into the productive regions of the ACC after passing over continental margin sediments (Nolting et al. 1991, de Baar et al. 1995). Especially the Argentinean shelf and slope have been favoured as an important source region because of the northward veering ACC that follows closely the continental shelf edge. Yet, iron-enrichment is less pronounced with increasing distance to the suggested South American source region and has also been ascribed to wet deposition of aeolian material (Croot and Turner 1998, de Jong et al. 1999).

²²⁸Ra with a shallow water source is a suitable tracer to study the fate of shelfwater in land-remote areas. The distribution of ²²⁸Ra activities along the oceanic fronts in the ACC reveals an ambiguous picture and will be discussed from north to south.

Chapter 7.2.1 has demonstrated that higher activities in the subantarctic zone could be correlated with anticyclones of subtropical origin and rings from the Agulhas Retroflection Area (Fig. 41). However, there is no evidence that intrusions of subtropical water can account for elevated ²²⁸Ra activities south of 45° S. None of the cruises revealed a distinctive enrichment coinciding with the Subantarctic Front (SAF).

As to the PF, two strong signals (R 6 and S 5; Fig. 22) coincide indeed with the approximate position of the PF at 9.3° E and 0° during the respective cruises and represent the highest values for ²²⁸Ra that were determined in the course of this study. In contrast, a grid survey of the PF at 20° E a year later did not reveal increased activities. In view of the high activities associated with samples R 6 and S 5, the more easterly position should not have been a limiting factor for the detection of a shelfwater signal during this survey. Surface water iron concentrations, determined during the same grid survey, were patchy and correlated rather with rain events than with the position of the frontal jet (de Jong et al. 1999).

The PF proper does not get in contact with the continental shelf or slope sediments of South America but passes between the Falkland Islands and South Georgia over the North Scotia Arc. Here, water depths generally exceed 2000 m and impede the accumulation of ²²⁸Ra activities in the water column. Evidence comes from sample R 202 which shows that the northward flowing subantarctic water does not carry a significant ²²⁸Ra signal. In contrast, the returning branch of the ACC is higher enriched in ²²⁸Ra (Fig. 26). At 40° W, the SAF and the PF are found in close proximity to each other and can merge at times to form a single powerful frontal jet (Peterson and Whitworth 1989). This seems a likely mechanism for the PF to "inherit" a signal brought up by the SAF. The SAF itself is more prone for getting enriched in ²²⁸Ra due to the large loop it describes along the Argentinean shelf edge into subtropical latitudes. ²²⁸Ra can either be gained from the south, entrained by the Falkland Current, or from the north, collected by the Brazil Current on its flow along the South American continental margin.

Indication that shallow water masses find their way regularly into the PF comes from the repeated occurrence of the drifting seaweed (van Franeker pers. comm. 1999, Rutgers van der Loeff pers. comm. 2000, Wiencke pers. comm. 2001). *Macrocystis pyrifera* kelp has been ascribed a crucial role in the dispersal of animals and plants in circumpolar waters (Edgar 1987). Its distribution in the Atlantic Ocean is confined to coastal waters at the tip of South America and the subantarctic islands (Lüning 1990) - regions, that are not directly affected by the flow of the PF. However, the hydrographic processes seem to concentrate the detached patches of kelp efficiently along the PF. It can only be speculated whether the high ²²⁸Ra signal of samples R 6 and S 5 originate from a merging of or water exchange between the SAF and the PF at 40° W. It must be assumed that ²²⁸Ra enriched water, possibly within the Brazil/Falkland Current confluence, has entered the frontal jet west of the sampling position and experienced rapid eastward transport.

An inconsistency to this model is the fact that the SAF is proposed as the link between the shelf source and the PF but does not show increased activities along the frontal jet itself. Further, increased activities along the PF are about 13% higher than measurements made on the Argentinean shelf, the proposed source region. Both observations might be the result of the spatial and temporal variability of the ²²⁸Ra signals.

At 60° S, sample R 11 yields substantially higher ²²⁸Ra activities compared to adjacent samples (Fig. 22). The Antarctic Peninsula and neighbouring islands have been shown to be a strong source for both ²²⁸Ra and iron, and admixture of fresher shelfwater along the WSC can be traced as far as 22° E (Orsi et al. 1993). It can be concluded that the signal originates from the Peninsula region, transported with the Southern ACC Boundary which constitutes the eastward extension of the WSC.

To sum up, it can be said that increased ²²⁸Ra activities along the oceanic fronts of the open ACC are not a recurrent feature. In cases where elevated activities occur, the enrichment is spatially very restricted as none two adjacent samples in the ACC show similar high activities. As to the question, to what extent input of shelfwater increases iron levels in the HNLC waters of the ACC, the present study cannot give a satisfying answer. Judging from the ²²⁸Ra distribution determined in this work, shallow water signals in the Atlantic sector of the Southern Ocean are not regularly detectable. It remains unclear whether this is due to a true sporadic occurrence and to what extent factors like e.g. dilution or seasonality are of importance. Transects across the ACC at a more westerly position and downstream of the subantarctic islands are suggested to clarify the processes involved into ²²⁸Ra, and hence iron entrainment, into the open South Atlantic.

7.3 Comparison of ²²⁸Ra with other geochemical tracer data

Advection of shelfwater has been proposed as one possibility to sustain iron levels in the South Atlantic. Other processes are aeolian input, input by ice rafted debris

released from melting icebergs and deep upwelling. The collection of ²²⁸Ra samples on several cruises was done in conjunction with sampling for the geochemical tracers Al, ϵ_{Nd} and ²²⁷Ac. Together, they provide more information about sources of iron for the HNLC waters of the South Atlantic.

7.3.1 Distribution of Al and ϵ_{Nd} as tracers for continental input

Geochemical parameters like Al and the isotopic composition of neodymium (Nd) are used as tracers for terrigenous material that is part of the particulate suspended matter in sea water. While the former one is a measure for the amount of continental input, the latter one provides information about its possible source regions. The isotopic composition of Nd is expressed as an epsilon function that describes the $^{143}\text{Nd}/^{144}\text{Nd}$ ratio compared to a "chondritic uniform reservoir" (CHUR) and is therefore independent of the actual Nd concentration:

$$\epsilon_{Nd} = \left[\frac{\left(\frac{^{143}\text{Nd}}{^{144}\text{Nd}} \right)_s}{\left(\frac{^{143}\text{Nd}}{^{144}\text{Nd}} \right)_c} - 1 \right] \times 10^4$$

s: $^{143}\text{Nd}/^{144}\text{Nd}$ ratio in the sample

c: $^{143}\text{Nd}/^{144}\text{Nd}$ ratio in a chondritic model reservoir named CHUR (Wasserburg et al. 1981)

Geological formations can be distinguished on the ground of their ϵ_{Nd} value. The continental land masses surrounding the Atlantic sector of the Southern Ocean can roughly be divided into two groups in terms of their geology: East Antarctica and the southern part of Africa are formed from consolidated continental crust of paleozoic and precambrian age with low ϵ_{Nd} between -7 and -23. In contrast, West Antarctica with the Antarctic Peninsula and Patagonia belong to much younger, mobile belts with the occurrence of mesozoic and cenozoic magmatism. ϵ_{Nd} values in this province ranges from -8 to +7 (Fig. 43; Hegner et al. in prep. and references therein).

In the process of erosion, rock fragments keep their characteristic ϵ_{Nd} values of the source region. Due to the pronounced geological differences between the eastern and western rock regions bordering the South Atlantic, a classification of the suspended particulate matter in sea water should be possible on the ground of its ϵ_{Nd} values.

Al and ϵ_{Nd} values have been measured in suspended particulate matter in South Atlantic surface waters during expeditions ANT XV/2+3 and ANT XVI/3 with most of the sampling being done parallel to the ²²⁸Ra sampling (Fig. 42 and Fig. 43; Hegner et al. in prep.).

²²⁸Ra activities have shown that shelfwater influence from South America, Africa and Antarctica does not reach far offshore into the Southern Ocean. The influence of the

Argentinean shelf on the ^{228}Ra activities, increasing steadily from the northern Drake Passage towards South America, is mirrored by ϵ_{Nd} values >-5 from the young volcanic material. At 20°W in the central South Atlantic, there is evidence for aeolian input from Patagonia as can be inferred from the Al and ϵ_{Nd} data that remain uniform over several hundred kilometres and major oceanic fronts.

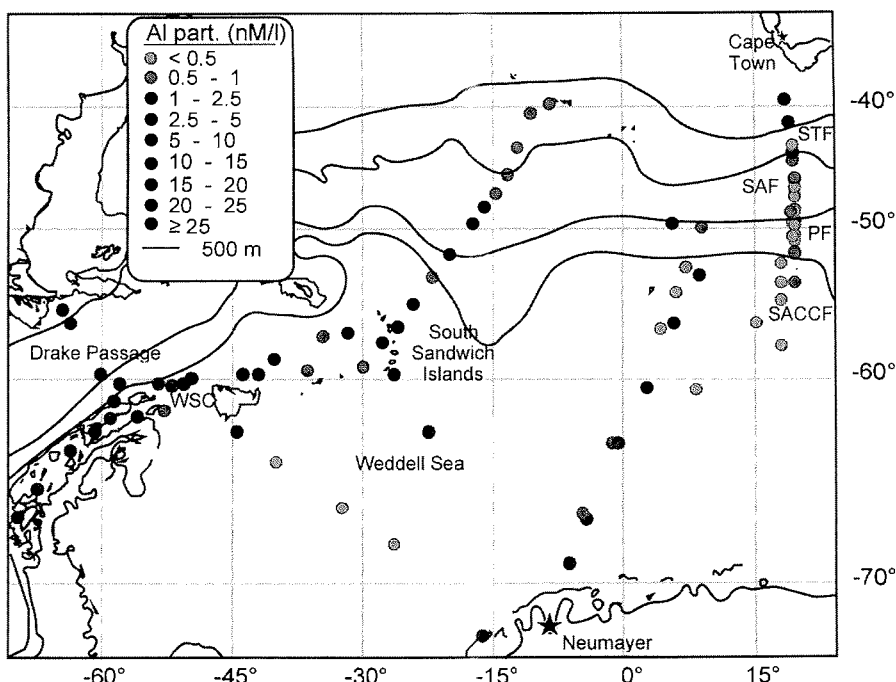


Fig. 42: Concentration of Al (nM/l) in suspended particulate matter collected from surface water in the Atlantic sector of the Southern Ocean (unpublished data from Dauelsberg & Hegner). Samples have been taken with a continuous flow centrifuge and were analyzed by ICP-MS. Oceanic fronts after Orsi et al. (1995). STF: Subtropical Front; SAF: Subantarctic Front; PF: Polar Front; SACC: Southern ACC Front. WSC: Weddell-Scotia-Confluence.

The Antarctic Peninsula has been associated with a confined continental signal, expressed as elevated ^{228}Ra activities, that decreases rapidly along the WSC. This picture is supported by Al concentrations measured in particulate suspended matter from surface water which are highest close to the Peninsula. The distribution supports previous observations of a significant resuspension of shelf material (Abelmann and Gersonde 1991, Westerlund and Öhman 1991). Material derived from South Africa yields ϵ_{Nd} values <-12 . Sample R 6 at 50°S with an extremely high ^{228}Ra activity has an associated ϵ_{Nd} of -9.2 which is untypical for South African material. As satellite altimetry revealed that subtropical anticyclones do not travel beyond 45°S , the

negative ε_{Nd} values south of the SAF must have another source than the African continent.

The Weddell Gyre and the overwhelming part of the ACC have been identified as areas with extremely low ²²⁸Ra activities that are cut off from continental influence. In contrast, elevated Al concentrations indicate that input of terrigenous material can be high in the eastern Weddell Gyre. The ε_{Nd} values give more insight into probable sources of the particulate material in the surface water. While the ε_{Nd} values in the proximity of South America and the Antarctic Peninsula are consistent with the signatures on the respective neighbouring continents, a gradual admixture of material from another source with lower ε_{Nd} can be depicted along the WSC. In accordance with the clockwise rotation of the central Weddell Gyre, this material must have its origin further east.

Significant aeolian input can be excluded as Antarctica is covered for > 98% by ice and the prevailing westerlies prevent dust input from South Africa. The very low ²²⁸Ra activities in the southern ACC waters and the Weddell Gyre do not indicate advection of shelfwater from Antarctica. Hence, Hegner et al. (in prep.) postulate transport and subsequent release of ice-raftered debris by icebergs. They calve along the coast of Enderby Land in East Antarctica, follow the Coastal Current and the clockwise gyre of the Weddell Sea (Tchernia and Jeannin 1984, Drinkwater et al. 1999) before reaching warmer waters in the north where the sedimentary material is liberated by melting. Sporadic, but strong phytoplankton blooms could be the result of this iron fertilization by icebergs as far north as the PF.

The question arises if the high ²²⁸Ra activities determined at the PF can be linked to ice-raftered debris. ²²⁸Ra is the direct daughter product of ²³²Th, a strongly particle reactive element. The latter is supplied to the oceans solely by terrigenous material only of which it is part of the crystal lattice. The ²³²Th activity of the suspended particulate matter has been analyzed by ICP-MS (Dauelsberg, unpublished data), too, and found to be about two orders of magnitude lower than the detection limit of ²²⁸Ra. Taking further into account that ²²⁸Ra needs to grow into equilibrium with its parent nuclide and that only a small fraction of ²²⁸Ra produced is able to leave the crystal lattice, it becomes obvious that dissolved ²²⁸Ra activities cannot be explained from particulate matter.

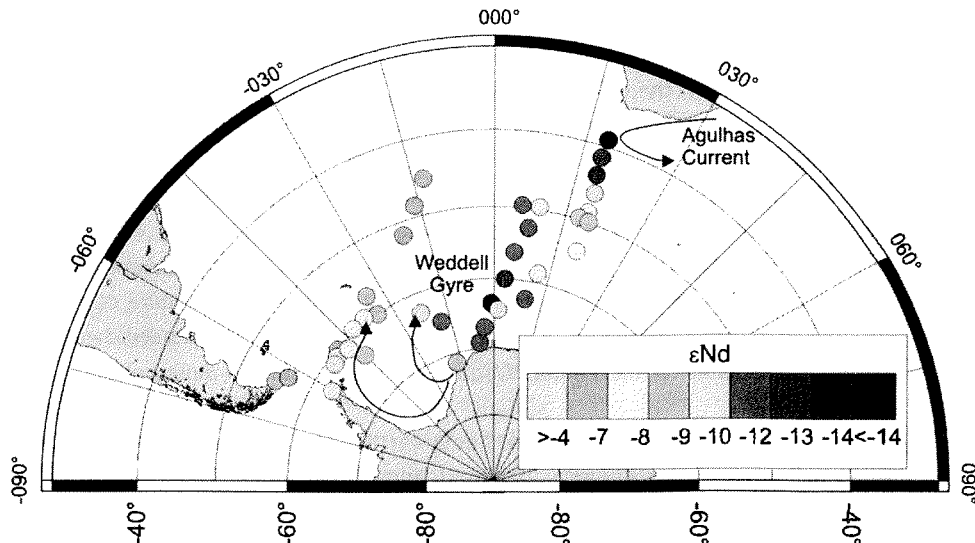


Fig. 43: ϵNd values of suspended particulate matter collected from surface water in the Atlantic sector of the Southern Ocean (unpublished data from Dauelsberg & Hegner). Samples have been taken with a continuous flow centrifuge. Iceberg trajectories in the Weddell Gyre after Tchernia and Jeannin (1984) and Drinkwater et al. (1999).

7.3.2 Distribution of $^{227}\text{Ac}_{\text{ex}}$ as a tracer for deep upwelling

^{227}Ac is a rather soluble nuclide with a half-life of 21.77 years and part of the natural ^{235}U -decay chain. The parent nuclide ^{231}Pa is rapidly scavenged from the water column and transported to the seafloor. In terms of their particle reactivity, the isotope couple $^{231}\text{Pa} - ^{227}\text{Ac}$ can be compared with $^{232}\text{Th} - ^{228}\text{Ra}$. But in contrast to ^{232}Th activities, the concentration of ^{231}Pa in sediments is correlated with depth. The fact that ^{227}Ac is mainly liberated from deep sea sediments makes it suitable as a tracer for water masses that were in contact with such sediments (Geibert 2001). The activity is expressed as excess over what is supported by the ^{231}Pa activity in the water column.

$^{227}\text{Ac}_{\text{ex}}$ was analyzed on stations 190, 197, 206 and 207 during expedition ANT XVI/3. The depth distribution displays a close similarity between $^{227}\text{Ac}_{\text{ex}}$ and nutrients, indicating the upwelling of CDW south of the PF. $^{227}\text{Ac}_{\text{ex}}$ can be measured in the surface waters of the open ACC, which implies that upwelling must occur sufficiently rapid compared to the half-life of ^{227}Ac . In contrast, the $^{228}\text{Th}/^{230}\text{Th}$ activity ratio did not indicate elevated ^{228}Ra activities in this area (Fig. 32).

These $^{227}\text{Ac}_{\text{ex}}$ values, the first ever to be measured in the Southern Ocean, strongly suggest this parameter to be a promising tracer for deep upwelling (Geibert 2001).

The vertical distributions of $^{228}\text{Th}/^{230}\text{Th}$ AR and $^{227}\text{Ac}_{\text{ex}}$ concentrations imply that the combination of ^{228}Ra and $^{227}\text{Ac}_{\text{ex}}$ should be ideal for future studies to distinguish between lateral advection and deep upwelling in regions nearer to the coast than the open ACC, like e.g. the area west of Maud Rise (64° S / 0°).

7.4 Iron pathways into the Atlantic Sector of the Southern Ocean: a synthesis

The advent of sensitive and exact analytics that allowed on board determination of iron (de Baar and de Jong 2001) as well as incubation experiments (de Baar et al. 1990, van Leeuwe et al. 1997) and in situ fertilization (Boyd et al. 2000, Smetacek et al. 2001) have shown that primary production in the Southern Ocean is co-limited by iron. While iron levels in southern ACC waters are reported to sustain only moderate productivity, concentrations along the PF allow the development of strong blooms. However, the total amounts of iron brought into the circumpolar High Nutrient Low Chlorophyll (HNLC) waters via the different pathways are still a matter of debate. Vertical mixing and upwelling of CDW has been estimated to contribute 2.9 mg/m²/year of soluble iron to the surface water (Löscher et al. 1997). According to Duce and Tindale (1991), atmospheric inputs should be about the same amount although there are huge discrepancies with calculated mean sedimentation rates of iron for holocene oceanic sediments (Kumar et al. 1995). Based on particulate Al concentrations, Hegner et al. (in prep.) calculate concentrations of potentially bioavailable iron between 0.3 and 3.1 nM for the Weddell Sea and up to 1 nM for the PF, released by terrigenous material from melting icebergs.

²²⁸Ra data from this study elucidate the role of advection of shelfwater in terms of iron supply. Southward transport of subtropical waters off southern Africa accounts for considerable cross-frontal water exchange. But as true iron-limitation only starts in the region, where macronutrients are in sufficient supply in surface waters, i.e. south of approximately 50° S (see chapter 6.1), this mechanism is of limited importance for the Southern Ocean HNLC waters.

Within the region where productivity is co-limited by iron, elevated ²²⁸Ra values can be associated with frontal structures of the ACC but are not a regular feature on all transects, indicating a rather sporadic input. Assuming that high ²²⁸Ra signals at the PF are caused by a temporary merging of the SAF and PF further west, then the advection of shallow water masses from the Argentinean shelf should indeed occur irregularly.

In contrast, the meandering flow of the PF will always pass over the North Scotia Arc and the Falkland Plateau with their reduced water depths. It is likely that fine-grained sedimentary material is picked up by the PF to be transported eastwards. Input of such particulate lithogenic material can account for elevated iron concentrations but will not lead to increased ²²⁸Ra activities as had been shown for suspended particulate matter released from icebergs. Indeed, high particulate concentrations of Al and Fe have been found along the PF at 6° W (Löscher et al. 1997). These signals could as well originate from terrigenous material released from melting icebergs but would then represent a highly variable source term dependant on the abundance of icebergs. Aeolian input of dust would affect the iron concentrations over a large area rather than specifically along a frontal structure which is nicely demonstrated by the constant Al concentrations and ϵ_{Nd} values on a transect between 40 and 55° S in the central SE-Atlantic (Fig. 42 and Fig. 43).

In summary, the iron distribution in the Atlantic sector of the Southern Ocean seems to be the result of a combination of rather constant processes combined with more sporadic and locally restricted events.

Aeolian input, upwelling of deep water and sedimentary input collected with the PF are likely to account for a quasi steady iron supply. At times when Argentinean shelfwater enters the Polar Frontal jet due to merging of the SAF and PF or during large sediment-laden iceberg melts in the ACC, iron levels should get further increased and facilitate the development of plankton blooms. A better distinction of the two groups of processes and a differentiation of their regional importance might in the future bring more light into the debate of iron transport paths.

8 NATURALLY OCCURRING RADIUM FROM MAN-MADE SOURCES

The shelf areas surrounding the Atlantic sector of the Southern Ocean, and especially the broad Argentinean shelf, have been hypothesized as sources for ^{228}Ra in this work. It was suggested that, due to its higher solubility over ^{232}Th , ^{228}Ra escapes into the water column and is subsequently subject to advection processes. It can hence be used as a tracer for iron which is believed to be equally liberated to the water column overlying shelf sediments.

Shelf areas often bear extensive hydrocarbon reservoirs. Associated with the exploitation of these gas and oil reservoirs is the production of highly mineralized waters, so-called "produced water" that is known for its high content in radium isotopes (Gott and Hill 1953, Pierce et al. 1964, Kraemer and Reid 1984, Lysebo et al. 1996).

This chapter aims to address the problem, to what extent discharges of produced waters on the South American shelf can lead to enhanced radium signals downstream of the platform installations. Such a link in whatever region has to my knowledge never been investigated or established. A strong focus is therefore put on a compilation of

existing publications to outline the amount of radium released to the marine environment.

Note the different unit for radionuclide activities as compared to the rest of this work. While publications dealing with natural radioactivity in the marine environment consistently use disintegrations per minute (dpm), monitoring studies currently quote the results as Becquerel (Bq). The conversion is: 1 Bq = 60 dpm.

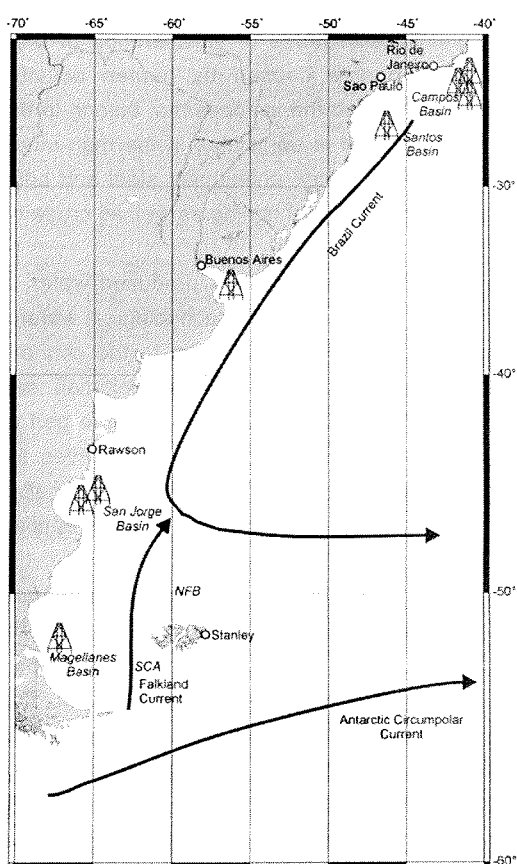


Fig. 44: Map showing the major exploration fields on the Brazilian and Argentinean shelf (compiled and modified from Petroconsultants (1996) and Admiralty List of Lights and Fog Signals 2000/2001). Licensing for future exploration has started in the North Falkland Basin (NFB) and is planned for the Special Co-operation Area (SCA).

8.1 Hydrocarbon exploitation on the Argentinean shelf

The Argentinean shelf hosts a number of important sedimentary basins that contain hydrocarbon reservoirs. Fig. 44 shows the location of the major offshore exploration fields that are currently in operation east of Brazil, Chile and Argentina. All are situated in the influence of either the Falkland or the Brazil Current. Exploration around the Falkland Islands is expected to be developed in the near future in the North Falkland Basin and the Special Co-operation Area shared by the UK and Argentina (Falkland Islands Government 1999). The fate of radium released from producing oil and gas rigs in these fields will be closer examined in chapter 8.4.

8.2 Naturally occurring radioactive material

"Naturally occurring radioactive material" (NORM) has been defined as "*any radionuclides or radioactivity disturbed by man-made activities or technologically-enhanced state, which may result in a relative increase in radiation exposure and risks to the public above background radiation levels*" (Health Physics Society). Although misleading in its expression, the definition implies a technological enhancement of naturally occurring radionuclides in terms of an alteration of their composition, concentration or proximity to people caused by human activity. Radioactive elements in NORM usually involve ^{40}K and the isotopes that belong to the natural decay chains of ^{238}U , ^{235}U and ^{232}Th . NORM is ubiquitous in the man-made environment. Typical producers are the fertilizing industry, phosphate, steel and brick production, support industries of the nuclear fuel cycle, coal mining as well as crude oil and gas operations (Kershaw 1999).

The primary source of NORM during hydrocarbon exploitation is produced water, a term that comprises the entity of formation water, injection and technological waters. Formation water, sometimes also called oilfield brine effluent, refers to the connate water that is inherent in most natural hydrocarbon reservoirs. During exploitation, sea water is injected into the reservoir to maintain the pressure and may become part of produced water whereas technological waters comprise a variety of additives for various purposes to facilitate the extraction. Produced water from gas fields consists mainly of formation water and condensed water as no water injection is applied (Jacobs et al. 1992).

Produced waters considerably dominate over other wastes and their volumes generally increase with the ongoing depletion of the reservoir (Neff et al. 1989, Røe et al. 1996). In older fields, they can represent up to 95% of the production (Neff et al. 1989). Johnsen (1996) assumes a discharge volume of 500-25000m³/d per platform. The composition of produced waters is highly variable, can be different from field to field and changes with the maturity of the reservoir. They usually show a high degree of natural mineralization with salinities up to 300g/l (Neff et al. 1989) and are often saturated with dissolved gases including CO₂ and H₂S (Jacobs et al. 1992). For technological purposes, compounds like BaSO₄, emulsifiers, organophilic clays,

organic polymers, zinc carbonate, lime and biocides are added. Once brought to the surface, produced waters are either reinjected into the well or adjacent geological formations or disposed of into the sea.

8.3 Radium in produced water

8.3.1 Chemical composition of formation water

Jacobs et al. (1992) characterize formation water as a salt solution that has a cationic composition comparable to sea water but with much higher concentrations. Elements of the alkaline and alkaline-earth group generally show the highest concentrations. The high salt content is due to leaching processes within the reservoir. Radium has been shown to be positively correlated to salinity (Reid 1983, Kraemer and Reid 1984, Rabalais et al. 1992), chlorine content (Alekseev et al. 1958) or total organic carbon (Neff et al. 1992) in produced water, but due to the limited number of investigations it is uncertain whether these findings represent general relationships. As has been stated above, the composition of produced water depends on different factors and any apparent relationship might only hold for a certain type of reservoir or a distinctive period of time during the exploration cycle. A low Ba content in the effluent of platforms has been considered as evidence for precipitation of BaSO_4 subsequent to contact of produced water with injected sea water (McCourt and Peers 1987). These precipitates will to a certain extent remove radium by coprecipitation out of the effluent, too.

8.3.2 Process of radium enrichment in formation water

The main source of radioactivity in produced waters are naturally occurring ^{226}Ra and ^{228}Ra that originate from the rocks associated with petroleum reservoirs. Among those, shales contain the highest level of radioactivity. Average values are 44 Bq/kg for both ^{238}U and ^{232}Th (UNSCEAR 1977). The organic-rich Kimmeridge Clay for example that is found in wide parts underlying the North Sea is known for its elevated uraniferous activities (Jones and Manning 1994). ^{238}U activities of 115000 Bq/kg have been reported for dense black organic matter, so-called "asphaltite" (Pierce et al. 1955). However, shales are characterized by low permeabilities that counteract an efficient release of radium to the formation water. ^{238}U and ^{232}Th contents in carbonates (26 and 8 Bq/kg, respectively) and sandstones (18 and 11 Bq/kg, respectively; UNSCEAR 1977) are somewhat lower, but both rock types provide better release conditions.

Thermal cracking of organic matter trapped in sedimentary rocks leads to the formation of oil. Upon migration, the naturally occurring radionuclides may be entrained and get enriched in connate waters. Radium is preferentially leached from the reservoir under reducing conditions by formation water and is subsequently brought to the surface with produced waters. Increased temperatures at great depths favour its enrichment in the formation water together with other earth alkaline elements like Ca, Sr and Ba. In

contrast, the activities of thorium and uranium isotopes are low in the aqueous phase due to their adsorption onto rock particles and the generally reducing environment (Shawky et al. 2001). As a consequence, radium isotopes are hardly ever in secular equilibrium with their parent nuclides in the effluent and their enrichment can be by factors up to 10000 (Bland 2001).

Kraemer and Reid (1984) suggested a combination of alpha-recoil effect and chemical leaching to explain the high enrichment of radium in formation waters. Within the ^{238}U and ^{232}Th decay chains, three and one alpha-decay, respectively, have taken place to produce ^{226}Ra and ^{228}Ra (see Appendix A 6). The production of helium nuclei and their emission from the crystal lattice should facilitate the migration of soluble nuclides into the pore water. Upon release, radium is readily adsorbed onto negatively charged mineral surfaces, notably clay minerals, and an equilibrium will develop between radium ions in solution versus radium ions that are adsorptively bound (Feige and Wiegand 1999). However, the high salinity in combination with an extraordinarily high concentration of bivalent ions like Ba^{2+} or Sr^{2+} favour the desorption process by ion exchange and lead to an enrichment of radium isotopes in the brine. Experimental elution results show that anions like Cl^- and NO_3^- lead to a four- to eightfold increase of ion exchange by disturbing the hydration capacity of Ra^{2+} that will be released into the fluid phase (Wiegand and Feige, in prep.). In principle, this process of enrichment applies to both ^{226}Ra and ^{228}Ra . The ultimate quantities are regulated by the activities of the respective parent nuclides ^{238}U and ^{232}Th in the aquifer rock and the migration time of the formation water as ^{228}Ra decays two orders of magnitudes faster than ^{226}Ra .

8.3.3 Radium concentrations in produced water

While reliable studies about the fate of effluents from offshore oil and gas operations in general are rare, hardly any studies exist about the special case of radioactivity in produced waters when released to the marine environment.

As soon as produced water reaches the surface, mixing with sea water in combination with the general drop in pressure and temperature decrease lead to the formation of sulfate and carbonate precipitations. Radium is co-precipitated with Sr and Ba as celestobarite or radiobarite (Lysebo 1996, Kraemer and Reid 1984). These deposits accumulate within the pipe system and the production equipment as well as in the surrounding of the platforms and present a severe problem for the oil and gas industry concerning the maintenance of industrial health and safety standards and a trouble-free production process. Hence, the fate of radium isotopes released during hydrocarbon exploitation from a reservoir has hitherto been considered mainly with regard to radioactive contamination of platform material and its proper disposal and safety aspects for platform workers. A few studies have addressed the subject of ecological and health risks due to radioactivity accumulation in marine organisms in coastal areas (Lysebo et al. 1996, Meinhold et al. 1996, Olsgaard and Gray 1995, Hamilton et al. 1992, Meinhold and Hamilton 1992).

Measurements about radioactivity levels in produced water have mostly been performed on a sporadic basis rather than in comprehensive studies that cover temporal and spatial variations in the effluents' composition. In some studies, the activities of both ^{226}Ra and ^{228}Ra have been grouped together, often the exact sampling place with respect to its position in the separation and production line is not clear and discharge volumes for specific concentrations are missing or represent an integrated amount of released radioactivity. It must be assumed that most of the values represent total activities (dissolved and particulate phase added) as no information is given about prefiltering of the samples. Further uncertainties arise as to how fast the measurement took place after the sampling time. Kraemer and Reid (1984) showed that within two months, the ^{226}Ra activity in a brine sample had decreased by a factor of four, caused by formation of radiobarite crystals. Table 6 gives an overview of existing data, compiled for oil and gas fields on- and offshore in the USA, the North Sea and Egypt. Data from coal mining in Germany and Poland as well as concentration levels for natural springs that discharge highly-mineralized waters are given for means of comparison. Although these figures represent only a snapshot of the radiochemistry of produced water, they give an idea about the enormous quantities of radioactivity liberated to the (marine) environment during exploration. A five-day survey at the Norwegian Brage oilfield revealed only minor variations in the concentration of radium isotopes in the produced water (Røe Utvik 1999) and sporadic repetitions at selected locations could reproduce former measurements in the same order of magnitude (Mulino and Rayle 1992).

Activities for ^{226}Ra and ^{228}Ra are 100 to more than 1000 times higher than usual concentrations away from platforms (Lysebo et al. 1996, Rabalais et al. 1992). Record values are reported from petroleum brines in Oklahoma and Arkansas that yield up to 5000 Bq/l for ^{226}Ra and 1500 Bq/l for ^{228}Ra (Armbrust and Kuroda 1956). Formation water derived fluids from natural hydrocarbon seeps in the Gulf of Mexico yielded enrichment factors over ambient levels up to 45000 for radium and 150000 for Ba. On the basis of the ^{228}Ra content, the migration time from the source to the sediment-water interface has been calculated to be less than 20 years (Aharon et al. 2001). In general, Ba in produced waters shows enrichment factors similar to radium by a factor 100-1000 (Table 6).

8.4 Discharge volumes and fate of radium after release to the marine environment

A comparison of natural versus man-made radium inputs would require an exact quantification of the total yearly discharge of radium in general and ^{228}Ra in special from a certain production field or a whole region which is nearly impossible on the basis of the data in Table 6. An approximation can be made by taking average radium activities and assuming them to be relatively constant. For the North Sea, the volume of produced water has been estimated at 340 million m³ for 1997 (Røe et al. 1996).

Naturally occurring radium from man-made sources

This would yield a total release of 1.7 TBq for ^{226}Ra and 3.4 TBq for ^{228}Ra , taking an average activity of 5 Bq/l and 10 Bq/l, respectively (Table 6).

In the absence of discharge volumes and associated radium concentrations for South American produced waters, an estimation can be tried on the grounds of the production figures. The approximate offshore oil production from Argentina and Brazil for the fields displayed in Fig. 44 in 1995 was 30 million m³ (Petroconsultants 1996). Combined with averaged produced water discharges from the North Sea, an expected mean discharge can be calculated. Assuming the same mean radium activities in the produced water as for the North Sea, a yearly release of 0.65 TBq for ^{226}Ra and 0.33 TBq for ^{228}Ra can be expected. This is probably a conservative estimate as gas production figures have not been taken into account. The local variations, however, might be by one to two orders of magnitude.

These numbers can be compared to natural ^{228}Ra release from shelf sediments. Working with the same flux of 3000 dpm/m²/year as in chapter 7.1.2 and a surface area of 1.5×10^6 km² for the South American shelf between 33 and 55° S results in a yearly release of ^{228}Ra of 75 TBq. At first glance, this implies that for the South American shelf region as a whole, artificial ^{228}Ra input is insignificant compared to natural diffusion from the shelf sediments. When looking on a more regional scale, the relationship might indeed be inverse. The platforms must be considered as point sources with extremely high concentrations compared to ambient sea water activities. Also, the discharges occur close to the sea surface whereas natural input is by diffusion from the bottom. Therefore, it is highly questionable to what extent these different sources in terms of their fluxes can be compared.

Whether the discharges have an impact on downstream ^{228}Ra activities depends more on the degree of dilution of the initially high concentrations and the time of transport into offshore waters. As open ACC waters yield ^{228}Ra activities close to the detection limit, they represent a very sensitive region where, even diluted, signals can still be important.

Some of the oil and gas fields on the South American shelf are likely to be situated in a favourable position regarding a rapid transport of their produced waters away from the source. The oil and gas rigs in the Campos Basin, Brazil, are situated on the continental slope in water depths exceeding 1300 m. Due to their more offshore position, discharges from these fields are under the direct influence of the Brazil Current which follows the continental slope. Under the influence of the strong westerly winds, the drift on the shelf south of 42° S is over large areas seaward, sweeping the shelfwater into the direct influence of the Falkland and Brazil Currents (Perillo et al. 2001). On the Patagonian shelf, the hydrocarbon fields situated in the estuary of the Strait of Magellanes are directly affected by the outflow of the Strait in direction of the Falkland Current (Fig. 44).

The fact that a lot of the radium liberated with produced water precipitates as radiobarite as soon as produced and sea waters mix, must not necessarily be a limitation to the model of an eastward transport of radium away from platforms into the

open ocean. Precipitation will never be complete due to equilibrium reactions. Controlled precipitation of radium together with Ba and sulfate ions is a common method to decrease the radium content in effluents from uranium mining and milling sites (Huck and Anderson 1990). Reported activities for ^{226}Ra in effluents for the Elliot Lake region, Canada, are between 10 and 20 Bq/l prior to and between 0.3 and 3 Bq/l after treatment (IJC 1997; Table 6). This means that up to 15% of the original ^{226}Ra content are still discharged into the natural environment. Furthermore, it has been shown that radium fixed in barite can still be subject to transport processes in the form of tiny crystals (Moore and Dymond 1991, Aharon 2001). Dissolution processes of both organic and inorganic origin may also continue to take place despite the low solubility product of barite. Radiobarite is degraded by reducing bacteria like *Desulfovibrio* for example, resulting in a net release of Ba^{2+} , Ra^{2+} and H_2S (Ritcey 1990).

The question in the context of this study is, if there are ways to distinguish between ^{228}Ra released from platforms and from the shelf sediments. A strong release of ^{226}Ra could indeed show in the downstream open ocean values, because the natural activities are mostly just above the detection limit. ^{226}Ra in contrast is naturally present in sea water in easily measurable amounts and an additional input might simply be hidden in the normal variation. Assuming that the samples R 6 and S 5 (see chapter 5.2.2) have indeed gained radium input from produced water, then this attribution does not show in their ^{226}Ra activities. The concentrations for both samples are consistent with their neighbouring values. Hence the $^{228}\text{Ra}/^{226}\text{Ra}$ activity ratio alone does not help unless it yields very exotic values.

A differentiation between both radium sources could best be done with tracers typical for produced water that are not released by the shelf sediments, like organic compounds for example.

These, surely speculative, considerations show that increased ^{228}Ra signals in the open ACC downstream of southern South America could in part originate from man-made sources on the continental shelf or slope. Yet a distinction between diffusion from sediments and produced water discharges as the source for ^{226}Ra is not possible and was not intended on the grounds of the data presented in this study. To my knowledge, a clear evidence of such an effect has not been described in the scientific literature. A brief mention that highly mineralized waters can indeed have an effect on natural radium activities distant to the source is given in Aharon et al. (2001) in the context of natural hydrocarbon seeps (p. 132): "... regional surveys should also address the question of Ra and Ba dispersion from the seeps into the water column in view of data suggesting an 'unexplained' increase in the downstream Ra concentrations in the Gulf of Mexico."

Table 6 (next 2 pages): Concentrations of ^{226}Ra , ^{228}Ra , Ba and iron in produced waters from oil and gas fields worldwide. Note the different unit (Bq/l) as compared to the natural sea water activities determined in the course of this work.

Naturally occurring radium from man-made sources

²²⁶ Ra (Bq/l)	²²⁸ Ra (Bq/l)	²²⁶ Ra+ ²²⁸ Ra (Bq/l)	Salinity (g/l)	Barium (mg/l)	Iron (mg/l)	Discharge
1 - 10	0.3 - 10					2100 - 18000 m ³ /d
10	17			228	11.3	
6	11			107	4.2	
7	<2			142	7.7	
6	7			147	4.3	
				1.3	1.8	
				1.9	3.8	
				3.4	5.9	
				0.7	66.1	
				6.6		
		0.007 - 0.03 *		0.1	<0.02	
		5 - 39	43 - 192 *	2 - 230		587 - 23176 m ³ /d
6 - 19	6 - 7		134 - 137 *			210 - 2576 m ³ /d
4 - 9	9 - 14					
0.01 - 0.03	0.01 - 0.1					
		<7.4 - >22.2	34 - 227 *			32 - 954 m ³ /d
		1 - 104	10 - 274 *			
		26 - 45	163 - 167 *	37 - 98		249 - 477 m ³ /d
		31	143 *	11454		249 - 477 m ³ /d
		22	220 *	15		
0.002 - 58		nd - 56	8 - 274			
13		14				34 MBq/d
3 - 5000	33 - 1500					
nd - 141	nd - 888					
22 - 59	11 - 52					
40	60					
5	1					
1 - 390						650 Bq/d
0.04 - 13				2500		>0.82 GBq/d
1						
63	28		250	1500		
330						
0.5 - 61	1 - 41		45 - 155 *	0.12 - 1173		
10 - 20						
0.3 - 3						

Naturally occurring radium from man-made sources

Type of sample or sampling place	Locality	Source
Flotation cells & degassing tanks	North Sea	Lysebo et al. 1996
Produced Water	North Sea, Brage Oil Field	Røe Utvik 1999
Produced Water	North Sea, Oseberg F Oil Field	Røe Utvik 1999
Produced Water	North Sea, Oseberg C Oil Field	Røe Utvik 1999
Produced Water	North Sea, Troll Oil Field	Røe Utvik 1999
Produced Water	North Sea, Brent Oil Field	Jacobs et al. 1992
Produced Water	Northern North Sea Oil Fields	Jacobs et al. 1992
Produced Water	Central North Sea Oil Fields	Jacobs et al. 1992
Produced Water	North Sea Gas Fields, UK Sector	Jacobs et al. 1992
Produced Water	North Sea Gas Fields, Dutch Sector	Jacobs et al. 1992
Sea Water	Background level North Sea water	Jacobs et al. 1992
Produced Water	Louisiana, Gulf of Mexico	Rabalais et al. 1992
0-100m from discharge point	Louisiana, Gulf of Mexico	Mulinio and Rayle 1992
Discharge water	Louisiana, Gulf of Mexico	Hamilton et al. 1992
Water 50 feet from discharge	Louisiana, Gulf of Mexico	Hamilton et al. 1992
Produced Water	Louisiana, coastal wetlands	Rayle and Mulinio 1992
Produced Water	Louisiana & Texas, gas, oil & geoth. wells	Reid 1983
Produced Water	Gulf of Mexico, Eugene Island oil platform	Neff et al. 1989, 1992
Produced Water	Gulf of Mexico, Lake Peito oil platform	Neff et al. 1989, 1992
Produced Water	Gulf of Mexico, Ship Shoal oil platform	Neff et al. 1989, 1992
Produced Water	Louisiana & Texas gas wells	Kraemer and Reid 1984
Produced Water	Gulf of Mexico	Randolph et al. 1992
Petroleum brine	Oklahoma and Arkansas	Armbrust & Kuroda 1956
Gas Brine	New York State	NYSDEC 2001
Oil Brine	New York State	NYSDEC 2001
Unspecified petroleum waste water	Western Egypt	Shawky et al. 2001
Unspecified petroleum waste water	Red Sea	Shawky et al. 2001
Pit water from coal mining	Silesia, Poland	Pociask-Karteczka 1997
Pit water from coal mining	Ruhr District, Germany	Feige and Wiegand 1999
Tributary downstream of colliery	Ruhr District, Germany	Feige and Wiegand 1999
Pit water from hard coal mining	Ruhr District, Germany	Wiegand & Feige, in prep.
Hot spring fluids	Iran	Pociask-Karteczka 1997
Fluid emissions	Gulf of Mexico, natural hydrocarbon seeps	Aharon et al. 2001
Effluent prior to treatment	Elliot Lake (Canada) uranium mining effluent	IJC 1997
Effluent after treatment	Elliot Lake (Canada) uranium mining effluent	IJC 1997

* Value refers to total radioactivity.

Unit for salinity in the original literature is ppt.

nd: Not detectable; activity was below the detection limit in the respective study.

8.5 Implications of man-made sources for the use of ^{228}Ra as a tracer for shelfwater

The data compiled for various hydrocarbon fields world-wide indicate high releases of ^{228}Ra with discharged produced waters. In a first approach, this does not interfere with the concept of ^{228}Ra as a tracer for shelfwater because oil and gas fields are situated on the continental shelves or slope. However, the natural concentrations are likely to get enhanced by the discharges. This effect should be more pronounced for platforms on the continental slope like e.g. in the Campos Basin because naturally occurring ^{228}Ra activities generally decrease with distance to the source region, i.e. the shelf.

In the context of iron transport paths into the open ocean, the suitability of ^{228}Ra as a tracer for shelfwater advection as suggested in this study has to be reconsidered. First, because the natural shelf source may no longer be the dominant source of ^{228}Ra and artificially enhanced ^{228}Ra activities could lead to an overestimation of iron.

Second, because iron concentrations can be elevated in produced waters, too, with an enrichment up to three orders of magnitude (Table 6). None of the studies cited gives the speciation of this iron and it must be assumed that precipitation occurs shortly after discharge due to changes in temperature, pH and Eh. It is unclear to what extent this iron is available to marine phytoplankton. But the situation might be such that the dominant source of ^{228}Ra is different to the dominant source of iron.

A differentiation of releases from the shelf versus releases with produced water requires knowledge of the $^{228}\text{Ra}/\text{Fe}$ ratios of both sources under consideration. The combination with other trace elements, especially those typical for platform discharges could help to resolve this conflict. Any attempt of quantification on the basis of this work would be highly speculative.

This outline has shown how the application of an otherwise approved marine tracer has to be questioned and might get affected in its applicability due to human activities. The extent of such perturbations has yet to be approved.

9 CONCLUSIONS

- Measurements of ^{228}Ra and ^{226}Ra surface water activities in the Atlantic sector of the Southern Ocean have for the first time been carried out in a high-resolution on several N-S-transects across the Antarctic Circumpolar Current (ACC). The sections cover the major oceanographic fronts at different seasons. The work also provides a solid set of ^{228}Ra data on the continental shelves bordering this region of the Southern Ocean. Several areas like the Larsen shelf and the Pacific side of the Antarctic Peninsula have been sampled for ^{228}Ra for the first time.
- Due to its remoteness from land and the corresponding paucity of neighbouring shallow water regions, the open Southern Ocean yields activities of ^{228}Ra that are amongst the lowest ones world-wide. Hence, sample collection and processing have been adjusted in a way to obtain a highest possible concentration factor of radium from as large a water volume as practicable. But even when analyzing several m³ of sea water with the sensitive ^{228}Th -ingrowth method, offshore activities in the central Weddell Gyre were below the detection limit. ^{228}Th activities and $^{228}\text{Th}/^{230}\text{Th}$ activity ratios can to some extent be used as indicators of the ^{228}Ra activity but are affected by scavenging processes.
- The high resolution sampling has shown that particulate uptake of ^{226}Ra continues north of the Polar Front after the near depletion of Si, indicating that both parameters are rather decoupled here. The ongoing radium depletion is likely to be caused by acantharians, a SrSO₄-forming group of microzooplankton, as well as by biogenic barite formation taking place in microenvironments. Acantharians, which have hitherto gone largely unnoticed in the biogeochemistry of radium, are proposed as a major carrier phase for radium in the upper ocean.
- In the context of iron input paths into the productive regions of the Atlantic sector of the Southern Ocean, ^{228}Ra was investigated here as a tracer for advection of shelfwater from the neighbouring continents. It could be shown that all sampled shelf areas are characterized by increased ^{228}Ra activities. Despite their great water depth, the offshore regions in the influence of the Brazil and the Agulhas Current show a clear continental influence, too. This could be attributed to enrichment of ^{228}Ra in these western boundary currents during their southbound flow. South of Africa, elevated ^{228}Ra activities could be correlated by satellite altimetry with subtropical anticyclones and rings that are spawned from the retroflecting Agulhas Current. These subtropical intrusions reach to about 45° S into the subantarctic regime. Within the open ACC, proof of increased ^{228}Ra activities remained difficult and a regular occurrence of increased concentrations coinciding with the oceanic fronts could not be observed. High, but sporadic activities along the Polar Front are suggested to originate from the merging of the

Conclusions

Subantarctic and Polar Front at 40° W. Overall, input of shelfwater seems to be of restricted importance for the area of investigation between 0° and 20° E.

It should be stressed that the main sampling area for this study was several thousand kilometres away from the postulated source regions of both ^{228}Ra and iron. Future studies on this topic should cover the area in-between which will help to clarify what processes account for the sporadic, but extremely high ^{228}Ra activities observed at 50° S. Additional surveys should also address the question of the true potential of the Argentinean shelf as a strong source for ^{228}Ra and iron. The contradiction of higher ^{228}Ra activities being found east of their postulated source could not be resolved to satisfaction in this study.

- The application of several geochemical tracers for the investigation of iron transport paths into the Atlantic sector of the Southern Ocean led to a better differentiation of the relative importance and regional influences of shelfwater advection, material released from melting icebergs and vertical upwelling. However, a quantification of any of these input mechanisms on the basis of this and the respective associated studies seems daring. The assumptions regarding the relative importance of each mechanism should be challenged by future studies carried out in carefully selected areas. The subantarctic islands, especially those forming the Scotia Arc, can be regarded as natural iron "supply stations" within the ACC that might give more insight into the linkage between the different forms of iron present in sea water and the distribution of tracers for continental origin like ^{228}Ra , Al and ε_{Nd} .
- Extensive literature research has shown that radium isotopes are considerably enriched in production waters which are discharged from oil and gas fields. Several exploitation fields are in operation along the South American East coast and their discharges can be dispersed with the Brazil and the Falkland Current. In principle, this artificial ^{228}Ra addition does not interfere with the concept of ^{228}Ra as a tracer for shelfwater advection into the open ocean. However, when used for quantitative approaches, a closer look at the released activities and their fate in the marine environment seems recommendable.

One never notices what has been done;
one can only see what remains to be done.

Marie Curie

10 REFERENCES

- Abelmann, A. and Gersonde, R. (1991): Biosiliceous particle flux in the Southern Ocean. – *Marine Chemistry*, 35, 503-536.
- Abraham, E.R., Law, C.S., Boyd, P.W., Lavender, S.J., Maldonado, M.T. and Bowle, A.R. (2000): Importance of stirring in the development of an iron-fertilized phytoplankton bloom. – *Nature*, 407, 727-730.
- Admiralty List of Light and Fog Signals (2000/20001): NP80 List of Lights, Volume G, Western side of South Atlantic Ocean and East Pacific Ocean. – Admiralty Charts and Publications, United Kingdom Hydrographic Office.
- Aharon, P., van Gent, D., Fu, B. and Scott, L.M. (2001): Fate and effects of barium and radium-rich fluid emissions from hydrocarbon seeps on the benthic habitats of the Gulf of Mexico offshore Louisiana. – OCS Study MMS 2001-004. Prepared by the Louisiana State University, Coastal Marine Institute, U.S. Department of the Interior, Minerals Management Service, Gulf of Mexico OCS Region, New Orleans, LA, 142pp. Internet: <http://www.mms.gov>
- Alekseev, F.A., Ermanov, V.I. and Filonov, V.A. (1958): K voprosu o soderzhanii radioelementov v vodakh neftyanykh mestorozhdenii (Radioactive elements in oil field waters). – *Geokhimiya*, 7, 642-649. Translated in *Geochemistry*, 7, 806-814.
- Allanson, B.R., Hart, R.C. and Lutjeharms, J.R.E. (1981): Observations on the nutrients, chlorophyll and primary production of the Southern Ocean south of Africa. – *South African Journal of Antarctic Research*, 10/11, 3-14.
- Ansorge, I.J. and Lutjeharms, J.R.E. (1999): Oceanic flow disturbance in the Antarctic Circumpolar Current at the Prince Edward Islands (Southern Ocean). – *EOS, Transactions of the American Geophysical Union*, 80 (49), 184.
- Arhan, M., Heywood, K.J. and King, B.A. (1999): The deep waters from the Southern Ocean at the entry to the Argentine Basin. – *Deep-Sea Research II*, 46, 475-499.
- Armbrust, B.F. and Kuroda, P.K. (1956): On the isotopic constitution of radium (Ra-224/Ra226 and Ra-228/Ra-226) in petroleum brines. – *Trans. Amer. Geophys. Union*, 37, 216-220.
- Bacon, M.P. and Anderson, R.F. (1982): Distribution of Thorium Isotopes Between Dissolved and Particulate Forms in The Deep Sea. – *Journal of Geophysical Research*, 87 (C3), 2045-2056.
- Bainbridge, A. E. (1971): GEOSECS: A program for the International Decade of Ocean Exploration. - *Marine Technology Society Journal*, 5(6), 23-26.
- Baskaran, M., Murphy, D.J., Santschi, P.H., Orr, J.C. and Schink, D.R. (1993): A method for rapid in situ extraction and laboratory determination of Th, Pb, and Ra isotopes from large volumes of seawater. – *Deep-Sea Research I*, 40, 849-865.
- Bathmann, U.V., Scharek, R., Klaas, C., Dubischar, C.D. and Smetacek, V. (1997): Spring development of phytoplankton biomass and composition in major water masses of the Atlantic sector of the Southern Ocean. – *Deep-Sea Research II*, 44, 51-67.
- Bathmann, U.V., Priddle, J., Treguer, P., Lucas, M., Hall, J. and Parslow, J. (2000): Plankton ecology and biogeochemistry in the Southern Ocean: A review of the Southern Ocean JGOFS. – In: Hansen, R.B., Ducklow, H.W. and Field, J.G. (Eds.): *The Dynamic Ocean Carbon Cycle: A Midterm Synthesis of the Joint Global Ocean Flux Study, International Geosphere-Biosphere Programme Book Series*, 5, 300-337.
- Bayer, R. and Schlosser, P. (1991): Tritium profiles in the Weddell Sea. – *Marine Chemistry*, 35, 123-136.
- Beers, J.R., Reid, F.M.H. and Stewart, G.L. (1975): Microplankton of the North Pacific central gyre. Population structure and abundance, June 1973. – *Internationale Revue der Gesamten Hydrobiologie*, 60, 607-638.

References

- Bernstein, R.E. and Betzer, R.H. (1991): Labile phases and the ocean's strontium cycle. In: Hurd, D.C. and Spencer, D.W. (Eds.): *Marine Particles: Analysis and Characterization*. - Geophysical Monograph 63, 369-374, American Geophysical Union, Washington DC, USA.
- Bernstein, R.E., Byrne, R.H., Betzer, P.R., Greco, A.M. (1992): Morphologies and transformations of celestite in seawater: the role of acantharians in strontium and barium geochemistry. – *Geochimica Cosmochimica Acta*, 56, 3273-3279.
- Bernstein, R.E., Byrne, R.H. and Schijf, J. (1998): Acantharians: a missing link in the oceanic biogeochemistry of barium. – *Deep-Sea Research I*, 45, 491-505.
- Bernstein, R.E., Kling, S.A. and Boltovskiy, D. (1999): Acantharia. - In: Boltovskiy, D. (Ed.): *South Atlantic Zooplankton*, Vol.1, 75-145, Backhuys, Leiden, Netherlands.
- Bishop, J.K.B. (1988): The barite-opal-organic-carbon association in oceanic particulate matter. – *Nature*, 332, 341-343.
- Bland, C.J. (2001): A review of NORM in Oil and Natural gas Extraction.
Internet: <http://www.c5plus.com/norm.htm>
- Boebel, O., Duncombe Rae, C., Garzoli, S., Lutjeharms, J., Richardson, P., Rossby, T., Schmid, C. and Zenk, W. (1998): Float experiment studies interocean exchanges at the tip of Africa. - *EOS, Transactions of the American Geophysical Union*, 79, 1, 6-8.
- Boebel, O., Lutjeharms, J., Schmid, C., Zenk, W., Rossby, T. and Barron, C. (2001): The Cape Cauldron: A regime of turbulent interocean exchange. – *Deep-Sea Research II*, submitted.
- Bollinger, M.S. and Moore, W.S. (1984): Radium fluxes from a salt marsh. – *Nature*, 309, 444-446.
- Boyd, P.W. et al. (2000): A mesoscale phytoplankton bloom in the polar Southern Ocean stimulated by iron fertilization. – *Nature*, 407, 695-702.
- Broecker, W.S. (1965): An application of natural radon to problems on ocean circulation. - In: Ichijo, T. (Ed.): *Symposium on Diffusion in Oceans and Fresh Waters*, Lamont-Doherty Geological Observatory, Palisades, NY, 116-145.
- Broecker, W.S. and Peng, T.-H. (1982): *Tracers in the Sea*. – Lamont-Doherty Geological Observatory, New York, 690pp.
- Broecker, W.S., Li, Y.-H. and Cromwell, J. (1967): Radium-226 and radon-222: concentration in Atlantic and Pacific Oceans. – *Science*, 158, 1307-1310.
- Broecker, W.S., Kaufman, A. and Trier, R. (1973): Residence time of thorium in surface sea water and its implications regarding the rate of reactive pollutants. – *Earth Planetary Science Letters*, 20, 35-44.
- Broecker, W.S., Goddard, J. and Sarmiento, J.L. (1976): The distribution of ^{226}Ra in the Atlantic Ocean. - *Earth Planetary Science Letters*, 220-235.
- Brown et al. (Eds.; 1989): *Seawater: Its composition, properties and behaviour*. – The Open University, Pergamon Press, Oxford, 165pp.
- Bucciarelli, E., Blain, S. and Tréguer, P. (2001): Iron and manganese in the wake of the Kerguelen Islands (Southern Ocean). - *Marine Chemistry*, 73, 21-36.
- Buesseler, K.O., Cochran, J.K., Bacon, M.P., Livingston, H.D., Casso, S.A., Hirschberg, D., Hartman, M.C. and Fleer, A.P. (1992): Determination of thorium isotopes in seawater by non-destructive and radiochemical procedures. – *Deep-Sea Research I*, 39, 1103-1114.
- Callahan, J.E. (1972): The structure and circulation of deep water in the Antarctic. – *Deep-Sea Research*, 19, 563-575.
- CARUSO – Carbon Uptake in the Southern Ocean: Internet: <http://kellia.nioz.nl/projects/caruso>

References

- Chan, L.H., Edmond, J.M., Stallard, R.F., Broecker, W.S., Chung, Y.C., Weiss, R.F. and Ku, T.-L. (1976): Radium and barium at GEOSECS stations in the Atlantic and Pacific. – Earth Planetary Science Letters, 32, 258-267.
- Chen, J.H., Edwards, R.L. and Wasserburg, G.J. (1986): ^{238}U , ^{234}U and ^{232}Th in seawater. – Earth Planetary Science Letters, 80, 241-251.
- Cheney, R.E., Marsh, J.G. and Beckly, B.D. (1983): Global mesoscale variability from collinear tracks of Seasat altimeter data. – Journal of Geophysical Research, 88, 4343-4354.
- Chow, T.J. and Goldberg, E.D. (1960): Concentration profiles of barium. – Geochimica Cosmochimica Acta, 20, 192-198.
- Chung, Y. (1974): Radium-226 and Ra-Ba-relationships in Antarctic and Pacific waters. – Earth Planetary Science Letters, 23, 125-135.
- Chung, Y. (1980): Radium-barium-silica correlations and a two dimensional radium model for the world ocean. – Earth Planetary Science Letters, 49, 309-318.
- Chung, Y. (1981): ^{210}Pb and ^{226}Ra distributions in the Circumpolar waters. – Earth Planetary Science Letters, 55, 205-216.
- Chung, Y. (1987): ^{226}Ra in the western Indian Ocean. – Earth Planetary Science Letters, 85, 11-27.
- Chung, Y. and Applequist, M.D. (1980): ^{226}Ra and ^{210}Pb in the Weddell Sea. – Earth Planetary Science Letters, 49, 401-410.
- Chung, Y. and Craig, H. (1973): Ra-226 in the eastern equatorial Pacific. – Earth Planetary Science Letters, 17, 306-318.
- Cochran, J.K. (1980a): The flux of Ra-226 from deep-sea sediments. – Earth Planetary Science Letters, 49, 381-392.
- Cochran, J.K. (1980b): The use of naturally occurring radionuclides as tracers for biologically related processes in deep-sea sediment. - In: Ernst, W.G. and Morin, J.G. (Eds.): The environment of the deep-sea. pp. 55-72, Prentice Hall, Englewood Cliffs, NJ.
- Cochran, J.K. and Krishnaswami, S. (1980): Radium, thorium, uranium and Pb-210 in deep-sea sediments and sediment pore water from the North Equatorial Pacific. – American Journal of Science, 280, 849-889.
- Cochran, J.K., Livingston, H.D., Hirschberg, D.J. and Surprenant, L.D. (1987): Natural and anthropogenic radionuclide distributions in the northwest Atlantic Ocean. – Earth Planetary Science Letters, 84, 135-152.
- Croot, P. and Turner, D.R. (1998): Iron speciation in the Southern Ocean. – Abstract at Amsterdam Symposium Biogeochemistry of Iron in Seawater, SCOR, WG, 109, 27.
- Curie, M., Debierne, A., Eve, A.S., Geiger, H., Hahn, O., Lind, S.C., Meyer, S., Rutherford, E. and Schweidler, E. (1931): The radioactive constants as of 1930. – Reviews of Modern Physics, 3, 427-445.
- de Baar, H.J.W. and de Jong, J.T.M. (2001): Distributions, Sources and Sinks of Iron in Seawater. – In: Turner, D. and Hunter, K.A. (Eds.): Biogeochemistry of Iron in Seawater, IUPAC Book Series on Analytical and Physical Chemistry of Environmental Systems, 7, 123-253.
- de Baar, H.J.W., Buma, A.G.J., Nolting, R.F., Cadée, G.C., Jacques, G. and Tréguer, P.J. (1990): On iron limitation of the Southern Ocean: experimental observations in the Weddell and Scotia seas. – Marine Ecology Progress Series, 65, 105-122.
- de Baar, H.J.W., de Jong, J.T.M., Bakker, D.C.E., Löscher, B.M., Veth, C., Bathmann, U. and Smetacek, V. (1995): Importance of iron for plankton blooms and carbon dioxide drawdown in the Southern Ocean. – Nature, 373, 412-415.
- de Jong, J.T.M., den Das, J., Bathmann, U., Stoll, M.H.C., Kattner, G., Nolting, R.F. and de Baar, H.J.W. (1998): Dissolved iron at subnanomolar levels in the Southern Ocean as determined by ship-board analysis. – Analytica Chimica Acta, 377, 113-124.

References

- Deacon, G.E.R. (1982): Physical and biological zonation in the Southern Ocean. – Deep-Sea Research, 29, 1-15.
- Dehairs, F., Chesselet, R. and Jedwab, J. (1980): Discrete suspended particles of barite and the barium cycle in the open ocean. – Earth Planetary Science Letters, 49, 528-550.
- Dehairs, F., Shopova, D., Ober, S., Veth, C. and Goeyens, L. (1997): Particulate barium stocks and oxygen consumption in the Southern Ocean mesopelagic water column during spring and early summer: relationship with export production. – Deep-Sea Research II, 44, 497-516.
- Dreisigacker, E. and Roether, W. (1978): Tritium and ^{80}Sr in the North Atlantic Surface Water: sources, rates, and pathways. – Earth Planetary Science Letters, 38, 301-312.
- Drinkwater, M.R., Liu, X., Maslanik, J. and Fowler, C. (1999): Optimal analysis products combining buoy trajectories and satellite-derived ice-drift fields. – In: Report of the second session of the WCRP Antarctic Buoys (Naples, Italy, 11-13 May 1998), International Programme for World Climate Research, Informal Reports 5 (1999).
- Duce, R.A. and Tindale, N.W. (1991): Atmospheric transport of iron and its deposition in the ocean. – Limnology and Oceanography, 36 (8), 1715-1726.
- Edgar, G.J. (1987): Dispersal of faunal and floral propagules associated with drifting *Macrocystis pyrifera* plants. – Marine Biology, 95, 599-610.
- Edmond, J.M. (1970): Comments on the paper by T.L. Ku, Y.H. Li, G.G. Mathieu and H.K. Wong, "Radium in the Indian-Antarctic Ocean south of Australia". – Journal of Geophysical Research, 75, 6878-6883.
- Elsinger, R.J. and Moore, W.S. (1983): Ra-224, Ra-228 and Ra-226 in Winyah Bay and Delaware Bay. – Earth Planetary Science Letters, 64, 430-436.
- Elsinger, R.J. and Moore, W.S. (1984): Ra-226 and Ra-228 in the mixing zones of the Pee Dee River-Winyah Bay, Yangtze River and Delaware Bay estuaries. – Estuarine Coastal Shelf Science, 18, 601-613.
- Elsinger, R.J., King, P.T. and Moore, W.S. (1982): ^{224}Ra in natural waters measured by γ -ray spectrometry. – Analytica Chimica Acta, 144, 227-281.
- Erdtmann, G. and Soyka, W. (1979): The Gamma Rays of the Radionuclides. – Verlag Chemie, Weinheim, 862pp.
- Evans, R.D., Kip, A.F. and Moberg, E.G. (1938): The radium and radon content of Pacific Ocean water, life and sediments. – American Journal of Science, 36, 241-259.
- Falkland Islands Government (1999): Internet: <http://www.falklands.gov.fk/oildept.htm>
- Faure, G. (1986): Principles of Isotope Geology. – 2nd edition, Wiley, New York, 589pp.
- Feige, S. and Wiegand, J. (1999): The influence of coal mining on radon potential. – Il Nuovo Cimento, 22(C), 345-352.
- Fisher, N.S. and Teissié, J.-L. (1987): Accumulation of Th, Pb, U, and Ra in marine phytoplankton and its geochemical significance. – Limnology and Oceanography, 32, 131-142.
- Fleer, A.P. and Bacon, M.P. (1984): Determination of ^{210}Po and ^{210}Pb in seawater and marine particulate matter. – Nuclear Instruments and Methods in Physics Research, 223, 243-249.
- Fleer, A.P. and Bacon, M.P. (1991): Notes on some techniques of marine particle analysis used at WHOI. In: Hurd, D.C. and Spencer, D.W. (Eds.): Marine Particles: Analysis and Characterization. - Geophysical Monograph 85, 223-226, American Geophysical Union, Washington DC, USA.
- Flynn, W.W. (1968): The determination of low levels of Polonium-210 in environmental materials. – Analytica Chimica Acta, 43, 221-227.
- Fogelqvist, E. (1985): Carbon tetrachloride tetrachloroethylene 1,1,1-trichloroethane and bromoform in Arctic seawater. – Journal of Geophysical Research, 90, 9181-9193.

References

- Foster, T.D. and Carmack, E.C. (1976): Frontal zone mixing and Antarctic Bottom Water formation in the southern Weddell Sea. – Deep-Sea Research, 23, 301-317.
- Francois, R., Bacon, M.P. and Suman, D.O. (1990): Thorium-230 profiling in deep-sea sediments: High-resolution records of flux and dissolution of carbonate in the equatorial Atlantic during the last 24,000 years. – Paleoceanography, 5, 761-787.
- Friedrich, J. (1997): Polonium-210 und Blei-210 im Südpolarmeer: Natürliche Tracer für biologische Prozesse im Oberflächenwasser des Antarktischen Zirkumpolarstroms und des Weddellmeeres. – Berichte zur Polarforschung, 235, 155pp.
- Fu, L.-L., Dudley, B.C. and Zlotnicki, V. (1988): Satellite Altimetry: Observing Ocean Variability from Space. – Oceanography, 1 (2), 4-11+58.
- Gammon, R.H., Cline, J. and Wisegarver, D. (1982): Chlorofluoromethanes in the northeast Pacific Ocean: Measured vertical distributions and application as transient tracers of upper ocean mixing. – Journal of Geophysical Research, 87, 9441-9454.
- Geibert, W. (2001): Actinium-227 als Tracer für Advektion und Mischung in der Tiefsee. – Berichte zur Polarforschung, 385, 112pp.
Internet: <http://www.awi-bremerhaven.de/GEO/Publ/PhDs.html>
- Gilmore, G. and Hemingway, J.D. (1996): Practical Gamma-Ray Spectrometry. – Wiley & Sons, Chichester, 314pp.
- Gmelin (1997): Handbuch der Anorganischen Chemie. – Main series, 8th edition, System-Number 31, Springer Verlag, Heidelberg.
- Gordon, A.L. (1967): Structure of Antarctic waters between 20°W and 170°W. – In: Bushnell, V.C. (Ed.): Antarctic map folio series, Folio 6, American Geophysical Society, 10pp.
- Gordon, A.L. (1988): The South Atlantic: An overview of results from 1983-1988 research. – Oceanography, 1 (2); 12-17+58.
- Gordon, A.L. and Nowlin Jr., W.D. (1978): The Basin Waters of the Bransfield Strait. – Journal of Physical Oceanography, 8, 258-264.
- Gordon, A.L., Taylor, H.W. and Georgi, D.T. (1977): Antarctic oceanographic zonation. In: Dunbar, M.J. (Ed.): Polar Oceans. – Arctic Institute of North America, 45-67.
- Gordon, A.L., Jutjeharms, J.R.E. and Gründlingh, M.L. (1987): Stratification and circulation at the Agulhas Retroflection. - Deep-Sea Research A, 34, 565-599.
- Gordon, R.M., Johnson, K.S. and Coale, K.H. (1998): The behaviour of iron and other trace elements during the IronEx-I and PlumEx experiments in the Equatorial Pacific. – Deep-Sea Research, 45, 995-1041.
- Gott, G.B. and Hill, J.W. (1953): Radioactivity in Some Oil Fields of Southeast Kansas. – USGS Bulletin, 988E, 69-112.
- Gouretski, V.V. and Danilov, A.I. (1993): Weddell Gyre: structure of the eastern boundary. – Deep-Sea Research I, 40, 561-582.
- Gran, H.H. (1931): On the conditions for the production of plankton in the sea. – Rapports et Procès Verbaux des Réunions, Conseil Permanent International pour l'Exploration de la Mer, 75, 37-46.
- Grotti, M., Soggia, F., Abelmoschi, M.L., Rivaro, P., Magi, E. and Frache, R. (2001): Temporal distribution of trace metals in Antarctic coastal waters. – Marine Chemistry, 76, 189-209.
- Grousset, F.E., Biscaye, P.E., Revel, M., Petit, J.-R., Pye, K., Joussaume, S. and Jouzel, J. (1992): Antarctic (Dome C) ice-core dust at 18 k.y. B.P.: Isotopic constraints on origins. – Earth Planetary Science Letters, 111, 175-182.
- Hamilton, L.D., Meinhold, A.F. and Nagy, J. (1992): Health risk assessment for radium discharged in produced waters. In: Ray, J.P. and Engelhart, F.R. (Eds.): Produced Water: Technological/Environmental Issues and Solutions. – Plenum Press, New York, 303-314.

References

- Hancock, G.J. and Martin, P. (1991): The determination of radium in environmental samples by alpha-particle spectrometry. – *Applied Radiation and Isotopes*, 42, 63-69.
- Hancock, G.J., Webster, I.T., Ford, P.W. and Moore, W.S. (2000): Using Ra isotopes to examine transport processes controlling benthic fluxes into a shallow estuarine lagoon. – *Geochimica Cosmochimica Acta*, 64, 3685-3699.
- Health Physics Society. – Internet: <http://www.hps.org>
- Hegner, E., Dauelsberg, H.J., Jeandel, C., Rutgers van der Loeff, M.M. and de Baar, H.J.W. (in prep.): Distribution and sources of terrigenous matter in surface waters and seawater composition in the South Atlantic sector of the Southern Ocean as inferred from Nd isotopes.
- Howard Jr., E.G. and O'Brien, T.C. (1999): Water-bouyant particulate materials containing micronutrients for phytoplankton. – United States Patent 5965117; United States Patent and Trade Mark Office. Internet: <http://www.uspto.gov/patft/index.html>
- Huck, P.M. and Anderson, W.B. (1990): Removal of ^{226}Ra from uranium mining effluents and leaching from sludges. – In: International Atomic Energy Agency: The environmental behaviour of radium, Vol.2. – Technical Report Series 310, 135-162.
- IJC – International Joint Commission (1997): Inventory of radionuclides for the Great Lakes. Internet: <http://www.ijc.org/boards/nuclear/invrep/index.htm>
- Iriondo, M. (2000): Patagonian dust in Antarctica. – *Quaternary International*, 68-71, 83-86.
- IUPAC International Commission on Atomic Weights (1999): Pure Appl. Chemistry, 71, 1593-1607.
Internet: http://www.iupac.org/publications/pac/1999/71_08_pdf/7108vocke_1593.pdf
- Ivanovich, M. and Harmon, R.S. (1992): Uranium-series Disequilibrium, Applications to Earth, Marine, and Environmental Sciences. – 2nd edition, Clarendon Press, Oxford, 910pp.
- Jacobs, R.P.W.M., Grant, R.O.H., Kwant, J., Marquenie, J.M. and Mentzer, E. (1992): The composition of produced water from Shell operated oil and gas production in the North Sea. In: Ray, J.P. and Engelhart, F.R. (Eds.): Produced Water: Technological/Environmental Issues and Solutions. – Plenum Press, New York, 13-22.
- Jenkins, W.J. and Clarke, W.B. (1976): The distribution of ^3He in the Western Atlantic Ocean. – *Deep-Sea Research*, 23, 481-494.
- Johnsen, S. (1996): Produced water control in the North Sea. – 6th Annual Produced Water Seminar, American Filtration Society, Texas.
- Johnson, K.S., Chavez, F.P. and Friedrich, G.E. (1999): Continental-shelf sediments as a primary source of iron for coastal phytoplankton. – *Nature*, 398, 697-700.
- Joly, J. (1908): On the radium-content of deep-sea sediment. – *Philosophical Magazine*, 16, 190-197.
- Jones, B. and Manning, D.A.C. (1994): Comparison of geochemical indices used for the interpretation of palaeoredox conditions in ancient mudstones. – *Chemical Geology*, 111, 111-129.
- KAPEX – Cape of Good Hope Experiments. Internet: <http://www.ifm.uni-kiel.de/ph/woce/kapex/>
- Kaufman, A., Trier, R.M. and Broecker, W.S. (1973): Distribution of ^{228}Ra in the World Ocean. – *Journal of Geophysical Research*, 78, 8827-8848.
- Kershaw, P. (1999): Pilot Study for the update of the MARINA Project on the radiological exposure of the European Community from radioactivity in North European marine waters, final Report: December 1999. Prepared for the European Commission Directorate-General XI, Environment, Nuclear Safety and Civil Protection. Internet: <http://www.europa.eu.int/comm/environment/radprot/index.htm#studies>
- Key, R.M., Sarmiento, J.L. and Moore, W.S. (1985): Distribution of Ra-228 and Ra-226 in the Atlantic Ocean. – Technical Reports #85-1, TTO Test Cruise, NAS legs 1-3, 78pp.

References

- Koczy, F.F. (1958): Natural radium as a tracer in the ocean. – Proceedings of the Second UN International Conference on the Peaceful Uses of Atomic Energy, Geneva, 18, 351-357.
- Koczy, F.F., Picciotto, E., Poulaert, G. and Wilgain, S. (1957): Mesure des isotopes du thorium dans l'eau de mer. – *Geochimica Cosmochimica Acta*, 11, 103-129.
- Kraemer, T.F. and Reid, D.F. (1984): The occurrence and behaviour of radium in saline formation water of the US Gulf coast region. – *Isotope Geoscience*, 2, 153-174.
- Krest, J.M., Moore, W.S. and Rama (1999): ^{226}Ra and ^{228}Ra in the mixing zones of the Mississippi and Atchafalaya Rivers: indicators of groundwater input. – *Marine Chemistry*, 64, 129-152.
- Ku, T.-L. and Lin, M.C. (1976): Ra-226 distributions in the Antarctic Ocean. – *Earth Planetary Science Letters*, 31, 236-248.
- Ku, T.-L. and Luo, S. (1994): New appraisal of Radium 226 as a large-scale oceanic mixing tracer. – *Journal of Geophysical Research*, 99 (C5), 10255-10273.
- Ku, T.-L., Li, Y.H., Mathieu, G.G. and Wong, H.K. (1970): Radium in the Indian-Antarctic Ocean south of Australia. – *Journal of Geophysical Research*, 75, 5286-5292.
- Ku, T.-L., Li, Y.H., Mathieu, G.G. and Wong, H.K. (1976): Radium in the Indian-Antarctic Ocean South of Australia. – *Journal of Geophysical Research*, 75, 5286-5292.
- Ku, T.-L., Huh, C.A. and Chan, P.S. (1980): Meridional distribution of Ra-226 in the eastern Pacific along GEOSECS cruise tracks. – *Earth Planetary Science Letters*, 49, 293-308.
- Ku, T.-L., Luo, S., Kusakabe, M. and Bishop, J.K.B. (1995): ^{228}Ra -derived nutrient budgets in the upper equatorial Pacific and the role of "new" silicate in limiting productivity. – *Deep-Sea Research II*, 42, 479-497.
- Kumar, N., Anderson, R.F., Mortlock, R.A., Froelich, P.N., Kubik, P., Dittrich-Hannen, B. and Suter, M. (1995): Increased biological productivity and export production in the glacial Southern Ocean. – *Nature*, 378, 675-680.
- Legeleux, F. and Reyss, J.-L. (1996): $^{228}\text{Ra}/^{226}\text{Ra}$ activity ratios in oceanic settling particles: implications regarding the use of barium as a proxy for paleoproductivity reconstruction. – *Deep-Sea Research I*, 1857-1863.
- Leisegang, E.C. and Orren, M.J. (1966): Trace Element Concentrations in the Sea off South Africa. – *Nature*, 211, 1166-1167.
- Levy, D.M. and Moore, W.S. (1985): Ra-224 in continental shelf waters. – *Earth Planetary Science Letters*, 73, 226-230.
- Li, Y.-H., Ku, T.L., Mathieu, G.G. and Wolgemuth, K. (1973): Barium in the Antarctic Ocean and implications regarding the marine geochemistry of Ba and ^{226}Ra . – *Earth Planetary Science Letters*, 19, 352-358.
- Li, Y.-H., Feely, H.W. and Santschi, P.H. (1979): ^{228}Th - ^{228}Ra radioactive disequilibrium in the New York Bight and its implications for coastal pollution. – *Earth Planetary Science Letters*, 42, 13-26.
- Li, Y.-H., Feely, H.W. and Toggweiler, J.R. (1980): ^{228}Ra and ^{228}Th concentrations in GEOSECS Atlantic surface waters. – *Deep-Sea Research*, 27A, 545-555.
- Lide, D.R. (1995): CRC Handbook of Chemistry and Physics. – 75th edition, CRC Press, Boca Raton, 2496pp.
- Ljunggren, P. (1955): Geochemistry and radioactivity of some Mn and Fe bog ores. – *Geologiska Föreningens Förhandlingar*, 77, 33-44.
- Löscher B.M., de Baar, H.J.W., de Jong, J.T.M., Veth, C. and Dehairs, F. (1997): The distribution of Fe in the Antarctic Circumpolar Current. – *Deep-Sea Research II*, 44, 143-187.

References

- Lüning, K. (1990): Seaweeds. Their environment, biogeography and ecophysiology. – Wiley & Sons, Chichester, 527pp.
- Lutjeharms, J.R.E. (1985): Location of frontal systems between Africa and Antarctica: some preliminary results. – Deep-Sea Research, 32 (12), 1499-1509.
- Lutjeharms, J.R.E. (1996): The Exchange of Water Between the South Indian and South Atlantic Oceans. In: Wefer, G., Berger, W.H., Siedler, G. and Webb, D.J. (Eds.): The South Atlantic: Present and past circulation. – Springer Verlag, Berlin, 125-162.
- Lutjeharms, J.R.E. (1999): Frontal systems south of Africa. – EOS, Transactions of the American Geophysical Union, 80 (49), 294-295.
- Lutjeharms, J.R.E. and Valentine, H.R. (1984): Southern Ocean thermal fronts south of Africa. – Deep-Sea Research, 31 (12), 1461-1475.
- Lutjeharms, J.R.E. and van Ballegooyen, R.C. (1984): Topographic control in the Agulhas Current system. – Deep-Sea Research, 31, 1321-1337.
- Lutjeharms, J.R.E., Fromme, G.A.W. and Valentine, H.R. (1981): Die termiese oseaan struktuur suid van Afrika. – Verslag oor sestien navorsingsm vaarte. WNNR Navorsingsverlag, 390.
- Lutjeharms, J.R.E., Walters, N.M. and Allanson, B.R. (1985): Oceanic frontal systems and biological enhancement. – In: Siegfried, W.R., Condy, P.R. and Laws, R.M. (Eds.): Antarctic Nutrient Cycles and Food Webs, 11-21, Springer, Berlin.
- Lysebo, I., Birovljev, A. and Strand, T. (1996): NORM in Oil Production – Occupational Doses and Environmental Aspects. – Proceedings of the Nordic Society for Radiation Protection, Meeting Reykjavik 1996. Internet: <http://www.gr.is/nsfs/lysebo.htm>
- Markels Jr., M. (2000): Method of sequestering carbon dioxide. – United States Patent 6056919; United States Patent and Trade Mark Office. Internet: <http://www.uspto.gov/patft/index.html>
- Martin, J.H. (1990): Glacial-interglacial CO₂ change: The iron hypothesis. – Paleoceanography, 5, 1-13.
- Martin, J.H., Gordon, R.M. and Fitzwater, S.E. (1990): Iron in Antarctic waters. – Nature, 345, 156-158.
- Martin, W.R. (1985): Transport of Trace Metals in Nearshore Sediments. – PhD thesis, MIT/WHOI, WHOI-85-18, 302pp.
- Mathieu, G.G., Biscaye, P.E., Lupton, R.A. and Hammond, D.E. (1988): System for measurement of 222Rn at low levels in natural waters. – Health Physics, 55, 989-992.
- McCourt, C.B. and Peers, D.M. (1987): Environmental Monitoring of Trace Elements in Water Discharges from Oil Production Platforms. – Petroanalysis 1987, Development in Analytical Chemistry in the Petroleum Industry, John Wiley & Sons.
- Meinhold, A.F. and Hamilton, L.D. (1992): Radium concentration factors and their use in health and environmental risk assessment. In: Reed, M. and Johnsen, S. (Eds.): Produced Water 2: Environmental Issues and Mitigation Techniques. – Plenum Press, New York, 293-314.
- Meinhold, A.F., Holtzman, S. and DePhillips, M.P. (1996): Risk assessment for produced water discharges to open bays in Louisiana. In: Reed, M. and Johnsen, S. (Eds.): Produced Water 2: Environmental Issues and Mitigation Techniques. – Plenum Press, New York, 395-409.
- Michaels, A.F. (1988): Vertical distribution and abundance of Acantharia and their symbionts. – Marine Biology, 97, 559-569.
- Michaels, A.F., Caron, D.A., Swanberg, N.R., Howse, F.A. and Michaels, C.M. (1995): Planktonic sarcodines (Acantharia, Radiolaria, Foraminifera) in surface waters near Bermuda: abundance, biomass and vertical flux. – Journal of Plankton Research, 17, 131-163.

References

- MODAS – Modular Ocean Data Assimilation System.
Internet: <http://www7320.nrlssc.navy.mil/modas2/logo.html>
- Moise, T., Starinsky, A., Katz, A. and Kolodny, Y. (2000): Ra isotopes and Rn in brines and ground waters of the Jordan-Dead Sea Rift Valley: Enrichment, retardation, and mixing. – *Geochimica Cosmochimica Acta*, 64, 2371-2388.
- Monnin, C., Jeandel, C., Cattaldo, T and Dehairs, F. (1999): The marine barite saturation of the world's oceans. – *Marine Chemistry*, 65, 253-261.
- Moore, W.S. (1969a): Measurement of ^{228}Ra and ^{228}Th in sea water. – *Journal of Geophysical Research*, 74 (2), 694-704.
- Moore, W.S. (1969b): Oceanic concentrations of radium-228. – *Earth Planetary Science Letters*, 6, 437-446.
- Moore, W.S. (1972): Radium-228: Application to thermocline mixing studies. – *Earth Planetary Science Letters*, 16, 421-422.
- Moore, W.S. (1984): Radium isotope measurements using germanium detectors. – *Nuclear Instruments and Methods in Physics Research*, 223, 407-411.
- Moore, W.S. (1987): Radium 228 in the South Atlantic Bight. – *Journal of Geophysical Research*, 92 (C5), 5177-5190.
- Moore, W.S. (1997): 226Ra, 228Ra, 223Ra, and 224Ra in coastal waters with application to coastal dynamics and groundwater input. - *Radioprotection*, 32 (C2), 137-146; 1997
- Moore, W.S. (2000): Ages of continental shelf waters determined from 223Ra and 224Ra. – *Journal of Geophysical Research*, 105(C9), 22117-22122.
- Moore, W.S. and Arnold, R. (1996): Measurement of ^{223}Ra and ^{224}Ra in coastal waters using a delayed coincidence counter. – *Journal of Geophysical Research*, 101 (C1), 1321-1329.
- Moore, W.S. and Astwood, H. (1990): Advection of Amazon water into the Atlantic Ocean. – *EOS, Transactions of the American Geophysical Union*, 71, 1366.
- Moore, W.S. and Dymond, J. (1991): Fluxes of ^{226}Ra and barium in the Pacific Ocean: The importance of boundary processes. – *Earth Planetary Science Letters*, 107, 55-68.
- Moore, W.S. and Sackett, W.M.: (1964): Uranium and thorium series in equilibrium in sea water. – *Journal of Geophysical Research*, 69, 5401-5405.
- Moore, W.S. and Santschi, P.H. (1986): Ra-228 in the deep Indian Ocean. – *Deep-Sea Research*, 33 (1), 107-120.
- Moore, W.S. and Todd, J.F. (1993): Radium isotopes in the Orinoco estuary and eastern Caribbean Sea. – *Journal of Geophysical Research*, 98 (C2), 2233-2244.
- Moore, W.S., Feely, H.W. and Li, Y.-H. (1980): Radium isotopes in sub-arctic waters. – *Earth Planetary Science Letters*, 49, 329-340.
- Moore, W.S., Key, R.M. and Sarmiento, J.L. (1985): Techniques for precise mapping of ^{226}Ra and ^{228}Ra in the ocean. – *Journal of Geophysical Research*, 90 (C4), 6983-6994.
- Moore, W.S., Sarmiento, J.L. and Key, R.M. (1986): Tracing the Amazon component of surface Atlantic water using ^{228}Ra , salinity and silica. – *Journal of Geophysical Research*, 91 (C2), 2574-2580.
- Moore, W.S., DeMaster, D.J., Smoak, J.M., McKee, B.A. and Swarzenski, P.W. (1996): Radionuclide tracers of sediment-water interactions on the Amazon shelf. – *Continental Shelf Research*, 16 (5/6), 645-665.
- Mulino, M.M. and Rayle, M.F. (1992): Produced water radionuclides fate and effects. In: Ray, J.P. and Engelhart, F.R. (Eds.): *Produced Water: Technological/Environmental Issues and Solutions*. – Plenum Press, New York, 281-292.

References

- Naveira Garabato, A.C., Allen, J.T., Leach, H., Strass, V.H. and Pollard, R.T. (2001): Mesoscale Subduction at the Antarctic Polar Front Driven by Baroclinic Instability. – *Journal of Physical Oceanography*, 31, 2087-2107.
- Neff, J.M., Sauer, T.C. and Maciolek, N. (1989): Composition, fate and effects of produced water discharges to nearshore marine waters: final report. – American Petroleum Institute, API Publication 4472, Washington DC.
- Neff, J.M., Sauer, T.C. and Maciolek, N. (1992): Composition, fate and effects of produced water discharges to nearshore marine waters. In: Ray, J.P. and Engelhart, F.R. (Eds.): *Produced Water: Technological/Environmental Issues and Solutions*. – Plenum Press, New York, 371.
- Nolting, R.F., de Baar, H.J.W., van Bennekom, A.J. and Masson, A. (1991): Cadmium, copper and iron in the Scotia Sea, Weddell Sea and Weddell/Scotia Confluence (Antarctica). – *Marine Chemistry*, 35, 219-243.
- Nozaki, Y. and Yamamoto, Y. (2001): Radium-228 based nitrate fluxes in the eastern India Ocean and the South China Sea and a silicon-induced "alkalinity pump" hypothesis. – *Global Biogeochemical Cycles*, 15, 555-567.
- Nozaki, Y., Dobashi, F., Kato, Y. and Yamamoto, Y. (1998): Distribution of Ra isotopes and the ^{210}Pb and ^{210}Po balance in surface seawaters of the mid Northern Hemisphere. – *Deep-Sea Research I*, 45, 1263-1284.
- NYSDEC – New York State Department of Environmental Conservation, Division of Solid & Hazardous Materials (1999): An Investigation of Naturally Occurring Radioactive Materials (NORM) in Oil and Gas Wells in New York State. – New York, 86pp. Internet: <http://www.dec.state.ny.us/website/dshm/hazrad/norm.htm>
- Olsgaard, F. and Gray, J. (1995): A comprehensive analysis of the effects of offshore oil and gas exploration and production on the benthic communities of the Norwegian continental shelf. – *Marine Ecology Progress Series*, 122, 277-306.
- Ormerod, B. and Angel, M. (1998): Ocean fertilization as a CO₂ sequestration option. – Cheltenham: CRE Group for IEA Greenhouse Gas R&D Programme, 50pp.
- Orr, J.C. (1988): ^{222}Rn , ^{226}Ra , and ^{228}Ra as tracers for the evolution of warm core rings. – PhD thesis, Texas A&M University, 324pp.
- Orr, J.C., Maier-Reimer, E., Micolajewicz, U., Monfray, P., Sarmiento, J.L., Toggweiler, J.R., Taylor, N.K., Palmer, J., Gruber, N., Sabine, C.L., Le Quéré, C., Key R.M., and Boutil, J. (in press): Global oceanic uptake of anthropogenic carbon dioxide as predicted by four 3-D ocean models. – *Global Biogeochemical Cycles*.
- Orsi, A.H., Nowlin Jr., W.D. and Whitworth III, T. (1993): On the circulation and stratification of the Weddell Gyre. – *Deep-Sea Research I*, 40 (1), 169-203.
- Orsi, A. H., Whitworth III, T. and Nowlin Jr., W.D. (1995): On the meridional extent and fronts of the Antarctic Circumpolar Current. – *Deep-Sea Research I*, 42 (5), 641-673.
- Östlund, H.G. (1982): The Residence Time of the Freshwater Component in the Arctic Ocean. – *Journal of Geophysical Research*, 87 (C3), 2035-2043.
- Östlund, H.G., Craig, H., Broecker, W.S. and Spencer, D. (1987): GEOSECS Atlantic, Pacific and Indian Ocean Expeditions, Vol.7. Shorebased data and graphics. – US Government Printing Office, Washington DC.
- Pangaea (1997): Panmap. – Internet: <http://www.pangaea.de/Software/PanMap/>
- Park Y.-H., Charriaud, E., Crabeguy, P. and Kartavtseff, A. (2001): Fronts, transport, and Weddell Gyre at 30 degrees E between Africa and Antarctica. – *Journal of Geophysical Research*, 106 (C2), 2857-2879.
- Perillo, G.M.E., Piccolo, M.C., Bastida, R. and Marcovecchio, J. (2001): Coastal oceanography on the western South Atlantic continental shelf (33 to 55° S, 5° W).

References

- Perisinotto, R., Laubscher, R.K. and Mcquaid, C.D. (1992): Marine productivity enhancement around Bouvet and South Sandwich Islands (Southern Ocean). – *Marine Ecology Progress Series*, 88, 41-53.
- Peterson, R.G. (1992): The boundary currents in the western Argentine Basin. – *Deep-Sea Research*, 39, 623-644.
- Peterson, R.G. and Stramma, L. (1991): Upper-level circulation in the South Atlantic Ocean. – *Progress in Oceanography*, 26, 1-73.
- Peterson, R.G. and Whitworth III, T. (1989): The Subantarctic and Polar fronts in relation to deep water masses through the Southwestern Atlantic. – *Journal of Geophysical Research*, 94, 10817-10838.
- Petroconsultants – Internet: <http://www.petroconsultants.com>
- Pierce, A.P., Mytton, J.W. and Gott, G.B. (1955): Radioactive elements and their daughter products in the Texas Panhandle and other gas fields in the USA. – *Proceedings of the 1st Int. Conf. Peaceful Use of Atomic Energy*, Geneva, Pergamon Press.
- Pierce, A.P., Gott, G.B. and Mytton, J.W. (1964): Uranium and Helium in the Panhandle Gas Fields and Adjacent Areas. – *USGS Prof. Paper* 454-G.
- Pociask-Karteczka, J. (1997): The influence of radionuclides released by Silesian coal mine activity on the natural environment. – *Annales Universitatis Mariae Curie-Sklodowska, Sectio B*, 52, 173-184.
- Pollard, R.T., Read, J.F. and Lucas, M.I. (2000): Relationships between physical and biogeochemical regimes in the Southern Ocean. – *Southern Ocean JGOFS Symposium: "The Southern Ocean – climatic changes and the cycle of carbon"*, 8th – 12th July 2000, Brest.
- Rabalais, N.N., McKee, B.A., Reed, D.J. and Means, J.C. (1992): Fate and effects of produced water discharges in coastal Louisiana, Gulf of Mexico, USA. In: Ray, J.P. and Engelhart, F.R. (Eds.): *Produced Water: Technological/Environmental Issues and Solutions*. – Plenum Press, New York, 355-369.
- Rama, Todd, J.F., Butts, J.L. and Moore, W.S. (1987): A new method for the rapid measurement of Ra-224 in natural waters. – *Marine Chemistry*, 22, 43-54.
- Randolph, T.M., Ayers, R.C. Jr., Shaul, R.A., Hart, A.D., Shebs, W.T., Ray, J.P., Savant-Malhiel, S.A. and Rivera, R.V. (1992): Radium fate and oil removal for discharged produced sand. In: Ray, J.P. and Engelhart, F.R. (Eds.): *Produced Water: Technological/Environmental Issues and Solutions*. – Plenum Press, New York, 267-279.
- Rayle, M.F. and Mulino, M.M. (1992): Produced water impacts in Louisiana coastal waters. In: Ray, J.P. and Engelhart, F.R. (Eds.): *Produced Water: Technological/Environmental Issues and Solutions*. – Plenum Press, New York, 343-354.
- Reid, D.F. (1983): Radium in formation waters: How much and is it of concern? – *Proceedings 4th Annual Gulf of Mexico Information Transfer Meeting*. OCS Report/MMS 84-0026, US Dpt. of Interior.
- Reid, D.F., Moore, W.S., Sackett, W.M. (1979): Temporal variation of ²²⁸Ra in the near-surface gulf of Mexico. – *Earth Planetary Science Letters*, 43, 227-236.
- Reyss, J.-L., Schmidt, S., Legeleux, F. and Bonté, P. (1995): Large, low background well-type detectors for measurements of environmental radioactivity. – *Nuclear Instruments and Methods in Physics Research, A* 357, 391-397.
- Rhein, M. and Schlitzer, R. (1988): Radium-226 and barium sources in the deep East Atlantic. – *Deep-Sea Research*, 35 (A9), 1499-1510.
- Rhein, M., Chan, L.H., Roether, W., and Schlosser, P. (1987): ²²⁶Ra and Ba in Northeast Atlantic Deep Water. – *Deep-Sea Research*, 34, 1541-1564.

References

- Ritcey, G.M. (1990): Weathering processes in uranium tailings and the migration of contaminants. In: International Atomic Energy Agency: The environmental behaviour of radium, Vol.2. – Technical Report Series 310, 27-82.
- Røe Utvik, T.I. (1999): Chemical characterisation of produced water from four offshore oil production platforms in the North Sea. – Chemosphere, 39, 2593-2606.
- Røe, T.I., Johnsen, S. and the Norwegian Oil Industry Association (1996): Discharges of produced water to the North Sea: Effects in the water column. In: Reed, M. and Johnsen, S. (Eds.): Produced Water 2: Environmental Issues and Mitigation Techniques. – Plenum Press, New York, 13-26.
- Rutgers van der Loeff, M.M. (1994): ^{228}Ra and ^{228}Th in the Weddell Sea. In: Johannessen, O.M., Muench, R.D., and Overland, J.E. (Eds.): The Polar Oceans and their role in shaping the global environment: The Nansen centennial volume. - Geophysical Monograph 85, 177-186, American Geophysical Union, Washington DC, USA.
- Rutgers van der Loeff, M.M. and Berger, G.W. (1993): Scavenging of ^{230}Th and ^{231}Pa near the Antarctic Polar Front in the South Atlantic. – Deep-Sea Research I, 40 (2), 339-357.
- Rutgers van der Loeff, M.M. and Moore, W.S. (1999): Determination of natural radioactive tracers. - In: Grasshoff, K., Kremling, K. and Ehrhardt, M. (Eds.): Methods of Seawater Analysis. pp. 365-397, Wiley-VCH, Weinheim.
- Rutgers van der Loeff, M.M., Key, R.M., Scholten, J., Bauch, D. and Michel, A. (1995): ^{228}Ra as a tracer for shelf water in the Arctic Ocean. – Deep-Sea Research II, 42 (6), 1533-1553.
- Rutgers van der Loeff, M.M., Friedrich, J. and Bathmann, U.V. (1997): Carbon export during the Spring Bloom at the Antarctic Polar Front, determined with the natural tracer ^{234}Th . – Deep-Sea Research II, 44, 457-478.
- Sakanoue, M., Okubo, T. and Furuyama, K. (1980): ^{228}Ra in Sea Water. In: Goldberg, E.D. (Ed.): Isotope Marine Chemistry. - Geochemistry Research Association, 247-258, Tokio.
- Sanudo-Wilhelmy, S.A., Olsen, K.A., Scelfo, J.M., Foster, T.D. and Flegal, A.R. (in press): Trace metal distributions off the Antarctic Peninsula in the Weddell Sea. – Marine Chemistry.
- Sarmiento, J. (1988): A chemical tracer strategy for WOCE: Report of a Workshop held in Seattle, Washington, 22 and 23 January 1987. - U.S. WOCE Planning Report 10, U.S. Planning Office for WOCE, College Station, TX, 181pp.
- Sarmiento, J.L. (1991): Oceanic uptake of anthropogenic CO_2 : The major uncertainties. – Global Biogeochemical Cycles, 5, 309-313.
- Schlitzer, R. (2001): Ocean Data View, version 5.4.
Internet: <http://www.awi-bremerhaven.de/GEO/ODV>
- Schlosser, P., Bönisch, G., Kromer, B., Loosli, H.H., Bühler, R., Bonani, G. and Koltermann, K.P. (1995): Mid 1980s distribution of tritium, ^3He , ^{14}C and ^{39}Ar in the Greenland/Norwegian Seas and the Nansen basin of the Arctic Ocean. – Progress in Oceanography, 35, 1-28.
- Schröder, M. and Fahrbach, E. (1999): On the structure and the transport of the eastern Weddell Gyre. – Deep-Sea Research II, 46, 501-527.
- SeaWiFS - Sea-viewing Wide Field-of-view Sensor.
Internet: <http://seawifs.gsfc.nasa.gov/SEAWIFS.html>
- Shannon, L.V. and Cherry, R.D. (1971): Radium-226 in marine phytoplankton. – Earth Planetary Science Letters, 11, 339-343.
- Shawky, S., Amer, H., Nada, A.A., Abd El-Maksoud, T.M. and Ibrahim, N.M. (2001): Characteristics of NORM in the oil industry from Eastern and Western deserts of Egypt. – Applied Radiation and Isotopes, 55, 135-139.

References

- Sievers, H.A. and Nowlin Jr., W.D. (1988): Upper ocean characteristics in Drake Passage and adjoining areas of the Southern Ocean, 39°W-95°W. – In: Sahrage, D. (Ed.): Antarctic and resources variability, 57-80, Springer, Berlin.
- Simon, H. (1974): Messung von radioaktiven und stabilen Isotopen. Anwendung von Isotopen in der organischen Chemie und Biochemie. – Springer, Heidelberg, 430pp.
- Smetacek, V., de Baar, H.J.W., Bathmann, U.V., Lochte, K. and Rutgers van der Loeff, M.M. (1997): Ecology and biogeochemistry of the Antarctic Circumpolar Current during austral spring: a summary of Southern Ocean JGOFS cruise ANT X/6 of R.V. Polarstern. – Deep-Sea Research II, 44, 1-21.
- Smetacek, V., Bathmann, U., El Naggar, S. (2001): The expeditions ANTARKTIS XVIII/1-2 of the Research Vessel "Polarstern" in 2000. – Berichte zur Polarforschung, 400, 232pp.
- Somayajulu, B.L.K. and Goldberg, E.D. (1966): Thorium and uranium isotopes in seawater and sediments. – Earth Planetary Science Letters, 1, 102-106.
- Spindler, M and Beyer, K. (1990): Distribution, Abundance and Diversity of Antarctic Acantharian Cysts. – Marine Micropaleontology, 15, 209-218.
- Steger, H.F. and Bowman, W.S. (1980): DL-1a: A certified uranium-thorium reference ore. – Canada Centre for Mineral and Energy Technology (CANMET), Report 80-10E.
- Strass, V. and Langreder, J. (2000): Underway measurements of currents with the vessel-mounted Acoustic Doppler Current Profiler. In: Bathmann, U. et al. (Eds.): The expeditions ANTARKTIS XVI/3-4 on the Research Vessel "POLARSTERN" in 1999. – Berichte zur Polarforschung, 364, 31-33.
- Strass, V.H., Leach, H., Naveira Garabato, A.C., Gonzalez, S., Bathmann, U.V. and Smetacek, V. (1999): Mesoscale dynamics of the Antarctic Polar Front: Subduction and phytoplankton sedimentation. – EOS, Transactions of the American Geophysical Union, 80 (49), 200.
- Strass, V.H., Naveira Garabato, A.C., Pollard, R.T., Fischer, H.I., Hense, I., Allen, J.T., Read, J.F., Leach, H. and Smetacek, V.: Mesoscale Frontal Dynamics: Shaping the Environment of Primary Production in the Antarctic Circumpolar Current. – submitted to Deep-Sea Research II.
- Stuiver, M. and Östlund, H.G. (1980): GEOSECS Atlantic Radiocarbon. – Radiocarbon, 22, 1-24.
- Szabo, B.J. (1967): Radium content in plankton and sea water in the Bahamas. – Geochimica Cosmochimica Acta, 31, 1321-1331.
- Tchernia, P. and Jeannin, P.F. (1984): Circulation in Antarctic waters as revealed by iceberg tracks 1972-1983. – Polar Record, 22 (138), 263-269.
- Tomczak, M. and Godfrey, J.S. (1994): Regional Oceanography: An Introduction. – 1st edition, Pergamon Press, 422pp.
- Torgensen, T.E., Deangelo, E.C., O'Donell, J., Turekian, K.K., Tanaka, N. and Turekian, V.C. (1996): ²²⁴Ra distribution in surface and deep water of Long Island Sound, summer 1991. – Continental Shelf Research, 16, 1545-1559.
- Trier, R.M., Broecker, W.S. and Feely, H.W. (1972): Radium-228 profile at the second GEOSECS Intercalibration Station, 1970 in the North Atlantic. – Earth Planetary Science Letters, 16, 141-145.
- Tsoulfanidis, N. (1995): Measurement and Detection of Radiation. – 2nd edition, Taylor & Francis, Washington DC, 614pp.
- Turekian, K.K., Tanaka, N., Turekian, V.C., Torgensen, T. and Deangelo, E.C. (1996): Transfer rates of dissolved tracers through estuaries based on ²²⁸Ra: a study of Long Island Sound. – Continental Shelf Research, 16 (7), 863-873.
- Tynan, C.T. (1998): Ecological importance of the Southern Boundary of the Antarctic Circumpolar Current. – Nature, 392, 708-710.

References

- UNSCEAR – United Nations Scientific Commission (1977): Sources and Effects of Ionizing Radiation, United Nations, New York. Internet: <http://www.unscear.org>
- Usbeck, R., Rutgers van der Loeff, M., Hoppema, M. and Schlitzer, R. (in press): Shallow remineralization in the Weddell Gyre. – *Geochemistry, Geophysics, Geosystems*.
- van Bennekom, A.J., Berger, G.W., van der Gaast, S.J. and de Vries, R.T.P. (1988): Primary productivity and the silica cycle in the Southern Ocean (Atlantic Sector). – *Palaeogeography Palaeoclimatology Palaeoecology*, 67, 19-30.
- van den Berg, C.M.G. (1995): Evidence for organic complexation of iron in seawater. – *Marine Chemistry*, 50, 139-157.
- van Franeker, J.A. (1999): Census of marine birds and mammals. In: Bathmann, U. et al. (Eds.): *The expeditions ANTARKTIS XVI/3-4 on the Research Vessel "POLARSTERN"* in 1999. – *Berichte zur Polarforschung*, 364, 101-109.
- van Leeuwe, M.A., Scharek, R., de Baar, H.J.W., de Jong, J.T.M. and Goeyens, L. (1997): Iron enrichment experiments in the Southern Ocean: Physiological responses of a plankton community. – *Deep-Sea Research II*, 44, 189-208.
- van Leeuwen, P.J., de Ruijter, W.P.M. and Lutjeharms, J.R.E (2000): Natal pulses and the formation of Agulhas rings. - *Journal of Geophysical Research*, 105 (C3), 6425-6436.
- Veth, C., Peeken, I. and Scharek, R. (1997): Physical anatomy of fronts and surface waters in the ACC near the 6°W meridian during austral spring 1992. – *Deep-Sea Research II*, 44, 23-49.
- Wallace, D.W.R., Beining, P. and Putzka, A. (1994): Carbon tetrachloride and chlorofluorocarbons in the South Atlantic Ocean, 19S. – *Journal of Geophysical Research*, 99, 7803-7819.
- Walter, H.-J., Rutgers van der Loeff, M.M. and Hoeltzen, H. (1997): Enhanced scavenging of ^{231}Pa relative to ^{230}Th in the South Atlantic south of the Polar Front: Implications for the use of the $^{231}\text{Pa}/^{230}\text{Th}$ ratio as a paleoproductivity proxy. – *Earth Planetary Science Letters*, 149, 85-100.
- Walter, H.J., Geibert, W., Rutgers van der Loeff, M.M., Fischer, G. and Bathmann, U. (2001): Shallow vs. deep-water scavenging of ^{231}Pa and ^{230}Th in radionuclide enriched waters of the Atlantic sector of the Southern Ocean. – *Deep-Sea Research I*, 48, 471-493.
- Warren, B.A. (1981): Transindian hydrographic section at Lat. 18°: property distributions and circulation in the South Indian Ocean. – *Deep-Sea Research*, 28, 759-788.
- Wassburg, G.J., Jacobsen, S.B., Depaolo, D.J., McCulloch, M.R. and Wen, T. (1981): Precise determination of Sm/Nd ratios, Sm and Nd isotopic abundances in standard solutions. – *Geochimica Cosmochimica Acta*, 45, 2311-2323.
- Weppernig, R., Schlosser, P., Khatiwala, S. and Fairbanks, R.G. (1996): Isotope data from Ice Station Weddell: Implications for deep water formation in the Weddell Sea. – *Journal of Geophysical Research*, 101 (C 10), 25723-25739.
- Westerlund, S. and Öhman, P. (1991): Iron in the water column of the Weddell Sea. – *Marine Chemistry*, 35, 199-217.
- Whitworth III, T. and Nowlin Jr., W.D. (1987): Water masses and currents of the Southern Ocean at the Greenwich Meridian. – *Journal of Geophysical Research*, 92 (C6), 6462-6476.
- Wiegand, J. and Feige, S. (in prep.): Origin of radium in high-mineralized waters.

ACKNOWLEDGEMENTS

Sincere thanks go to Prof. Dieter Fütterer for offering this thesis as well as for his continuous support of and faith into the radionuclide "enclave" at the Handelshafen. Prof. Monika Rhein is thanked for kindly taking on the co-referate.

Dr. Michiel Rutgers van der Loeff has accompanied and supported the work with constant interest, unforgettable "explain"s and most useful, helpful and motivating comments. His door (or, recently, email-box) has been open at any time for any worry whatsoever, and having done a cruise together will be one of the many things to remember!

I am grateful to Dr. G. Shimmield who introduced me to the world of naturally occurring radionuclides and to Tim Brand, who filled this world with life, patiently teaching me the art of "producing something vaguely looking scientific with tubing, tape and connectors". These skills have proven to be the basis for becoming a radionuclide geochemist.

Various colleagues assisted in the progress of this work: Dr. Volker Strass had a critical eye on the oceanography chapter and provided CTD data from expedition ANT XVI/3. Dr. Olaf Boebel was most helpful in combining Agulhas eddies and radium signals south of Africa by means of satellite altimetry. Prof. W. Moore kindly provided ^{228}Th data from the Drake Passage. Susanne Gatti sampled the prime meridian for radium during expedition ANT XV/4. Ulrike Westernströer provided excellent help during expedition ANT XVI/3. Dr. Walter Geibert took charge of the sampling in the Argentine Basin during expedition ANT XVII/4 and Prof. E. Dormack collected samples at an otherwise inaccessible region of the Larsen shelf area during expedition NBP00-03. Ingrid Vöge's diligent and practised hand took care of many a sample in the home lab.

Heike, Rainer and Martin helped through the obstacles of the first southbound cruise and the crew of RV Polarstern has facilitated so many things that at first glance seemed to be impossible. For sure, the Southern Ocean would have lost a lot less radium to my filters without the help of Helmut Muhle.

Michiel, Walter, Regina, Ralph, Ingrid, Björn, Hans-Jürgen, Ellen and so many others have been or are still a most colourful and lively group of colleagues that made the work pleasant and varied, often surprising, sometimes demanding, but never boring. Thank you all for companionship, fruitful discussions, endless proof-reading, coffee breaks on the flat roof and counting raindrops from inside.

Of the many friends that accompanied this work in the one or the other way, I'd like to mention deputy especially Andreas as well as Astrid, Claudia, Franzl, Daniela, Florian and Hedi for sharing wonderful moments together, for helping through the difficult times and for never complaining about having been neglected so often.

My parents are thanked for their unfailing support in every respect throughout my academic career and their patience that even this daughter will finally do something serious.

Financial support of this work by the German Science Foundation is kindly acknowledged.

APPENDIX

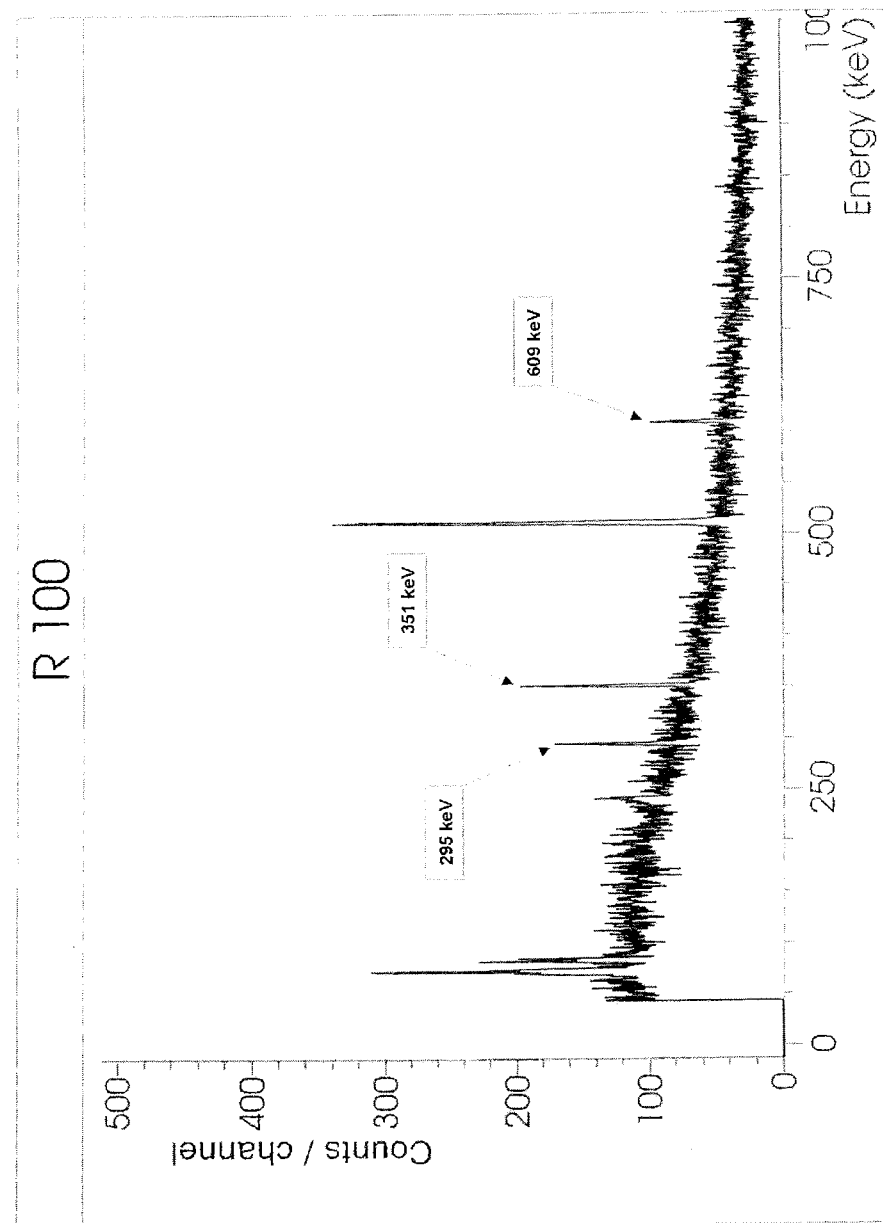
- A 1 Abbreviations
- A 2 γ -spectrum for determination of ^{226}Ra in BaSO_4
- A 3 γ -spectrum for determination of ^{226}Ra and ^{228}Ra in cartridge ash
- A 4 α -spectrum for the determination of ingrown ^{228}Th
- A 5 Conversion of the activity of a radionuclide into mass units
- A 6 Reference chart of ^{238}U and ^{232}Th decay chains
- A 7 Table of surface water results for ^{226}Ra , ^{228}Ra , $^{228}\text{Ra}/^{226}\text{Ra}$ AR and ^{228}Th
- A 8 Table of water column results for ^{226}Ra and $^{228}\text{Th}/^{230}\text{Th}$ AR

A 1: Frequently used abbreviations within the text:

AABW	Antarctic Bottom Water
AAIW	Antarctic Intermediate Water
AASW	Antarctic Surface Water
Ac	Actinium
ACC	Antarctic Circumpolar Current
AF	Agulhas Front
Al	Aluminium
AR	Activity Ratio
Ba	Barium
Bi	Bismuth
Bq	Becquerel
Ca	Calcium
CC	Coastal Current
CDW	Circumpolar Deep Water
cpm	counts per minute
dpm	disintegrations per minute
ε_{Nd}	isotopic composition of Nd ($^{143}\text{Nd}/^{144}\text{Nd}$) compared to a standard
GBq	Gigabecquerel
GEOSECS	Geochemical Ocean Sections
HNLC	High Nutrient Low Chlorophyll
ISW	Ice Shelf Water
LCDW	Lower Circumpolar Deep Water
NADW	North Atlantic Deep Water
Nd	Neodymium
Pb	Lead
PF	Polar Front
Po	Polonium
Ra	Radium
Rn	Radon
SACCF	Southern ACC Front
SAF	Subantarctic Front
SASF	Subantarctic Surface Water
Si	Silicon
Sr	Strontium
STF	Subtropical Front
TBq	Terabecquerel
Th	Thorium
U	Uranium
UCDW	Upper Circumpolar Deep Water
WDW	Warm Deep Water
WSBW	Weddell Sea Bottom Water
WSC	Weddell-Scotia-Confluence
WSDW	Weddell Sea Deep Water
WW	Winter Water

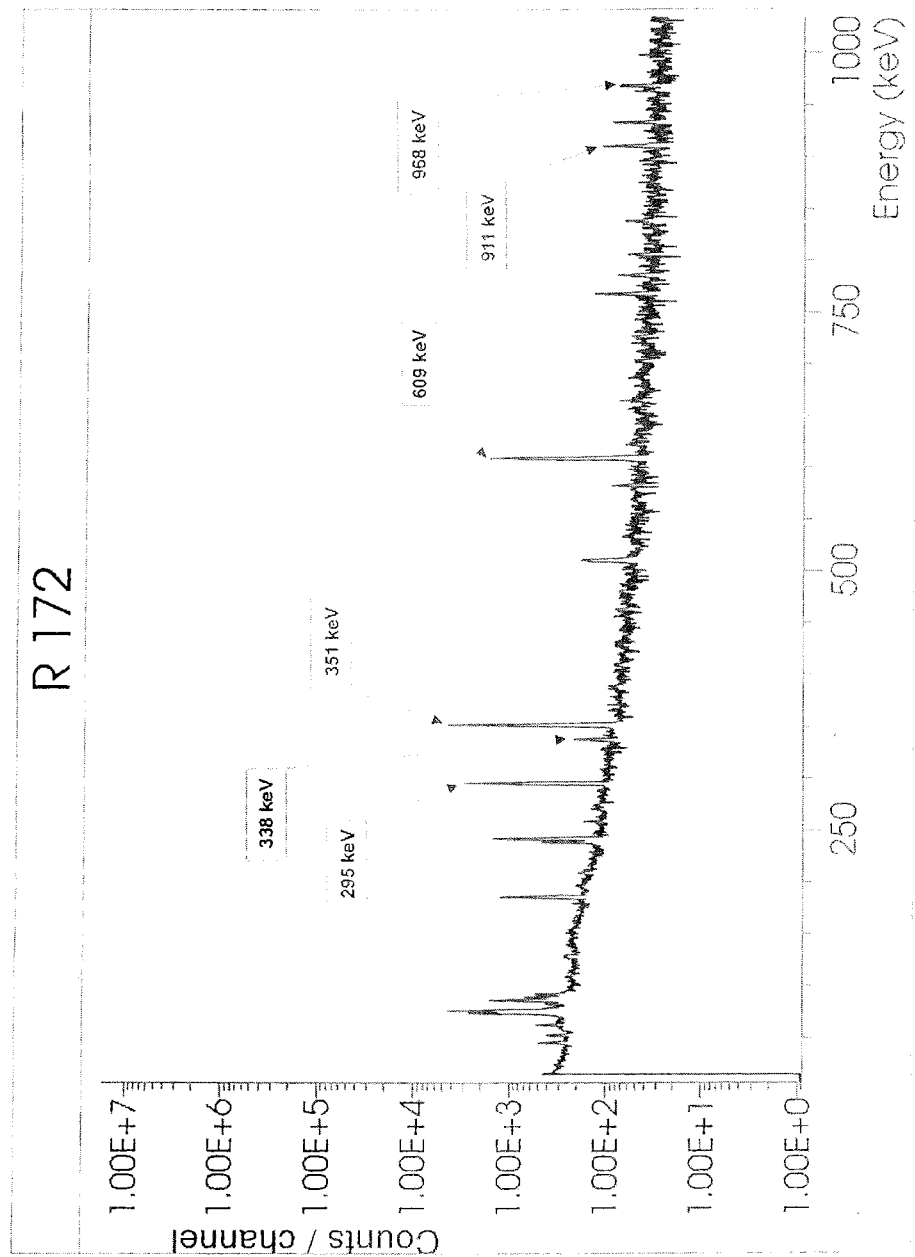
Appendix

A 2: Example of a typical γ -spectrum for the determination of ^{226}Ra , measured on BaSO_4 -precipitation from a 20 l surface water sample. The lines used for analysis of the spectrum are the decay lines of the ^{226}Ra daughters ^{214}Pb (295 and 351 keV) and ^{214}Bi (609 keV).



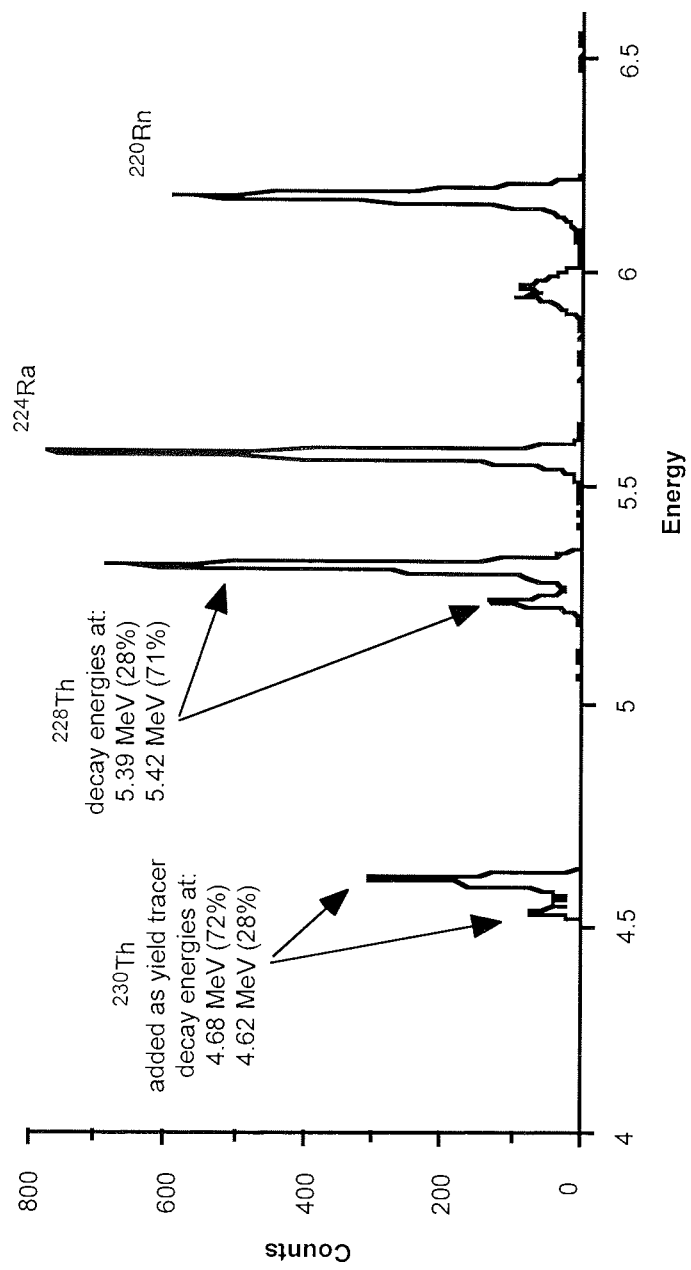
Appendix

A 3: Example of a typical γ -spectrum for the determination of ^{228}Ra and ^{226}Ra , measured on cartridge ash from a surface water sample. The lines used for analysis of ^{228}Ra are the decay lines of its daughter ^{228}Ac at 338, 911 and 969 keV.



Appendix

A 4: Example of an α -spectrum for the determination of ingrown ^{228}Th in a surface water sample. ^{230}Th was added as a yield tracer.



Appendix

A 5: Derivation of the relationship between the molar concentration of an isotope and its activity.

For a conversion in either direction, the following parameters are needed:

- 1 Avogadro's Number $N_A = 6.022 \times 10^{23}$
- 2 the molar weight m of the isotope
- 3 half-life $t_{1/2}$ of the isotope (convert to minutes to be in accordance with dpm)
- 4 the decay constant λ , derived from the half-life by:

$$\lambda = \frac{\ln(2)}{t_{1/2}}$$

The number of atoms (N) of a radioactive nuclide is related to its activity (A) as follows:

$$N = \frac{A}{\lambda}$$

Dividing by Avogadro's Number N_A and the sample's weight or volume V gives the molar concentration C_m :

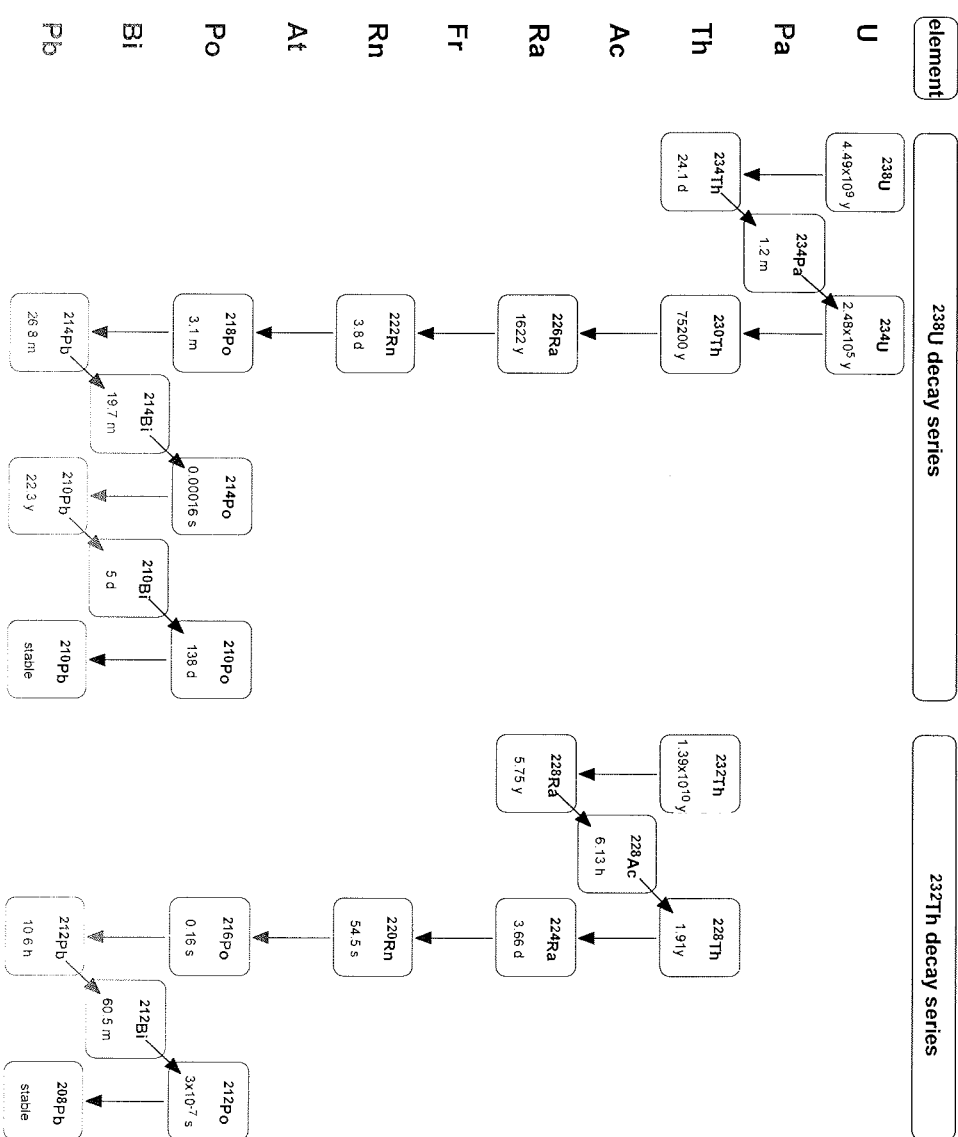
$$C_m = \frac{\frac{N}{N_A}}{V} = \frac{\frac{A}{\lambda N_A}}{V}$$

To convert to mass units, multiply by the molar weight m :

$$C_{ms} = \frac{\frac{A}{\lambda N_A} \times m}{V}$$

Appendix

A 6: Reference chart of the naturally occurring decay series ^{238}U and ^{232}Th (after Broecker and Peng 1962). Each isotope is given with its specific half-life. Decay modes are indicated by arrows: \downarrow : α -decay; \nearrow : β -decay.



Appendix

A 7: Surface water results for ^{226}Ra , ^{228}Ra , $^{228}\text{Ra}/^{226}\text{Ra}$ AR and ^{228}Th .

SAMPLE	SAMPLING DATE	LAT.	LONG.	^{226}Ra (dpm/100kg)	^{228}Ra (dpm/100kg)	$^{228}\text{Ra}/^{226}\text{Ra}$	$^{228}\text{Th}_{\text{extrdiss.}}$ (dpm/100kg)
ANT XV/2							
SWC 1	11.11.1997	-41.37	12.98	9.31 ± 0.38			0.0671 ± 0.0015
SWC 2	12.11.1997	-42.53	9.93	9.10 ± 0.30			0.0661 ± 0.0017
SWC 3	13.11.1997	-45.66	6.95	11.08 ± 0.33	0.099 ± 0.014	0.0089 ± 0.0013	0.0502 ± 0.0020
SWC 4	13.11.1997	-46.72	6.18	11.63 ± 0.22	0.073 ± 0.012	0.00631 ± 0.00099	0.0291 ± 0.0011
SWC 5	13.11.1997	-47.67	5.95				0.02595 ± 0.00094
SWC 6	14.11.1997	-48.54	5.88	14.44 ± 0.51	0.068 ± 0.010	0.00472 ± 0.00067	0.02346 ± 0.00081
SWC 7	14.11.1997	-49.52	5.87	15.13 ± 0.53	0.062 ± 0.012	0.00409 ± 0.00079	0.0188 ± 0.0021
SWC 8	14.11.1997	-50.26	6.10	14.41 ± 0.51	0.063 ± 0.010	0.00435 ± 0.00070	0.0265 ± 0.0012
SWC 9	15.11.1997	-51.11	6.87	12.44 ± 0.35	0.0481 ± 0.0076	0.00387 ± 0.00060	0.02196 ± 0.00090
SWC 10	15.11.1997	-52.48	8.08	14.31 ± 0.38	0.0648 ± 0.0099	0.00453 ± 0.00068	0.0243 ± 0.0010
SWC 11	15.11.1997	-53.47	8.99	16.07 ± 0.42	0.148 ± 0.013	0.00919 ± 0.00077	0.0361 ± 0.0014
SWC 12	16.11.1997	-55.64	7.26	16.72 ± 0.67	0.0462 ± 0.0079	0.00276 ± 0.00046	0.0192 ± 0.0016
SWC 13	16.11.1997	-56.98	6.17	15.81 ± 0.54	0.0160 ± 0.0030	0.00101 ± 0.00019	0.01412 ± 0.00089
SWC 14	17.11.1997	-59.04	4.46	15.94 ± 0.36	0.0379 ± 0.0072	0.00238 ± 0.00045	0.02107 ± 0.00087
SWC 15	17.11.1997	-60.67	2.89	17.96 ± 0.45	0.0219 ± 0.0037	0.00122 ± 0.00021	0.01585 ± 0.00058
SWC 16	18.11.1997	-63.03	0.72	16.89 ± 0.51			0.02109 ± 0.00067
SWC 17	18.11.1997	-63.65	-0.28	16.50 ± 0.39			0.01710 ± 0.00057
SWC 18	19.11.1997	-65.66	-2.01	16.61 ± 0.54			0.0209 ± 0.0010
SWC 19	19.11.1997	-67.32	-3.97	14.39 ± 0.31			0.0142 ± 0.0010
SWC 20	20.11.1997	-69.07	-6.07	13.62 ± 0.41			0.0615 ± 0.0016
SWC 21	20.11.1997	-69.97	-7.05	14.80 ± 0.36			0.0597 ± 0.0013
SWC 22	30.11.1997	-67.93	-13.04	15.86 ± 0.43			
SWC 23	30.11.1997	-66.81	-14.78	16.06 ± 0.52			
SWC 24	01.12.1997	-65.79	-16.63	17.20 ± 0.54			
SWC 25	01.12.1997	s -65.35	-17.05	16.63 ± 0.58			
SWC 26	02.12.1997	-63.83	-20.18	14.99 ± 0.46			
SWC 27	02.12.1997	-62.73	-22.52	15.38 ± 0.48			
SWC 28	03.12.1997	-61.25	-24.23	13.90 ± 0.30			
Z 9	03.12.1997	-59.68	-13.12	14.98 ± 0.28			
Z 10	04.12.1997	-59.38	-15.10	15.11 ± 0.38			
Z 11	05.12.1997	-59.60	-18.27	14.15 ± 0.27			
Z 12	06.12.1997	-59.85	-21.01	15.22 ± 0.53			
Z 13	06.12.1997	-59.67	-22.17	16.31 ± 0.55			
Z 14	07.12.1997	-60.10	-24.62	14.74 ± 0.47			
Z 15	07.12.1997	-60.50	-25.88	15.88 ± 0.48			
Z 16	11.12.1997	-62.40	-29.28	18.04 ± 0.44			
Z 17	no sample recovered						
Z 18	13.12.1997	-61.24	-29.56	13.75 ± 0.36			
Z 19	15.12.1997	-61.30	-29.53	13.77 ± 0.27			
Z 20	16.11.1997	-61.33	-29.08	13.92 ± 0.31			
Z 21	19.11.1997	-61.01	-29.69	13.99 ± 0.30			
Z 22	20.12.1997	s -60.39	-29.42	14.26 ± 0.39			
Z 23	21.12.1997	-60.37	-28.75	12.37 ± 0.24			
Z 24	22.12.1997	-60.36	-26.38	14.35 ± 0.48			
Z 25	22.12.1997	-60.33	-24.99	14.30 ± 0.38			
Z 26	23.12.1997	-59.93	-22.40	14.92 ± 0.38			
Z 27	24.12.1997	-58.94	-19.94	15.27 ± 0.51			
Z 28	25.12.1997	-57.44	-17.26	14.17 ± 0.51			
Z 29	26.12.1997	-57.30	-15.41	13.45 ± 0.50			
Z 30	29.12.1997	-57.81	-13.60	15.89 ± 0.55			
Z 31	01.01.1998	-56.94	-12.79	7.61 ± 0.27			
Z 32	03.01.1998	-55.33	-12.03	3.70 ± 0.16	?		
Z 33	03.01.1998	-53.36	-10.78	5.56 ± 0.18	?		
Z 34	03.01.1998	-51.66	-9.69	5.29 ± 0.25	?		
Z 35	04.01.1998	-49.50	-8.42	4.08 ± 0.15	?		
Z 36	04.01.1998	-48.41	-7.80	7.25 ± 0.21			
Z 37	04.01.1998	-47.22	-7.16	7.51 ± 0.23			
Z 38	05.01.1998	-45.54	-6.49				
Z 39	05.01.1998	-43.40	-5.91	9.05 ± 0.21			
Z 40	06.01.1998	-40.63	-5.08	8.92 ± 0.29			
Z 41	06.01.1998	-39.77	-3.93	6.99 ± 0.19			

Appendix

SAMPLE	SAMPLING DATE	LAT.	LONG.	^{226}Ra (dpm/100kg)	^{228}Ra (dpm/100kg)	$^{228}\text{Ra}/^{226}\text{Ra}$	$^{228}\text{Th}_{\text{total diss.}}$ (dpm/100kg)
ANT XV/3							
R 1	15.01.1998	-41.10	14.62	6.29 ± 0.23	nd	nd	
R 2	15.01.1998	-42.47	13.88	8.33 ± 0.30	0.668 ± 0.036	0.0802 ± 0.0031	
R 3	16.01.1998	-44.72	12.60	10.57 ± 0.34	0.053 ± 0.029	0.0050 ± 0.0028	
R 4	16.01.1998	-46.25	11.70	9.14 ± 0.34	0.664 ± 0.035	0.0726 ± 0.0027	
R 5	17.01.1998	-48.56	10.32	11.74 ± 0.29	nd	nd	
R 6	17.01.1998	-50.17	9.31	12.44 ± 0.31	4.23 ± 0.23	0.340 ± 0.016	
R 7	18.01.1998	-53.03	7.42	13.60 ± 0.45	0.0552 ± 0.0076	0.00406 ± 0.00054	
R 8	18.01.1998	-54.62	6.32	16.64 ± 0.45	nd	nd	
R 9	19.01.1998	-56.92	4.69	16.07 ± 0.52	nd	nd	
R 10	19.01.1998	-58.63	3.33	15.29 ± 0.44	nd	nd	
R 11	20.01.1998	-60.27	2.02	15.81 ± 0.42	0.215 ± 0.013	0.01360 ± 0.00071	
R 12	20.01.1998	-61.50	0.97	13.68 ± 0.37	nd	nd	
R 13	21.01.1998	-63.55	-0.83	16.59 ± 0.37	nd	nd	
R 14	21.01.1998	-65.18	-2.37	15.45 ± 0.51	nd	nd	
R 15	22.01.1998	-67.08	-4.29	17.63 ± 0.61	nd	nd	
R 16	22.01.1998	-68.31	-5.62	14.50 ± 0.49	2.65 ± 0.16	0.1830 ± 0.0095	
R 17	23.01.1998	s -70.57	-4.07	15.48 ± 0.46	0.647 ± 0.035	0.0418 ± 0.0019	
R 18	24.01.1998	-70.59	-9.89	15.45 ± 0.55	0.715 ± 0.032	0.0463 ± 0.0012	
R 19	25.01.1998	-71.47	-13.60	15.15 ± 0.44	0.450 ± 0.020	0.0295 ± 0.0012	
R 20	26.01.1998	-72.60	-18.79	16.17 ± 0.54	0.375 ± 0.018	0.02320 ± 0.00083	
R 21	26.01.1998	s -72.83	-19.25	a	0.448 ± 0.018	0.02958 ± 0.00097	
R 22	28.01.1998	-71.74	-14.63	14.14 ± 0.54	0.463 ± 0.024	0.0327 ± 0.0012	
R 23	30.01.1998	s -70.87	-10.48	13.79 ± 0.40	0.556 ± 0.021	0.0404 ± 0.0010	
R 24	04.02.1998	s -73.45	-22.72	13.40 ± 0.37			
R 25	09.02.1998	-73.87	-24.69	11.76 ± 0.27	0.230 ± 0.011	0.01959 ± 0.00085	
R 26	09.02.1998	s -74.53	-27.22	14.00 ± 0.40			
R 27	12.02.1998	s -75.43	-25.67	15.16 ± 0.26	0.509 ± 0.020	0.0336 ± 0.0012	
R 28	20.02.1998	-71.10	-11.52	15.53 ± 0.30			
R 29	21.02.1998	-72.01	-15.90	14.23 ± 0.49			
R 30	23.02.1998	-72.83	-19.36	14.79 ± 0.43			
R 31	26.02.1998	s -71.45	-15.13	15.38 ± 0.32			
R 32	27.02.1998	-70.90	-10.80	15.05 ± 0.37			
R 33	03.03.1998	-71.02	-15.63	16.38 ± 0.52			
R 34	04.03.1998	-69.70	-21.08	16.11 ± 0.43	nd	nd	
R 35	04.03.1998	-69.03	-23.74	14.63 ± 0.30			
R 36	04.03.1998	-68.40	-26.14	13.03 ± 0.46	nd	nd	
R 37	05.03.1998	-67.44	-29.72	12.13 ± 0.34			
R 38	05.03.1998	-66.83	-31.95	14.46 ± 0.28	nd	nd	
R 39	05.03.1998	-66.17	-34.22	13.82 ± 0.44			
R 40	06.03.1998	-65.21	-37.44	15.56 ± 0.44	nd	nd	
R 41	06.03.1998	-64.57	-39.60	13.75 ± 0.39			
R 42	06.03.1998	-63.87	-41.82	14.61 ± 0.44	nd	nd	
R 43	07.03.1998	-63.03	-44.17	14.69 ± 0.39			
R 44	08.03.1998	-61.76	-51.52	14.65 ± 0.33	0.232 ± 0.011	0.01585 ± 0.00065	
R 45	08.03.1998	-62.23	-55.47	15.96 ± 0.49	0.707 ± 0.040	0.0443 ± 0.0021	
R 46	09.03.1998	-63.00	-60.10	15.70 ± 0.35	0.825 ± 0.025	0.0525 ± 0.0011	
R 47	09.03.1998	-63.97	-63.24	11.09 ± 0.37			
R 48	10.03.1998	-65.88	-66.95	12.22 ± 0.39	0.945 ± 0.039	0.0774 ± 0.0021	
R 49	10.03.1998	-67.23	-69.38	9.73 ± 0.32	0.853 ± 0.034	0.0876 ± 0.0019	
R 50	11.03.1998	s -67.57	-68.12	14.80 ± 0.39	1.988 ± 0.076	0.1343 ± 0.0038	
R 51	12.03.1998	-65.82	-66.83	13.32 ± 0.39	0.843 ± 0.033	0.0633 ± 0.0016	
R 52	12.03.1998	-64.77	-65.03	13.60 ± 0.25			
R 53	13.03.1998	-63.50	-61.85	13.01 ± 0.37			
R 54	14.03.1998	s -62.25	-58.70	14.29 ± 0.39	0.771 ± 0.030	0.0593 ± 0.0016	
R 55	17.03.1998	-62.25	-29.35	14.58 ± 0.42	1.115 ± 0.039	0.0781 ± 0.0017	
R 56	18.03.1998	s -61.33	-58.18	17.70 ± 0.59	nd	nd	
R 57	21.03.1998	-61.86	-57.43	12.57 ± 0.43	0.602 ± 0.030	0.0479 ± 0.0017	
R 58	22.03.1998	-61.27	-57.94	10.21 ± 0.33			
R 59	22.03.1998	-60.40	-58.98	11.50 ± 0.28	0.0743 ± 0.0051	0.00646 ± 0.00041	
R 60	22.03.1998	-59.80	-59.72	12.23 ± 0.24			
R 61	22.03.1998	-59.05	-60.60	12.83 ± 0.42			
R 62	23.03.1998	-58.29	-61.46	12.11 ± 0.43	0.0181 ± 0.0049	0.00150 ± 0.00040	
R 63	23.03.1998	-57.46	-62.38	7.07 ± 0.25			
R 64	23.03.1998	-56.76	-63.12	6.55 ± 0.27			
R 65	23.03.1998	-56.09	-63.84	7.49 ± 0.29			
R 66	23.03.1998	-55.39	-64.58	8.49 ± 0.37	0.123 ± 0.010	0.01448 ± 0.00098	
R 67	24.03.1998	-54.92	-64.85	6.32 ± 0.23			
R 68	24.03.1998	-54.41	-65.26	8.15 ± 0.25	1.245 ± 0.072	0.1528 ± 0.0074	
R 69	24.03.1998	-53.79	-66.29	b	2.00 ± 0.23	0.200 ± 0.012	
R 70	24.03.1998	-53.32	-67.07	b	3.10 ± 0.14	0.310 ± 0.011	
R 71	25.03.1998	-53.13	-67.38	b	3.70 ± 0.13	0.3697 ± 0.0073	

Appendix

SAMPLE	SAMPLING DATE	LAT.	LONG.	^{228}Ra (dpm/100kg)	^{228}Ra (dpm/100kg)	$^{228}\text{Ra}/^{226}\text{Ra}$	$^{228}\text{Th}_{\text{mix}} \text{diss.}$ (dpm/100kg)
ANT XVI/4							
S 1	13.05.1998	-56.88	0.00	14.44 \pm 0.29	nd	nd	
S 2	14.05.1998	-54.24	0.00	14.20 \pm 0.42	nd	nd	
S 3	15.05.1998	s -52.03	0.00	13.90 \pm 0.39	nd	nd	
S 4	16.05.1998	-50.71	-0.01	8.10 \pm 0.32	nd	nd	
S 5	16.05.1998	s -49.00	-0.01	7.72 \pm 0.30	4.37 \pm 0.33	0.567 \pm 0.037	
S 6	17.05.1998	s -47.05	-0.48	9.36 \pm 0.26	nd	nd	
S 7	17.05.1998	s -46.13	-1.03	7.02 \pm 0.25	nd	nd	
S 8	18.05.1998	s -45.18	-1.52	8.25 \pm 0.33	0.066 \pm 0.103	0.008 \pm 0.012	
S 9	18.05.1998	s -44.25	-2.00	8.49 \pm 0.36	nd	nd	
S 10	18.05.1998	s -43.30	-2.50	c	0.090 \pm 0.120	0.010 \pm 0.014	
S 11	19.05.1998	s -42.00	-6.07	8.44 \pm 0.25	0.23 \pm 0.27	0.028 \pm 0.032	
ANT XVI/3							
R 100	20.03.1999	-41.93	19.90	8.14 \pm 0.33	2.82 \pm 0.18	0.346 \pm 0.017	
R 101	21.03.1999	s -46.00	20.00	11.17 \pm 0.41	0.283 \pm 0.017	0.0254 \pm 0.0012	
R 102	22.03.1999	-46.26	20.01	11.28 \pm 0.37	0.1660 \pm 0.0087	0.01471 \pm 0.00060	0.0494 \pm 0.0052
R 103	22.03.1999	-46.82	20.00	11.16 \pm 0.41	0.0692 \pm 0.0039	0.00620 \pm 0.00027	
R 104	22.03.1999	-47.39	20.00	11.59 \pm 0.47	0.0563 \pm 0.0035	0.00486 \pm 0.00022	
R 105	23.03.1999	-48.01	20.00	11.77 \pm 0.47	nd	nd	
R 106	23.03.1999	-48.49	20.00	10.53 \pm 0.39	nd	nd	0.0181 \pm 0.0019
R 107	23.03.1999	-49.02	20.00	10.43 \pm 0.41	0.0550 \pm 0.0033	0.00527 \pm 0.00024	0.0153 \pm 0.0016
R 108	23.03.1999	-49.61	20.00	10.68 \pm 0.44	0.0620 \pm 0.0036	0.00580 \pm 0.00024	
R 109	24.03.1999	-50.20	20.00	10.37 \pm 0.41	0.0550 \pm 0.0034	0.00530 \pm 0.00026	
R 110	24.03.1999	-50.80	20.00	14.30 \pm 0.54	0.0968 \pm 0.0055	0.00677 \pm 0.00029	0.0185 \pm 0.0019
R 111	24.03.1999	-51.38	20.00	14.53 \pm 0.49	0.0790 \pm 0.0045	0.00543 \pm 0.00025	
R 112	24.03.1999	-51.83	20.00	17.12 \pm 0.69	0.0746 \pm 0.0044	0.00436 \pm 0.00019	
R 113	26.03.1999	s -49.85	19.95	12.90 \pm 0.51	0.0832 \pm 0.0048	0.00645 \pm 0.00027	
R 114	27.03.1999	s -48.82	19.92	11.47 \pm 0.54	0.0618 \pm 0.0037	0.00539 \pm 0.00020	0.0125 \pm 0.0013
R 115	28.03.1999	s -49.33	19.90	12.15 \pm 0.40	nd	nd	
R 116	31.03.1999	-48.98	19.90	10.60 \pm 0.44	0.0690 \pm 0.0042	0.00651 \pm 0.00028	0.0888 \pm 0.0090
R 117	01.04.1999	-49.61	19.71	11.52 \pm 0.47	0.0625 \pm 0.0037	0.00542 \pm 0.00024	
R 118	03.04.1999	s -49.96	19.06	13.64 \pm 0.58	0.0843 \pm 0.0053	0.00618 \pm 0.00029	0.0199 \pm 0.0021
R 119	04.04.1999	-48.86	20.06	13.05 \pm 0.56	0.0800 \pm 0.0048	0.00613 \pm 0.00026	0.0126 \pm 0.0013
R 120	05.04.1999	-49.71	20.00	12.93 \pm 0.44	0.0768 \pm 0.0045	0.00594 \pm 0.00028	0.0099 \pm 0.0010
R 121	07.04.1999	-52.91	18.46	16.20 \pm 0.57	0.0543 \pm 0.0030	0.00333 \pm 0.00015	
R 122	07.04.1999	-53.92	18.49	16.45 \pm 0.66	0.0360 \pm 0.0023	0.00219 \pm 0.00011	0.0196 \pm 0.0021
R 123	07.04.1999	-55.01	18.52	16.63 \pm 0.61	0.0257 \pm 0.0022	0.00155 \pm 0.00012	
R 124	08.04.1999	-56.19	18.52	16.99 \pm 0.62	0.0193 \pm 0.0015	0.001138 \pm 0.00080	0.08843 \pm 0.00090
R 125	08.04.1999	-57.39	18.50	16.98 \pm 0.71	0.0316 \pm 0.0023	0.00184 \pm 0.00011	
R 126	08.04.1999	-58.59	18.49	15.55 \pm 0.52	nd	nd	0.0118 \pm 0.0013
R 127	08.04.1999	s -60.00	18.52	16.11 \pm 0.53	0.0406 \pm 0.0023	0.00252 \pm 0.00012	0.0103 \pm 0.0011
R 128	09.04.1999	-60.64	16.70	16.73 \pm 0.57	0.0311 \pm 0.0019	0.001858 \pm 0.00092	
R 129	10.04.1999	-61.38	14.50	16.04 \pm 0.59	0.0299 \pm 0.0018	0.001865 \pm 0.00086	
R 130	10.04.1999	-62.08	12.41	15.85 \pm 0.62	0.0254 \pm 0.0017	0.001604 \pm 0.00084	0.0129 \pm 0.0014
R 131	10.04.1999	-62.70	10.48	15.75 \pm 0.51	0.0288 \pm 0.0018	0.00183 \pm 0.00010	
R 132	10.04.1999	-63.41	8.27	16.48 \pm 0.58	0.0430 \pm 0.0025	0.00261 \pm 0.00012	0.0167 \pm 0.0017
R 133	11.04.1999	-63.97	6.10	14.90 \pm 0.57	0.0276 \pm 0.0019	0.00185 \pm 0.00011	
R 134	11.04.1999	-64.69	1.96	17.36 \pm 0.65	0.0670 \pm 0.0041	0.00386 \pm 0.00019	0.00868 \pm 0.00092
R 135	11.04.1999	-66.53	-1.88	15.47 \pm 0.59	0.0281 \pm 0.0016	0.001817 \pm 0.000076	
R 136	12.04.1999	-69.59	-6.51	d	0.330 \pm 0.024	0.0220 \pm 0.0012	0.266 \pm 0.027
R 137	16.04.1999	s -70.17	-6.85	14.74 \pm 0.53	0.486 \pm 0.027	0.0330 \pm 0.0014	0.575 \pm 0.060
R 138	19.04.1999	s -70.22	-6.12	16.50 \pm 0.66	0.605 \pm 0.036	0.0367 \pm 0.0016	0.0305 \pm 0.0032
R 139	21.04.1999	s -66.98	0.03	16.98 \pm 0.71	0.0307 \pm 0.0017	0.001807 \pm 0.000070	0.0192 \pm 0.0020
R 140	25.04.1999	s -54.02	19.97	15.73 \pm 0.67	0.0432 \pm 0.0026	0.00275 \pm 0.00012	0.0175 \pm 0.0018
R 141	29.04.1999	s -49.33	19.17	12.98 \pm 0.44	0.0844 \pm 0.0047	0.00650 \pm 0.00029	0.0139 \pm 0.0015
R 142	30.04.1999	s -49.33	20.62	14.94 \pm 0.59	0.0832 \pm 0.0052	0.00557 \pm 0.00027	
R 143	06.05.1999	-45.52	19.82	9.60 \pm 0.41	0.219 \pm 0.016	0.0228 \pm 0.0013	
R 144	06.05.1999	-44.54	19.65	10.79 \pm 0.42	0.1336 \pm 0.0077	0.01239 \pm 0.00053	0.0377 \pm 0.0040
R 145	07.05.2003	s -44.02	19.56	13.09 \pm 0.55	0.321 \pm 0.018	0.02453 \pm 0.00093	0.0573 \pm 0.0059
R 146	07.05.1999	-43.88	19.90	7.20 \pm 0.31	1.373 \pm 0.080	0.1907 \pm 0.0075	
R 147	07.05.1999	-43.39	19.80	8.77 \pm 0.35	?	0.752 \pm 0.076	
R 148	08.05.1999	-42.53	19.51	7.31 \pm 0.30	1.34 \pm 0.085	0.1837 \pm 0.0090	
R 149	08.05.1999	-41.33	19.21	5.45 \pm 0.23	1.04 \pm 0.058	0.1905 \pm 0.0071	
R 150	08.05.1999	-40.11	18.96	6.90 \pm 0.29	?	0.779 \pm 0.083	
R 151	08.05.1999	-39.02	18.78	8.51 \pm 0.30	4.23 \pm 0.22	0.497 \pm 0.018	0.823 \pm 0.083

Appendix

SAMPLE	SAMPLING DATE	LAT.	LONG.	^{226}Ra (dpm/100kg)	^{228}Ra (dpm/100kg)	$^{228}\text{Ra}/^{226}\text{Ra}$	$^{228}\text{Th}_{\text{initial}}$ diss. (dpm/100kg)
ANT XVIII/4							
R 200	14.05.2000	s -52.6	-66.9	e	<i>1.57 ± 0.34</i>	<i>0.157 ± 0.034</i>	
R 201	15.05.2000	s -49.8	-58.5	<i>10.78 ± 0.371</i>	<i>0.59 ± 0.14</i>	<i>0.055 ± 0.013</i>	
R 202	16.05.2000	s -48.6	-54.9	<i>11.60 ± 0.389</i>	<i>0.094 ± 0.032</i>	<i>0.0081 ± 0.0027</i>	
R 203	17.05.2000	s -47.2	-52.3	<i>9.85 ± 0.307</i>	<i>0.425 ± 0.092</i>	<i>0.0432 ± 0.0093</i>	
R 204	19.05.2000	s -43.9	-45.8	f	<i>0.45 ± 0.10</i>	<i>0.056 ± 0.013</i>	
R 205	22.05.2000	s -43.0	-32.5	f	<i>0.90 ± 0.16</i>	<i>0.113 ± 0.020</i>	
R 206	23.05.2000	s -43.0	-27.4	f	<i>0.87 ± 0.15</i>	<i>0.109 ± 0.019</i>	
R 207	25.05.2000	s -37.3	-27.4	f	<i>1.35 ± 0.22</i>	<i>0.168 ± 0.028</i>	
NBP 00-03							
R 160	15.05.2000	s -64.64	-58.63	g	<i>1.015 ± 0.051</i>	<i>0.0597 ± 0.0025</i>	
R 161	15.05.2000	s -64.56	-59.51	g	<i>0.588 ± 0.033</i>	<i>0.0346 ± 0.0016</i>	
R 162	16.05.2000	s -64.82	-60.52	g	<i>1.188 ± 0.054</i>	<i>0.0699 ± 0.0024</i>	
R 163	17.05.2000	s -64.78	-60.50	g	<i>1.002 ± 0.045</i>	<i>0.0589 ± 0.0020</i>	
R 164	17.05.2000	s -64.76	-60.16	g	<i>0.943 ± 0.045</i>	<i>0.0555 ± 0.0021</i>	
R 165	19.05.2000	s -64.81	-60.61	g	<i>1.319 ± 0.070</i>	<i>0.0776 ± 0.0035</i>	
R 166	19.05.2000	s -64.71	-59.91	g	<i>1.184 ± 0.045</i>	<i>0.0697 ± 0.0017</i>	
R 167	20.05.2000	s -64.71	-60.34	g	<i>0.890 ± 0.049</i>	<i>0.0523 ± 0.0025</i>	
R 168	20.05.2000	s -64.78	-60.36	g	<i>1.127 ± 0.086</i>	<i>0.0663 ± 0.0047</i>	
R 169	22.05.2000	s -64.76	-59.58	g	<i>1.035 ± 0.049</i>	<i>0.0609 ± 0.0023</i>	
R 170	23.05.2000	s -64.36	-58.48	g	<i>1.450 ± 0.077</i>	<i>0.0853 ± 0.0038</i>	
R 171	24.05.2000	s -64.28	-58.65	g	<i>1.549 ± 0.067</i>	<i>0.0911 ± 0.0029</i>	
R 172	24.05.2000	s -64.12	-58.57	g	<i>1.769 ± 0.084</i>	<i>0.1041 ± 0.0039</i>	

- s Sample has been taken during station time;
the geographic positions of all other samples represent the mean between sample start and end.
- nd Sample yielded no detectable activity above background, based on two times the background.
- ?
- Value questionable judging from adjacent values.
- italic* Values in italics indicate samples for which no ^{226}Ra subsamples exist.
The ^{228}Ra activity of these samples has been calculated on the basis of literature values or estimates for ^{226}Ra as follows:
- a 15.2 dpm/100kg, estimated from adjacent samples
 - b 10 dpm/100kg, after Ku and Lin (1976)
 - c 8.4 dpm/100kg, estimated from adjacent samples
 - d 15 dpm/100kg, estimated from adjacent samples
 - e 10 dpm/100kg, after Ku and Lin (1976)
 - f 8 dpm/100kg, after Ku and Lin (1976)
 - g 17 dpm/100kg, after Chung and Applequist (1980)

Appendix

A 8: Water column results for ^{226}Ra and $^{228}\text{Th}/^{230}\text{Th}$ AR.

STATION	SAMPLING DATE	LAT.	LONG.	MAX. DEPTH (m)	DEPTH (m)	^{226}Ra (dpm/100kg)	$^{228}\text{Th}/^{230}\text{Th}$ activity ratio
ANT 16/3							
PS 53-156	27.03.1999	-48.83	20.00	4831	0 200 600 1000 1800	11.47 ± 0.54 10.85 ± 0.44 15.47 ± 0.56 12.77 ± 0.48 16.82 ± 0.58	5.85 ± 0.44 2.75 ± 0.19 0.806 ± 0.049 0.521 ± 0.031 0.521 ± 0.018
PS 53-161	03.04.1999	-49.96	19.06	4684	0 600 1600		5.69 ± 0.43 0.809 ± 0.056 0.783 ± 0.043
PS 53-169	08.04.1999	-60.00	18.53	4849	0 250 400 750 1000	16.11 ± 0.53 16.43 ± 0.61	1.490 ± 0.075 0.764 ± 0.033 0.660 ± 0.024 0.600 ± 0.022 0.570 ± 0.031
PS 53-182	19.04.1999	-70.13	-6.22	1231	0 100 400 800 986	16.5 ± 0.66 18.45 ± 0.76	5.57 ± 0.41 9.16 ± 0.61 10.3 ± 1.4 2.55 ± 0.78 1.71 ± 0.37
PS 53-190	25.04.1999	-54.03	19.97	3517	0 130 200 400 800 1000	15.73 ± 0.67 17.06 ± 0.53 15.98 ± 0.59	1.470 ± 0.053 1.02 ± 0.14 0.370 ± 0.051 0.530 ± 0.044 0.780 ± 0.049
PS 53-197	02.05.1999	-52.01	20.00	3450	0 120 400 700 1000		2.05 ± 0.10 2.150 ± 0.046 1.110 ± 0.020 0.680 ± 0.016 0.6800 ± 0.0088
PS 53-206	05.05.1999	-47.00	20.00	5056	0 130 400 700 1000		5.4 ± 1.1 1.88 ± 0.14 1.02 ± 0.12 0.670 ± 0.074
PS 53-207	07.05.1999	-44.02	19.56	4576	0 120 427 510 1000	13.09 ± 0.55 8.85 ± 0.37 11.78 ± 0.47 12.85 ± 0.44	18.9 ± 2.1 22.5 ± 2.6 0.350 ± 0.029 0.1800 ± 0.0055 0.830 ± 0.043

"Berichte zur Polarforschung"

Eine Titelübersicht der Hefte 1 bis 376 (1981 - 2000) erschien zuletzt im Heft 413 der nachfolgenden Reihe "Berichte zur Polar- und Meeresforschung". Ein Verzeichnis aller Hefte beider Reihen sowie eine Zusammenstellung der Abstracts in englischer Sprache finden sich im Internet unter der Adresse:

<http://www.awi-bremerhaven.de/Resources/publications.html>

Ab dem Heft-Nr. 377 erscheint die Reihe unter dem Namen: "Berichte zur Polar- und Meeresforschung".

Heft-Nr. 377/2000 – „Rekrutierungsmuster ausgewählter Wattfauna nach unterschiedlich strengen Wintern“ von Matthias Strasser.

Heft-Nr. 378/2001 – „Der Transport von Wärme, Wasser und Salz in den Arktischen Ozean“, von Boris Cisewski.

Heft-Nr. 379/2001 – „Analyse hydrographischer Schnitte mit Satellitennaltimetrie“, von Martin Losch.

Heft-Nr. 380/2001 – „Die Expeditionen ANTARKTIS XVI/1-2 des Forschungsschiffes POLARSTERN 1998/1999“, herausgegeben von Eberhard Fahrbach und Saad El Naggar.

Heft-Nr. 381/2001 – „UV-Schutz- und Reparaturmechanismen bei antarktischen Diatomeen und *Phaeocystis antarctica*“, von Lieselotte Rieger.

Heft-Nr. 382/2001 – „Age determination in polar Crustacea using the autofluorescent pigment lipofuscin“, by Bodil Bluhm.

Heft-Nr. 383/2001 – „Zeitliche und räumliche Verteilung, Habitspräferenzen und Populationsdynamik benthischer Copepoda Harpacticoida in der Potter Cove (King George Island, Antarktis)“, von Gritta Veit-Köhler.

Heft-Nr. 384/2001 – „Beiträge aus geophysikalischen Messungen in Dronning Maud Land, Antarktis, zur Auffindung eines optimalen Bohrpunktes für eine Eiskerntiefbohrung“, von Daniel Steinhage.

Heft-Nr. 385/2001 – „Actinium-227 als Tracer für Advektion und Mischung in der Tiefsee“, von Walter Geibert.

Heft-Nr. 386/2001 – „Messung von optischen Eigenschaften troposphärischer Aerosole in der Arktis“, von Rolf Schumacher.

Heft-Nr. 387/2001 – „Bestimmung des Ozonabbaus in der arktischen und subarktischen Stratosphäre“, von Astrid Schulz.

Heft-Nr. 388/2001 – „Russian-German Cooperation SYSTEM LAPTEV SEA 2000: The Expedition LENA 2000“, edited by Volker Rachold and Mikhail N. Grigoriev.

Heft-Nr. 389/2001 – „The Expeditions ARKTIS XVI/1 and ARKTIS XVI/2 of the Research Vessel 'Polarstern' in 2000“, edited by Gunther Krause and Ursula Schauer.

Heft-Nr. 390/2001 – „Late Quaternary climate variations recorded in North Atlantic deep-sea benthic ostracodes“, by Claudia Didié.

Heft-Nr. 391/2001 – „The polar and subpolar North Atlantic during the last five glacial-interglacial cycles“, by Jan P. Helmke.

Heft-Nr. 392/2001 – „Geochemische Untersuchungen an hydrothermal beeinflußten Sedimenten der Bransfield Straße (Antarktis)“, von Anke Dähmann.

Heft-Nr. 393/2001 – „The German-Russian Project on Siberian River Run-off (SIRRO): Scientific Cruise Report of the Kara-Sea Expedition 'SIRRO 2000' of RV 'Boris Petrov' and first results“, edited by Ruediger Stein and Oleg Stepanets.

Heft-Nr. 394/2001 – „Untersuchungen der Photooxidantien Wasserstoffperoxid, Methylhydroperoxid und Formaldehyd in der Troposphäre der Antarktis“, von Katja Riedel.

Heft-Nr. 395/2001 – „Role of benthic cnidarians in the energy transfer processes in the Southern Ocean marine ecosystem (Antarctica)“, by Covadonga Orejas Saco del Valle.

Heft-Nr. 396/2001 – „Biogeochemistry of Dissolved Carbohydrates in the Arctic“, by Ralph Engbrodt.

Heft-Nr. 397/2001 – „Seasonality of marine algae and grazers of an Antarctic rocky intertidal, with emphasis on the role of the limpet *Nacilla concinna* Strebel (Gastropoda: Patelidae)“, by Dohong Kim.

Heft-Nr. 398/2001 – „Polare Stratosphärenwolken und mesoskalige Dynamik am Polarwirbelrand“, von Marion Müller.

Heft-Nr. 399/2001 – „North Atlantic Deep Water and Antarctic Bottom Water: Their Interaction and Influence on Modes of the Global Ocean Circulation“, by Holger Brix.

Heft-Nr. 400/2001 – „The Expeditions ANTARKTIS XVIII/1-2 of the Research Vessel 'Polarstern' in 2000“, edited by Victor Smetacek, Ulrich Bathmann, Saad El Naggar.

Heft-Nr. 401/2001 – „Variabilität von CH₂O (Formaldehyd) – untersucht mit Hilfe der solaren Absorptionsspektroskopie und Modellen“, von Torsten Albrecht.

Heft-Nr. 402/2001 – „The Expedition ANTARKTIS XVII/3 (EASIZ III) of RV 'Polarstern' in 2000“, edited by Wolf E. Arntz and Thomas Brey.

Heft-Nr. 403/2001 – „Mikrohabitatsprüche benthischer Foraminiferen in Sedimenten des Südatlantiks“, von Stefanie Schumacher.

- Heft-Nr. 404/2002** – "Die Expedition ANTARKTIS XVII/2 des Forschungsschiffes 'Polarstern' 2000", herausgegeben von Jörn Thiede und Hans Oerter.
- Heft-Nr. 405/2002** – "Feeding Ecology of the Arctic Ice-Amphipod *Gammarus wilkitzkii*. Physiological, Morphological and Ecological Studies", by Carolin E. Arndt.
- Heft-Nr. 406/2002** – "Radiolarienfauna im Ochotskischen Meer - eine aktuopaläontologische Charakterisierung der Biozönose und Taphozönose", von Anja Nimmergut.
- Heft-Nr. 407/2002** – "The Expedition ANTARKTIS XVIII/5b of the Research Vessel 'Polarstern' in 2001", edited by Ulrich Bathmann.
- Heft-Nr. 408/2002** – "Siedlungsmuster und Wechselbeziehungen von Seepocken (Cirripedia) auf Muschelbänken (*Mytilus edulis* L.) im Wattenmeer", von Christian Buschbaum.
- Heft-Nr. 409/2002** – "Zur Ökologie von Schmelzwassertümpeln auf arktischem Meereis - Charakteristika, saisonale Dynamik und Vergleich mit anderen aquatischen Lebensräumen polarer Regionen", von Marina Carstens.
- Heft-Nr. 410/2002** – "Impuls- und Wärmeaustausch zwischen der Atmosphäre und dem eisbedeckten Ozean", von Thomas Garbrecht.
- Heft-Nr. 411/2002** – "Messung und Charakterisierung laminarer Ozonstrukturen in der polaren Stratosphäre", von Petra Wahl.
- Heft-Nr. 412/2002** – "Open Ocean Aquaculture und Offshore Windparks. Eine Machbarkeitsstudie über die multifunktionale Nutzung von Offshore-Windparks und Offshore-Marikultur im Raum Nordsee", von Bela Hieronymus Buck.
- Heft-Nr. 413/2002** – "Arctic Coastal Dynamics. Report of an International Workshop. Potsdam (Germany) 26-30 November 2001", edited by Volker Rachold, Jerry Brown and Steve Solomon.
- Heft-Nr. 414/2002** – "Entwicklung und Anwendung eines Laserablations-ICP-MS-Verfahrens zur Multielementanalyse von atmosphärischen Einträgen in Eisbohrkernen", von Heiko Reinhardt.
- Heft-Nr. 415/2002** – "Gefrier- und Tauprozesse im sibirischen Permafrost – Untersuchungsmethoden und ökologische Bedeutung", von Wiebke Müller-Lupp.
- Heft-Nr. 416/2002** – "Natürliche Klimavariationen der Arktis in einem regionalen hochauflösenden Atmosphärenmodell", von Wolfgang Dorn.
- Heft-Nr. 417/2002** – "Ecological comparison of two sandy shores with different wave energy and morphodynamics in the North Sea", by Iris Menn.
- Heft-Nr. 418/2002** – "Numerische Modellierung turbulenter Umströmungen von Gebäuden", von Simón Domingo López.
- Heft-Nr. 419/2002** – "Scientific Cruise Report of the Kara-Sea Expedition 2001 of RV 'Academik Petrov': The German-Russian Project on Siberian River Run-off (SIRRO) and the EU Project 'ESTABLISH'", edited by Ruediger Stein and Oleg Stepanets.
- Heft-Nr. 420/2002** – "Vulkanologie und Geochemie pliozäner bis rezenter Vukanite beiderseits der Bransfield-Straße / West-Antarktis", von Andreas Veit.
- Heft-Nr. 421/2002** – "POLARSTERN ARKTIS XVII/2 Cruise Report: AMORE 2001 (Arctic Mid-Ocean Ridge Expedition)", by J. Thiede et al.
- Heft-Nr. 422/2002** – "The Expedition 'AWI' of RV 'L'Atalante' in 2001", edited by Michael Klages, Benoit Mesnil, Thomas Soltwedel and Alain Christophe with contributions of the participants.
- Heft-Nr. 423/2002** – "Über die Tiefenwasserausbreitung im Weddellmeer und in der Scotia-Sea: Numerische Untersuchungen der Transport- und Austauschprozesse in der Weddell-Scotia-Konfluenz-Zone", von Michael Schodlok.
- Heft-Nr. 424/2002** – "Short- and Long-Term Environmental Changes in the Laptev Sea (Siberian Arctic) During the Holocene", von Thomas Müller-Lupp.
- Heft-Nr. 425/2002** – "Characterisation of glacio-chemical and glacio-meteorological parameters of Amundsenisen, Dronning Maud Land, Antarctica", by Fidan Göktas.
- Heft-Nr. 426/2002** – "Russian-German Cooperation SYSTEM LAPTEV SEA 2000: The Expedition LENA 2001", edited by Eva-Maria Pfeiffer and Mikhail N. Grigoriev.
- Heft-Nr. 427/2002** – "From the Inner Shelf to the Deep Sea: Depositional Environments on the Antarctic Peninsula Margin - A Sedimentological and Seismostratigraphic Study (ODP Leg 178)", by Tobias Mörz.
- Heft-Nr. 428/2002** – "Concentration and Size Distribution of Microparticles in the NGRIP Ice Core (Central Greenland) during the Last Glazial Period", by Urs Ruth.
- Heft-Nr. 429/2002** – "Interpretation von FCKW-Daten im Weddellmeer", von Olaf Klatt.
- Heft-Nr. 430/2002** – "Thermal History of the Middle and Late Miocene Southern Ocean - Diatom Evidence", by Bernd M. Censarek.
- Heft-Nr. 431/2002** – "Radium-226 and Radium-228 in the Atlantic Sector of the Southern Ocean", by Claudia Hanfland.

